NBSIR 81-2191 (DoE)

# The Use of the Slow Strain Rate Technique for the Evaluation of Structural Materials for Application in High-Temperature Gaseous Environments

C. E. Johnson and G. M. Ugiansky

Corrosion and Electrodeposition Group
Chemical Stability and Corrosion Division
Center for Materials Science
U.S. Department of Commerce
National Bureau of Standards
Washington, DC 20234

January 1981

Final Report

NBSIR 81-2191 (DoE)

# THE USE OF THE SLOW STRAIN RATE TECHNIQUE FOR THE EVALUATION OF STRUCTURAL MATERIALS FOR APPLICATION IN HIGH-TEMPERATURE GASEOUS ENVIRONMENTS

C. E. Johnson and G. M. Ugiansky

Corrosion and Electrodeposition Group
Chemical Stability and Corrosion Division
Center for Materials Science
U.S. Department of Commerce
National Bureau of Standards
Washington, DC 20234

January 1981

DISTRIBUTION OF THIS DOCUMENT IS UNLIMITED

Final Report

**U.S. DEPARTMENT OF COMMERCE, Malcolm Baldrige,** *Secretary*

**NATIONAL BUREAU OF STANDARDS, Ernest Ambler,** *Director*

# FOREWARD

Since 1974, the National Bureau of Standards has been engaged in research designed to address succinct materials problems and needs pertinent to coal conversion and utilization technologies. This work, sponsored in part, at first by the Office of Coal Research, then ERDA and currently the DOE, focuses on test method development, particularly accelerated procedures for materials behavior and durability; on the determination of the mechanisms of materials degradation; and on the development and operation of materials data centers to provide evaluated information on properties and performance including failures occurring in operating plants.

During the FY 77-79 period the NBS program, entitled "Materials Research for the Clean Utilization of Coal", consisted of a number of interrelated tasks including:

1.      Metal Corrosion

        a.  Slow Strain Rate Test
        b.  Pre-cracked Fracture Test


2.      Ceramic Deformation, Fracture and Erosion


3.      Chemical Degradation of Ceramics

        a.  Reactions and Transformations
        b.  Slag Characterization (viscosity)
        c.  Vaporization and Chemical Transport


4.      Failure Prevention

        a.  Failure Information Center
        b.  Materials Properties Data Center

The results of the research have been disseminated through quarterly reports of progress (available from NTIS; report designation EA-6010; Dist. Category (UC-90C) as well as numerous scientific publications in technical journals.  Further, as individual tasks are completed, an overall report is prepared detailing the results and accomplishments of the project.  This present publication is the final report for the project on <u>Metal Corrosion-Slow Strain Rate Test Technique.</u>

SAMUEL J. SCHNEIDNER
Program Manager
Center for Materials Science
National Bureau of Standards

# ABSTRACT

The slow strain rate technique has been evaluated as an accelerated test for determining the performance of structural materials in simulated coal gasification environments. Seven alloys, namely Types 309, 310, 310S, 347 and 446 stainless steels; Incoloy 800; and Inconel 671, were tested at temperatures from 370°C to 1040 C(700°F to 1900°F) at strain rates from $10^{-4}$ to $10^{-7}$/s in $H_2S$ plus water, gaseous mixtures of CO, $CO_2$, $H_2$, $CH_4$, $H_2S$, and $H_2O$, and in nominally inert environments of He and Ar. Type 310 steel, the most extensively studied material, showed a marked reduction in mechanical properties at low strain rates ($<10^{-5}$/s) in $H_2S/H_2O$ at 540°C(1000°F), and this was associated with the occurrence of a large degree of secondary intergranular cracking in addition to the main ductile fracture mode. The occurrence of the secondary cracking was taken as the primary indication of embrittlement in subsequent tests. Of particular significance, it occurred to some degree in all alloys tested in the simulated coal-gasification environments at 600°C(1100°F). Comparison of the results for the nonstabilized austenitic steels with those for the stabilized grade, Type 347, indicated that sensitization had a detrimental effect with respect to intergranular cracking, although it was not clear that it is a necessary condition for this type of failure. The secondary cracking was surface-initiated in all alloys except the Inconel 671, which failed by the formation of internal cracks associated with the temperature and strain-induced α-chromium phase. While there was clearly an effect of environment on the behavior of the former alloys, interpretation was hindered by the absence of base-line data for an inert environment, since the nominally inert media caused limited oxidation. Consequently, the mechanism(s) of the embrittlement phenomena remain uncertain; a number of possible causes including creep and several environmentally-induced fracture processes are outlined. it is shown that the overall results of the test program are in good agreement with in-plant experience. it is concluded that the slow strain rate technique is an effective method for evaluating the performance of structural materials in the elevated-temperature gaseous environments.

INTRODUCTION

This study of the mechanical behavior of structural alloys in gaseous environments at elevated temperatures was initiated primarily to support current efforts in the development of the technology to convert the Nation's abundant coal reserves to gases of both high and low BTU values. The behavior of materials under such conditions was largely unexplored at the start of this investigation. The thrust of the program was not to test specific alloys, but to evaluate an accelerated test method for materials selection for this demanding application. Specifically, the slow strain rate technique (SSRT) was investigated.

Previous work utilizing this technique had been confined largely to the study of stress-corrosion cracking (SCC) and hydrogen embrittlement in aqueous media.* The test involves the application of a slow strain rate to smooth, i.e., un-notched, tensile specimens which are simultaneously exposed to the environment being investigated, and yields data of the type shown in Fig. 1. Region A, where strain rates are too slow to lead to SCC, the rate of repassivation is thought to be rapid enough to prevent any damaging interaction between the environment and the bare metal exposed during straining. At the opposite extreme, Region C, the strain rate is so rapid that failure occurs by the normal ductile mode, the time being insufficient for environmental interaction to have a significant effect. It is only in the intermediate range of strain rates, Region B, where the rate of production of bare metal is sufficiently high so that the rate of repassivation does not effectively stifle environmental reaction and the strain rate is sufficiently slow so that ductile fracture does not predominate. Under these conditions, SCC takes place. If SCC is not possible for the system studied, the reduction in ductility shown in Region B does not occur; the presence or absence of this reduction of mechanical properties is the essence of the SSRT.

The SSRT has become widely used in the study of SCC, both for mechanistic investigations and as a routine method for materials/environment evaluation. The advantages of the method are the relatively short testing times required, and the severe nature of the test -- it will promote SCC where other tests will not, unless inordinately long times are used. While it is extremely useful for ranking materials, it should be noted that the detailed interpretation of the results is not clear. The reduction in area, strain to fracture, and maximum tensile stress are commonly used as measures of susceptibility, but it is not established whether the reduction in these parameters relates to crack initiation, propagation or a combination of these processes. Moreover, no clear relationship exists between the results of the SSRT and those of other test methods.

---

*A monograph has recently been published, describing the SSRT in considerable detail [1].

The environmental conditions encountered in coal gasification, i.e., high-temperature gases, are basically different from those in the aqueous SCC systems which have been studied by the SSRT. The present studies were carried out to determine whether the method can be used to evaluate materials for the gaseous case. The tests were carried out on several candidate materials for use in proposed coal-gasification systems, namely several austenitic stainless steels (Types 309, 310, 310S and 347), a ferritic stainless steel (Type 446), and two nickel-base alloys (Inconel 671 and Incoloy 800). These materials were also being included in a DOE-sponsored study of high-temperature corrosion-erosion [2]. The main test environments used were the gases He and Ar; $H_2S$ plus steam, and $H_2S$ saturated with water vapor at 23°C; and mixtures of CO, $CO_2$, $H_2$, $CH_4$, $H_2S$ and $H_2O$. He and Ar were used to provide baseline data. The wet $H_2S$ environments were employed because of the high probability of embrittlement in those environments, based on the known susceptibility of austenitic alloys to SCC in sulfide environments in oil refineries. The gaseous mixtures of CO, $CO_2$, $H_2$, $CH_4$, $H_2S$, and $H_2O$ simulated possible coal gasification environments.

## EXPERIMENTAL PROCEDURES

### Materials and Specimen Preparation

The compositions and heat treatments of the alloys used are given in Table 1. Note that two different batches of Type 310 steel were used. All the alloys were received in the form of 9.5 mm(0.375 in) diameter rods. The heat treatments were performed by the suppliers and no further heat treatment was carried out. The microstructures of the alloys are shown in Fig. 2.

The specimens were 58 cm(23 in) long by 9.5 mm(0.375 in) in diameter, and threaded on both ends for attachment to universal couplings outside the test cell. A central gauge section of effective length 2.5 cm(1.0 in) and diameter 4 mm(0.16 in) was produced by machining. The gauge section was subsequently polished using 320, 400, and 600 grit silicon carbide papers, respectively, followed by a final polish using CROCUS cloth. The surface was finally rinsed with acetone and alcohol, and air dried.

### Test Facility

The SSRT facility is capable of testing four specimens simultaneously and is equipped with automatic digital data acquistion and storage. The facility is illustrated schematically in Fig. 3. A range of strain rates from $10^{-3}$/s to $10^{-7}$/s (over the 2.5 cm(1.0 in) gauge length) was achieved through the use of different gear ratios, reduction gear boxes, and variable speed motors. The tensile load was measured by a load cell with a maximum capacity of 900 kg(2000 lb) and an output of 39.6 μV/kg(18 μV/lb). The strain was measured by means of a LVDT attached across the shoulders of the specimen, at points outside the furnace, Fig. 3; the LVDT was calibrated to

give an output of 13.33 V/m(0.34/in). The elongation was determined after fracture from gauge marks on the reduced section of the specimen. Reduction in area measurements were made by measuring the diameter of the reduced section before and after testing using a stage micrometer. The load cells and LVDTs were sequentially scanned and their outputs were read on a digital multimeter and stored in a programmable calculator. These data were transferred to magnetic tape or flexible magnetic disc memory for later use in constructing stress-strain curves or other curves of tensile strength, elongation, or reduction in area versus strain rate.

The test cells were Type 304 stainless steel tubes (38 cm(15 in) long by 5 cm(2.0 in) diameter sealed at both ends with Type 304 plates using Viton-A gaskets. The cells were mounted in furnaces capable of producing test temperatures up to 1100 C(200°F). Ports for entrant and exit gases, thermocouples, and specimens were available on the end plates, Fig. 3. Sliding seals of Teflon or high vacuum O-ring couplings provided freedom of movement for specimen extension while testing. These seals are limited in use to below 300 C(570°F) and therefore were located outside of the furnace and cooled with fresh air.

The specimens were positioned in the test cell so that the reduced section was in the center of the cell and furnace, Fig. 3. The cells were purged with either N, Ar, or He. The test gas then was introduced into the cells and the furnaces brought up to test temperature. The specimens were pre-loaded to 100 kg(220 lb) to produce a positive output from the load cell. Data were taken at predetermined load intervals (approximated by dividing the expected maximum load by the number of data registers available), usually 0.3 mV or 0.4 mV [corresponding to 7.5 kg(16.5 lb) or 10 kg(22 lb).

## Test Environments

The main environments were He, Ar, $H_2S$ plus steam, and $H_2S$ saturated at 23°C(73°F) with $H_2O$ vapor (wet $H_2S$), and gaseous mixtures of CO, $CO_2$, $H_2$, $CH_4$, $H_2S$, and $H_2O$; limited tests were conducted in air, $H_2$, and in vacuum. The inlet gas compositions and the calculated equilibrium compositions of the simulated coal gasification environments are given in Table 2.

## RESULTS AND DISCUSSION

## Austenitic Stainless Steels

Type 310: Specimens were initially tested at 540°C(1000°F) in the $H_2S$ environments. Typical stress-strain curves are shown in Fig. 4, and the various fracture parameters are presented in Fig. 5 and Table 3. It can be seen that the UTS, elongation and % reduction in area (RA) are markedly reduced at strain rates of $7.2 \times 10^{-6}$/s and slower. SEM examination indicated that the reduction in the tensile parameters was associated with the appearance of large numbers of surface cracks, Fig. 6. These formed throughout the gauge section and were approximately perpendicular to the stress axis, e.g., Fig. 6(d). In the case

of specimens showing reduced tensile properties, the central
region of the primary fracture surface was ductile with a flat
outer rim corresponding to the surface cracks.  These cracks,
seen below to be intergranular, are considered to be responsible
for the degradation of the tensile properties at the slower
strain rates.  It can be seen in Fig. 6(a) and (b) that failure
at the higher strain rates occurred by ductile shear; it should
be noted that secondary shear cracks formed near the primary
fracture, Figs. 6(a) and (b), are readily distinguished from the
intergranular cracks, cf.  Fig. 6(d).  A thick scale was formed
on the specimens and quantitative analysis indicated that it
consisted of a duplex oxide-sulfide layer, Appendix A.

For comparison purposes, specimens were also tested in He
at 540°C(1000°F).  The results, Fig. 5, indicated that the RA was
again decreased at the lower strain rates, and SEM examination
revealed the presence of intergranular cracks.  A visible oxide
film was observed, raising the possibility that this was
responsible for the reduced RA.  The supplier's analysis of the
He gave a value of $O_2$ content of 0.1 to 0.5% while $H_2O$ was listed
at 2-250 ppm.  Accordingly, further testing was carried out at a
strain rate of $10^{-6}$/s in He which was first passed through heated
Ti filings, phosphorus pentoxide, and a liquid-nitrogen trap;
tests were also carried out in Ar and vacuum (2 x $10^{-2}$ Torr).
Intergranular cracking occurred in each case, Fig. 7.  However, a
visible oxide film was detectable in each case, so that the
environments cannot be regarded as inert. A hard vacuum test cell
probably would have prevented the oxide on the specimens, but
equipment and time were not available to test this idea.

Subsequent testing in a reducing environment of $H_2$ also
produced a thin interference oxide film on the surface of the
specimens.  Cracking was also detected in these specimens in
tests at 540°C(1000°F) at a strain rate of $10^{-6}$/s.  Figure 8
shows the intergranular cracking on the surfaces of the gauge
section, and the intergranular facets on the primary fracture
surface.  The rim of intergranular cracking extended 250-400 μm
from the free surface, and the remaining fracture surface
corresponded to ductile shear.

It is probable that sensitization, detected from a
chemical etch test, occurred during testing at 540°F(1000°F), and
that carbide precipitation at grain boundaries and the associated
chromium depletion played a role in the intergranular failures.
To pursue this possibility, tests were run at a strain rate of
$10^{-6}$/s at 815°C(1500°F) and 1040°C(1900°F).  The former was
designed to give information near the top of the sensitization
range, while the latter would give results above the temperature
range for sensitization.  These tests were run in air because the
seals of the test chambers were not designed for these high
temperatures.  At 815°C(1500°F), the UTS was only 173 MPa(25 KSI)
versus 414 MPa(60 KSI) when tested in He at 540°C(1000°F) at the
same rate; the RA was 14.5% which was a lower value than obtained
for that parameter for any test at 540°C(1000°F).  Many secondary
intergranular cracks were observed in this specimen, Fig. 9(a)
and (b), and the primary fracture consisted largely of
intergranular facets, in contrast to the shallow rim of

intergranular cracking observed at 540°C(1000°F). The
intergranular nature of the secondary cracks is evident from Fig.
9(c). Intergranular cracking also occurred in the test at
1040°C(1900°F), thus ruling out the possibility that
sensitization is necessary for this form of failure. The RA was
21%, UTS 76 MPa(11 KSI) in this case, and the elongation 41%.
The latter was probably due to the more uniform yielding over the
entire reduced section at the higher temperature.

To further investigate the role of sensitization,
specimens were tested at a strain rate of $10^{-6}$/s in dry He and $H_2$
at 370°C(700°F) and 450°C(840°F), both below the nominal
temperature range for sensization. Examination of fractured
specimens suggested that partial sensitization had in fact
occurred, Figs. 10(b) and 11(b). However, the primary fracture
was entirely ductile and no secondary intergranular cracks were
detected, Figs. 10(a) and 11(a). The tensile properties were
higher than in comparable tests at 540°C(1000°F), e.g., Fig. 12.
In a further attempt to separate the effect of sensitization from
that of combined thermo-mechanical processes, a test was made by
heat-treating the unstressed specimen at 540°C(1000°F) for a time
equivalent to the time required for specimen failure when tested
at a strain rate of $10^{-6}$/s (approximately 60h). The Type 310
specimen failed in a ductile manner when subsequently tested at
540°C(1000°F) at a higher strain rate of $10^{-4}$/s. These tests
showed the need for simultaneous application of the slow strain
rate ($10^{-6}$/s) and the sensitization temperature (>450°C) for the
occurence of intergranular cracking.

Testing in simulated coal gasification environments, Table
2, was carried out at two test temperatures, one below the
nominal sensitization range (450°C) and one within this range
(600°C). A strain rate of $10^{-6}$/s was chosen, based on the
preceding tests. The tensile data are shown in Fig. 13. None of
the specimens failed by intergranular cracking when tested at
450°C(840°F) in any of the three environments (ultra-pure helium,
oxidizing/sulfidizing, or oxidizing/sulfidizing/carburizing).
Photomicrographs of the fractured specimens, scanning electron
micrographs of the fracture surfaces, and photomicrographs of the
sectioned specimens tested in the three environments are shown in
Figs. 14-16. These photographs show the ductile fracture and the
partially sensitized grain boundaries. The variation in the
measurements of the mechanical properties in each case are within
measurement error. When tested at 600°C(1100°F), a large amount
of intergranular cracking occurred in the three environments as
revealed in Figs. 17-19. The oxidizing/sulfidizing environment
seemed to produce the largest reductions in mechanical
properties, Fig. 13.

As a precaution against the possibility that the Type 310
material may be from a bad lot, or harbored some pecularities,
another lot of Type 310 Steel (RA 310) was tested in ultra-pure
He at 600°C(1100°F) at a strain rate of $10^{-6}$/s. The composition
of RA 310 is shown in Table 1. The RA 310 failed in the same
manner as the Type 310 SS, that is, with considerable amounts of
intergranular cracking. The UTS, elongation, and RA for both
lots tested in ultra-pure-He at 600°C(1100°F) are as follows:

|  | Type 310 | RA310 |
|---|---|---|
| UTS | 368 MPa(53,400psi) | 337 MPa(48,800psi) |
| Elongation | 19.9% | 19.2% |
| RA | 28.8% | 23.6% |

Type 310S:  The C content of this alloy was slightly lower than in Type 310, Table 1, and, if sensitization were important, this alloy should therefore be less susceptibile to intergranular cracking.  Initial tests were conducted in wet $H_2S$ at 540°C(1000°F).  In contrast to Type 310, no intergranular cracking was observed over the range of strain rates from $10^{-4}$ to $10^{-7}$/s.  There was a reduction in the magnitude of elongation and RA at the strain rates of $10^{-6}$/s and $10^{-7}$/s, but these did not reach the low levels found in the Type 310, Table 4, Fig. 20.

Type 310S specimens tested in He and "house" vacuum (726mm Hg) at 540°C(1000°F) at a strain rate of $10^{-6}$/s exhibited elongation and RA values twice as great as were seen for Type 310 tested under the same conditions, see Fig. 20.  However, numerous intergranular cracks were present in the Type 310S specimens. Clearly, the lower C content does not eliminate intergranular cracks.  The reason for the absence of such cracks in the wet $H_2S$ is not known, though it may be speculated that the scale formed in this environment protects the specimens from damaging environmental interaction.  It should also be noted that creep resistance of materials has been reported to be greater in air than in He and vacuum [3,4]; this will be discussed further below.

Further testing was done in the simulated coal gasification environments.  Test tempeatures of 450(840°F) and 600°C(1100°F), and a strain rate of $10^{-6}$/s were used for direct comparision with Type 310.  The stress-strain data are shown in Fig. 21.  The higher values of the tensile parameters at 450°C(840°F) are presumably due to the fact that no significant intergranular cracking occurred at 450°C(840°F), Figs. 22-24, whereas this form of cracking was prevalent at 600°C(1100°F), Figs. 25-27.  It can be concluded that the lower C content in Type 310S does not impart significantly greater resistance to intergranular cracking in coal-gasification environments.

Type 347:  This alloy was tested because it is stabilized with Nb and Ta, Table 1, to resist sensitization.  Specimens were initially tested in wet $H_2S$ at 540°C(1000°F) over a range of strain rates from $10^{-4}$ to $10^{-7}$/s.  The results are tabulated in Table 5 and shown graphically in Fig. 28.  The elongation was low compared with those for Type 310 and Type 310S, cf.  Tables 3-5, but the UTS and RA were comparable to the other alloys.  More importantly, the tensile properties of Type 347 specimens were not strongly sensitive to strain rate, Fig. 28, and this was consistent with the finding that no intergranular cracking occurred at any of the strain rates.  Further specimens were tested at 540°C(1000°F) in He, and house vacuum (723 mm Hg).  No intergranular cracking was detected over the range of strain rates of 5 x $10^{-5}$ to 8.4 x $10^{-7}$/s, and the mechanical properties were not significantly different from those in wet $H_2S$, see Fig.

28 for He.

Tests were carried out at 450°C(840°F) and 600°C(1100°F) in ultra-pure He and in the simulated coal gasification atmospheres, i.e., oxidizing/sulfidizing and oxidizing/sulfidizing/carburizing, using a strain rate of $10^{-6}$/s. The resulting stress-strain curves are shown in Fig. 29. No intergranular cracking was observed at 450°C(840°F) in either environment, Figs. 30-32. The UTS values were higher at 450°C(840°C) than at 540°C(1000°F). Elongation was still relatively low (17-19%), while RA was high (60-66%) due to necking. In some of the first tested specimens, tool marks were present on the reduced area, but these did not seem to act as stress-raisers. Subsequent specimens were polished to remove the tool marks. At 600°C(1100°F), the tensile properties were lower than at 450°C(840°C) in all of the test environments, Fig. 29. Small surface cracks were detected in the necked regions next to the fracture surface in specimens tested in He, Fig. 33, and in the oxidizing/sulfidizing/carburizing environment, Fig. 34, but no cracks were visible in the case of the oxidizing/sulfidizing case, Fig. 35. The cracks were shallow and were confined to the necked region, and there was no significant difference in mechanical properties for the three environments, Figs. 29 and 33-35. It is not clear whether the cracks shown in Figs. 33 and 34 are the same type as the intergranular cracks in the other alloys. However, it is clear that the stabilized alloy is far less susceptibile to this form of cracking. Thus the absence of sensitization may be beneficial with respect to intergranular cracking.

Type 309: Limited tests were carried out on this alloy, which is similar in composition to Type 310 except for its lower Ni and Cr contents and higher Si content, Table 1. The Type 309 specimens were tested at 600°C(1100°F), in various environments and at several strain rates and the results were compared to those for Type 310 tested under similar conditions. Stress-strain curves for both alloys tested at a strain rate of $10^{-6}$/s in He are shown in Fig. 36. The ductility of Type 309 is far greater, see also Table 6, and this correlates with the small amount of surface cracking observed in this alloy, Fig. 37, compared to that in Type 310, Fig. 17. The cracking in Type 309 is shallow and is confined to the necked region; no well defined rim of intergranular fracture could be detected at the main fracture, in contrast to the case of Type 310. Similar shallow secondary cracking was observed in tests on Type 309 specimens at 600°C(1100°F) in Ar and the oxidizing/sulfidizing/ carburizing atmosphere; the tensile parameters for these atmospheres are given in Table 6.

The microstructure of the Type 309 steel was found to contain ferrite, in which carbides were precipitated during testing at 600°C(1100°F), Fig. 38. There was no evidence for the formation of sigma phase, which is known to be formed from ferrite during long times at high temperatures. The presence of the ferrite may account for the greater resistance of Type 309 to intergranular cracking in our tests, but its specific role was not determined.

- 8 -

## Ferritic Stainless Steel

Tests were carried out on Type 446 steel, selected because of its resistance to corrosion and oxidation at high temperatures. Tests were carried out at 450°C(840°F) and 600°C(1100°F) in ultra-pure tank He and in the simulated coal gasification environments, i.e., oxidizing/sulfidizing and oxidizing/sulfidizing/carburizing, using a strain rate of $10^{-6}$/s. The resulting stress-strain curves are shown in Fig. 39. The data for 450°C(840°F) were not significantly different for the three environments, despite the fact that shallow surface cracks were visible within the necked region of specimens tested in the coal gasification environments, Figs. 41 and 42, but not in the He test, Fig. 40. The nature of the shallow cracks, i.e., interor transgranular, was not determined. At 600°C(1100°F), UTS values were significantly lower than at 450°C(840°F) in all test environments, and the elongation and RA were higher, Figs. 39 and 43-45. The mechanical properties can be seen to be significantly lower for the coal gasification environments compared to the specimen tested in He. Surface cracking was visible in the necked region in the three environments, Figs. 43-45, but the morphology was different in the coal gasification cases, the cracks adopting a mosaic pattern. Despite the apparent environmental effect, the overall failure was ductile in each case, as evidenced by the large values of elongation and RA. Moreover, the question of whether environmental reactions occur at this temperature is academic, since it is clear from a comparison of the UTS values at 450°C(840°F) and 600°C(1100°F) that the latter is above the temperature at which this alloy should be used under stress.

## Nickel Base Alloys

Incoloy 800: Specimens were initially tested at 540°C(1000°F) in the wet $H_2S$ environment over a range of strain rates from $10^{-4}$ to $10^{-7}$/s. However, severe scaling occurred in this environment, drastically reducing the cross-section, Fig. 46, so that the tensile data had no meaning. It is clear that the alloy cannot be used in this environment at elevated temperatures.

Further testing was carried out in the simulated coal gasification environments and in ultra-pure He at 450°C(840°F) and 600°C(1100°F) at a strain rate of $10^{-6}$/s. The stress-strain curves, Fig. 47, indicate that the properties were markedly affected by both the oxidizing/sulfidizing and oxidizing/sulfidizing/carburizing atmospheres. However, no secondary cracking was observed at 450°C(1100°F) in any of the three environments, and the values of RA were essentially the same, Figs. 48-50. At 600°C(1100°F), secondary cracks were found in the regions of the fracture in each environment, but were more shallow in the case of He, Figs. 51-53.

Inconel 617: This alloy was tested since it has found some use as a weld overlay in coal gasification pilot plants. Tests were confined to 450°C(840°F) and 600°C(1100°F) in the simulated coal gasification environments and ultra-pure He, using a strain rate of 10-6/s. The stress-strain curves were almost coincident for all three environments at each temperature, Fig. 54. However, shallow secondary cracks were visible near the primary fractures in both coal gasification atmospheres at 450°C(840°F), but not in the case of He, Figs. 55-57. The primary fractures were ductile in character in each case, but involved less necking than in other alloys tested; this is evident from the relatively low values of RA, Figs. 55-57. At 600°C(1100°F), the strengths and ductilities were considerably reduced, Fig. 54, and this was associated with the presence of α-chromium in each case, Figs. 58(c), 59(c) and 60(c). Studies of sections of the fractured specimens indicated that numerous secondary cracks, many of which were internal, occurred within the α-chromium or at the interface between this phase and the matrix. The amount of α-chromium was found to decrease with increasing distance from the primary fracture, Fig. 61, and thus it seems that the formation of this phase is assisted by strain. It is concluded that the poor mechanical properties of the alloy at 600°C(1100°F) are due to the presence of the α-chromium phase, which was both temperature- and strain-induced. Because of the internal nature of the cracking in many instances, it appears unlikely that the presence of the environments had any influence on the formation or fracture of this embrittling phase.

## COMPARISON OF RESULTS OBTAINED FROM THE SSRT WITH IN-PLANT EXPERIENCE*

The present results for the main environment/temperature combinations are summarized in Table 7. Embrittlement is identified by the occurrence of secondary cracking (SC); this was intergranular in the case of Type 310 specimens but was not characterized in some of the other materials. The results indicate that Type 310 steels undergo embrittlement at 540°C(1000°F) and 600°C in various gaseous media. Several in-plant failures are consistent with these findings. A Type 310 gasifier probe in the Consol plant was reported to fail by stress-enhanced intergranular corrosion [5]. Tests showed the sensitization of the steel when operated between 425 - 875°C (800 - 1600°F), which was thought to significantly reduce the corrosion resistance of the grain boundaries. A Type 310 $N_2$ purge line from the Hygas plant failed by brittle fracture due to grain boundary embrittlement and S corrosion when operated at 760 - 875°C (1400 - 1600°F)[6]. A Type 310 welded tube (inlet line to regeneration) in the $CO_2$ Acceptor plant failed [7],

---

*Information on our plant performance was obtained from the NBS Failure Prevention Information Center. The identification number of each report is given in the References so that they may be obtained from the Center.

Corrosion due to S was the fundamental cause of failure but was accentuated by the stress and strains from the fluidized bed and thermal cycling which was the immediate cause of failure . A cracking failure was reported in a Type 310 nozzle plate in the Westinghouse multi-stage coal gasification system [8]. Cracking was due to high thermal stresses set up during thermal cycling. The cracking progressed along massive carbide precipitates along grain broundaries. The synthesis gas environment could have been oxidizing or reducing at 980 - 1300°C(1800 - 2400°F). Failure of a Type 310 air distributor plate from an atmospheric fluidized bed combustor resulted from embrittlement due to sigma phase formation along with intergranular carbide precipitates [9]. Plant exposure of the plates resulted in a decrease in ductility at elevated temperatures, especially at 840°C(1550°F). Other plant reports have indicated that no failures have occurred with Type 310 when used at temperatures of 350 - 470°C(660 - 875°F) even at pressures up to 17 MPa(2500 psi).

Type 347 steel was seen to perform significantly better than Type 310 in the SSRT, and again this is consistent with pilot-plant experience. Thus, no evidence of cracking was found in the initial examination of Type 347 top closure flanges or inlet nozzles to the dissolver vessel in the Solvent Refined Coal plant operated at 525°C(975°F) at a pressure of 21 MPa(3000 psi) [10]. However, subsequent examination of the Type 347 cover plate on the SRC dissolver vessel revealed cracks that were very shallow and exhibited a pattern suggestive of a partially intergranular failure mode [11]. Thermal cycling during welding and residual stresses were expected in the cracked regions, and it was speculated that these effects contributed to this cracking. Four cracked ares were detected on the top surface of the Type 347 flange between the gasket grove and inner wall of the dissolver vessel. All appeared to be relatively shallow. From the location and appearance of the cracks, it was speculated that these occurred at regions that were mechanically damaged or perhaps repair welded.

Some secondary cracking was observed in our tests of the ferritic steel at both 450°C(840°F) and 600°C(1100°F), but it was clear that the latter is above the normal operating range for this material. An in-plant failure report also revealed the same results [12]. Two Type 446 thermowells failed in the Battelle's Agglomerating-Burner Process Development Unit and it was recommended that lower temperatures be used.

Incoloy 800 was seen to undergo embrittlement in the 600°C(1100°F) tests. There have been numerous in-plant service failures in this material. Fourteen cracking failures of schedule 40 Incoloy 800 pipe have occurred in the Westinghouse gasification PDU at temperatures of 315°C(600°F) [13]. These failures were closed to welds, but not necessarily in the weld metal or HAZ. Evidence indicates that the failures resulted from intergranular SCC. The material was heavily sensitized. The corroding agent was not identified. An Incoloy 800 nozzle reducer cracked and failed in the Synthane plant [14]. The operating environment was aqueous condensate at 205°C(400°F) and pressure of 4 MPa(600 psi). The crack appeared to have occurred

in the HAZ.  Failure was due to intergranular SCC of the sensitized
material, and caused a 5-week shutdown of the plant.  An Incoloy 800
pipe union developed a 360° circumferential crack in the central pipe
weld on the cyclone (C119) of the Westinghouse system [15].
Environmental conditions were product gas at 925 - 1035°C(1700-1900°F)
at a pressure of 1.5 MPa(200 psi).  Cracking was reported to be due to
SCC.  Cracking was observed in a schedule 40 Incoloy 800 pipe which
was part of a line in the second stage gasifier reactor in the Hygas
pilot plant [16].  The pipe transported char and gas at 815°C(750°F).
Fracture occurred immediately adjacent to a welded flange.  It was
noted that the cracking mode changed with increasing depth from
intergranular at the surface to transgranular at the crack tip.  It
was speculated that the change in crack mode might be due to an
increase in the effective stress as crack depth increases, chemical
effects at the surface, or chemical changes at the crack tip.  The
laboratory tests suggested that Incoloy 800 is an useful material at
400°C.  An in-plant service report bears this out.  An Incoloy 800
preheater coil in the Hygas plant has operated for 3820 h of coal
processing at a maximum temperature of 400°C(750°F) at a pressure of
17 MPa(2500 psi) [17].

The tests on Inconel 671 indicated that degradation of
mechanical properties resulted from the formation of the $\alpha$-chromium
phase at 600°C.  This is in essential agreement with the
recommmendation that in-plant use be restricted to cladding material
and not for structural purposes.  The alloy has been found to be a
good material for high temperature corrosion resistance, but the
elevated temperature mechanical properties are poor and cannot be
recommended for components subject to directional stresses [18].

GENERAL DISCUSSION AND CONCLUSIONS

The present results clearly demonstrate the usefulness of the
SSRT as a method of evaluating the performance of materials in gaseous
environments at elevated temperatures.  This is seen in the strong
correlation between the test data and in-plant experience, discussed
in the preceding section.  The results of Type 310 steel tested at
540°C(1000°F) in the $H_2S/H_2O$ environment show a reduction in
mechanical properties as the strain rate decreased from $10^{-4}$/s to
$10^{-5}$/s and below, Table 3 and Fig. 5; it was seen in the
Introduction that such a reduction is indicative of the operation of
an embrittling process.  The reduction in properties in the case of
Type 310 specimens was seen to be associated with the occurrence of
secondary intergranular cracking, and this was taken as an indication
of embrittlement in subsequent tests on this and other alloys.  It
should be noted that, while the RA exhibited a decrease with
decreasing strain rate, it did not show the increase at lower strain
rates commonly observed in the case of SCC in aqueous media, Fig. 1.
Thus, there does not appear to be an analogous effect to the
repassivation which occurs in aqueous environments.

The mechanism of the intergranular fracture observed in Type 310
steel and in certain of the other alloys was not determined.  In
particular, it was not established whether the failure was due to
creep or to some environmentally-induced fracture process.  For the
austenitic materials, temperatures of 540°C(1000°F) and above are in

the range where creep can occur [19]. To pursue this possibility, it would be necessary to carry out tests under constant load in inert environments (see below) as well as under the same environmental/temperature conditions used in the SSR tests. A number of environmentally-induced fracture processes could be proposed to account for the intergranular fractures. For example, it has been suggested that such failures can be produced by an oxide-rupture mechanism [20], similar to that advocated for certain aqueous stress-corrosion systems [21,22]. Alternatively, it could be speculated that embrittlement resulted from the penetration of grain boundaries by oxygen; or, in the S-bearing environment, by the formation of brittle sulfide compounds [23]. The present results do not permit us to distinguish between these possibilities, and it is clear that further work is necessary in this area.

A major uncertainity in the present work concerns the influence of the environments. This arises because of the absence of baseline data for inert environments -- it was seen that thin oxide layers were produced by each nominally inert medium such as He and Ar. As indicated in the text, it would be necessary to construct a test chamber capable of maintaining a hard vacuum ($\sim 10^{-9}$ torr) to resolve this question. Another parameter which was not evaluated is the influence of initial grain size. It was seen in Fig. 2 that significant variation existed between the different alloys, but no attempt was made to investigate the effect of this variation on mechanical behavior.

Comparison of the results for Type 310 and the stabilized austenitic steel, Type 347, indicates that sensitization has a detrimental effect on the high-temperature mechanical properties. Such an effect would be expected if the intergranular failures resulted from creep, since sensitization is known to adversely affect the creep resistance of austenitic stainless steels [19]. It could also be rationalized in terms of a stress-corrosion mechanism, since the chromium-depleted regions at the grain boundaries in sensitized material would be expected to be preferentially oxidized.

In summary, the SSRT has been shown to be a useful method for evaluating the performance of structural materials under conditions simulating those in coal-gasification plants. The mechanism(s) of the embrittlement phenomena encountered during the tests was not determined, and this serves to emphasize the need for further work in this important area.

## ACKNOWLEDGEMENTS

## PULICATIONS

Ugiansky, G. M. and Johnson, C. E., "Slow Strain-Rate Stress Corrosion Testing of Metals in Gaseous Atmospheres at Elevated Temperatures", Stress Corrosion Cracking-The Slow Strain-Rate Technique, ASTM, STP 665, G. M. Ugiansky and J. H. Payer, Eds., American Society for Testing and Materials, pp. 113-131, (1979).

Ugiansky, G. M. and Johnson, C. E., "Stress Corrosion Testing at Elevated Temperatures in Simulated Coal Conversion Gases", Proceedings of 7th International Congress on Metallic Corrosion, Vol. II, ABRACO, Rio de Janiero, pp. 915-924, (1979).

## TALKS

"Constant Strain-Rate Stress Corrosion Testing for Coal Gasification Systems", Workshop on Materials Technology for Coal Gasification (Gaithersburg, Maryland: National Bureau of Standards, September, 1975).

"Constant Strain-Rate Stress Corrosion Testing", ASM-AIME Joint National Meeting, 1975 Materials Science Seminar (Cincinnati, Ohio: November, 1975). (Invited).

"Constant Strain Rate Stress Corrosion Testing for Coal Gasification Systems", NACE Annual Meeting (Houston, Texas: March, 1976).

"Constant Strain Rate Stress Corrosion Testing of Metals at Elevated Temperatures", Mechanical Failures Prevention Group Symposium on Prevention of Failures in Coal Gasification Systems (Columbus, Ohio: April, 1976).

"Constant Strain Rate Stress Corrosion Testing at Elevated Temperatures", General Electric Co., Research and Development Center Staff Seminar (Schenectady, NY: February: 1977). (Invited).

"Constant Strain Rate Stress Corrosion Testing of Metals in Gaseous Environments at Elevated Temperatures", ASTM/NACE Symposium on Stress Corrosion Cracking - The Constant Strain Rate Technique (Toronto, Ontario: May 1977).

"Slow Strain Rate Stress Corrosion Testing in Coal Gasifier Environments", First International Conference on Materials for Coal Conversion and Utilization (NBS, Gaithersburg, Maryland: October, 1977).

"Stress Corrosion Testing at Elevated Temperatures in Simulated Coal Conversion Gases", 7th International Congress on Metallic Corrosion, (Rio de Janeiro, Brazil:  October, 1978).

## REFERENCES

[1]     Stress Corrosion Cracking - The Slow Strain Rate Technique,
        Ugiansky, G. M., and Payer, J. H., editors, ASTM STP 665, 1979.


[2]     Hill, V., Corrosion-Erosion Study of Materials for the
        Gasification of Coal, IITRI Reports to Metal Properties
        Council under DOE Contract Number EX-76-C-01-1784.


[3]     Shepard, O. C., and Schalliol, W., Symposium on Corrosion of
        Materials at Elevated Temperatures, ASTM STP 108, April 1951.


[4]     Hosoi, Y., and Abe, S., Met. Trans. A., 6A, 1975, p. 1171.

[5]     Leterle, J. F., Continental Oil Co. Technical Service Report,
        No. 116-74-1301, May 13, 1974; National Bureau of Standards -
        Failure Prevention Information Center Identification Number 98.


[6]     Danyluk, S., Argonne National Laboratory Service Failure
        Report, Dec. 22, 1976; NBS-Failure Prevention Information
        Center Identification Number 255.


[7]     Schulz, C. A., Conoco Materials and Component Failure Report,
        No. 75-8, Aug. 8, 1975; NBS-Failure Prevention Information
        Center Identification Number 144.


[8]     Albertin, L., et al., Westinghouse Technical Document Summary,
        No. 75-8D9-PDUOP-P1, Nov. 25, 1975; NBS-Failure Prevention
        Information Center Identification Number 191.


[9]     King, R. T., et al., Oak Ridge National Laboratory Report
        ORNL/TM-6444, Feb. 1979; NBS-Failure Prevention Information
        Center Identification Number 609.


[10]    King, R. T., et al., ORNL Intralaboratory Correspondence, May
        4, 1977; NBS-Failure Prevention Information Center
        Identification Number 397.


[11]    King, R. T., et al., ORNL Failure Analyses Reports, Oct-Nov.
        1977; NBS-Failure Prevention Information Center Identification
        Numbers 471 and 491.


[12]    Danyluk, S. and Dragel, G. M., Component Performance and
        Failure Analysis, Argonne National Laboratory, April-June,
        1977, ANL-77-62.

[13]    NBS-Failure Prevention Information Center Identification
        Number 409.

[14]    Greene, B. N., C. E. Lummus Summary to DOE Newsletter on
        Materials and Components in Fossil Energy Applications, Dec.
        5, 1977; NBS-Failure Prevention Informaion Center
        Identification Number 493.

[15]    Vandergrift, E., Westinghouse Failure Report to DOE, July 6,
        1977; NBS-Failure Prevention Information Center Identification
        Number 455.

[16]    Danyluk, S. and Dragel, G. M., Argonne National Laboratory
        Report, ANL-78-6, July-Dec 1977.

[17]    Barney, W. G., University of North Dakota, Letter to DOE
        Newsletter on Materials and Components in Fossil Energy
        Applications, May 31, 1978.

[18]    MacNab, A., Letter to Institute of Gas Technology, April 2,
        1975; NBS-Failure Prevention Information Center Identification
        Number 1.

[19]    Metals handbook, Vol. 10, Failure Analysis and Prevention, p.
        249, eighth edition, 1975.

[20]    Bleakney, H. H., Can. Met. Quart., Vol. 4, p. 13, 1965.

[21]    Forty, A. J. and Humble, P., Phil. Mag., Vol. 8, p. 247, 1963.

[22]    McEvily, Jr., A. J. and Bond, A. P., J. Electrochem. Soc.,
        Vol. 112, p. 131, 1965.

[23]    Floreen, S. and Kane, R. H., Met Trans. A, Vol. 10A, p. 1745,
        Nov. 1979.

## Appendix A

Qualitative microprobe analysis was made on the duplex corrosion products in the cracks on the profile of a Type 310 specimen that was tested in $H_2S$ plus steam at 540 °C (1000 °F) at a strain rate of $10^{-6}$/s. Figure A-1 shows the fracture surface and outside surface (a), the etched cross-section (b), and the cracks in the unetched profile (c). The corrosion products appear as two layers on the surface and in the cracks. The qualitative microprobe analysis was made on the largest crack seen in Fig. A-1c. The area of the crack was studied with a lithium-drifted silicon Si(Li), detector. This area is seen in the accompanying target current (TC) image (Fig. A-2a). The numbered regions in the TC image correspond to the numbers on the attached energy dispersive spectra (Figs. A-3 and A-4). Spectrum #1 (Fig. A-3) of the dark area in the crack shows mostly sulfur with some Cr, Mn, Fe, and Ni. These latter four elements are constituents of the matrix as seen in spectrum #2 (Fig. A-4). A small Si peak is usually expected in the energy spectra, and is an artifact of the Si(Li) detector. In this case, a Si peak is also expected from the matrix as 0.5 percent Si is present in the steel. The microprobe analysis was unable to determine whether the Si peak is the artifact or is, in fact, present in the matrix.

An x-ray scan of sulfur (Fig. A-2b) shows the distribution of this element throughout the crack and along the exterior edge of the sample. An x-ray scan of oxygen (Fig. A-2c) shows that this element is found mostly along the interior edge of the crack as well as along the surface of the sample.

The microprobe analysis has revealed that the duplex corrosion products on the surface of the specimen and in the cracks are mixed oxides and sulfides with the lighter colored corrosion product next to the bulk metal, rich in oxygen.
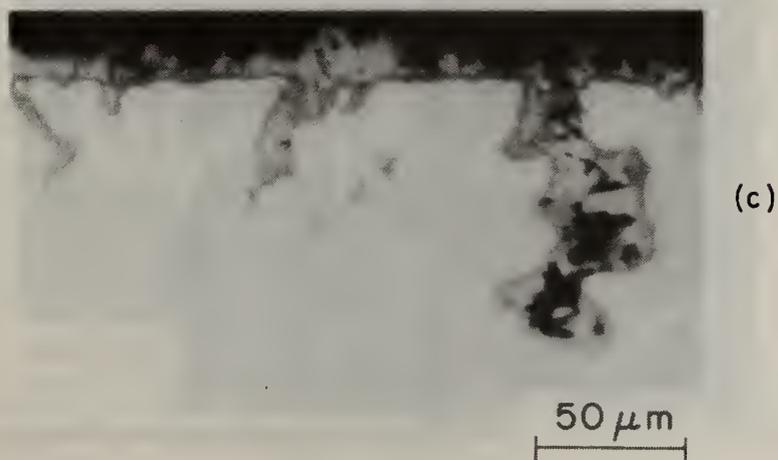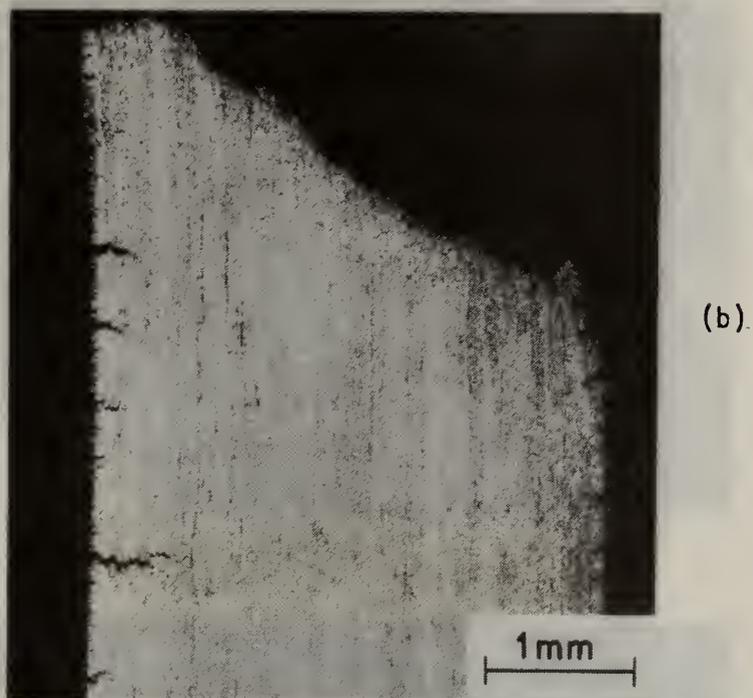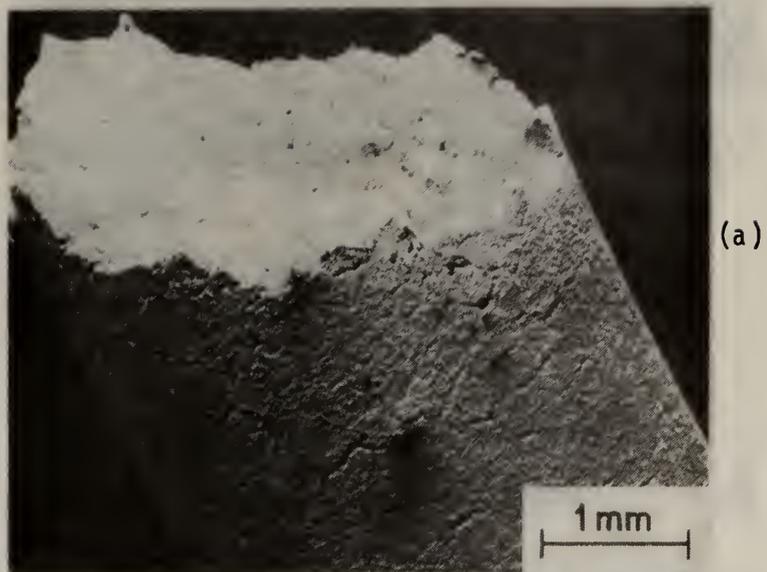
Fig. A-1. Type 310 specimen tested at 540 °C (1000 °F) at a strain rate
of $10^{-6}$/s in $H_2S$ plus steam. (a) SEM of specimen at region
of fracture. (b) Photomicrograph of etched cross-section
near fracture. (c) Photomicrograph of cracks in the unetched
profile.
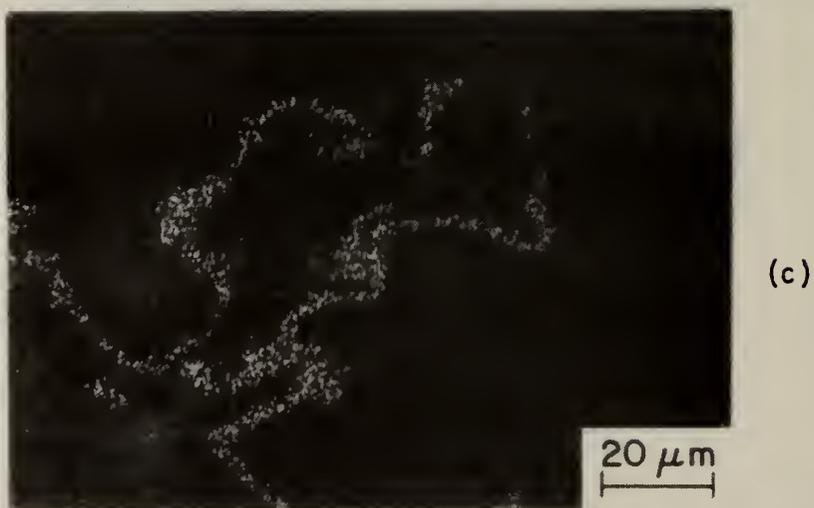
Fig. A-2. (a) Area of target current image for microprobe analysis.
(b) X-ray scan of crack showing sulfur distribution.
(c) X-ray scan of crack showing oxygen distribution.
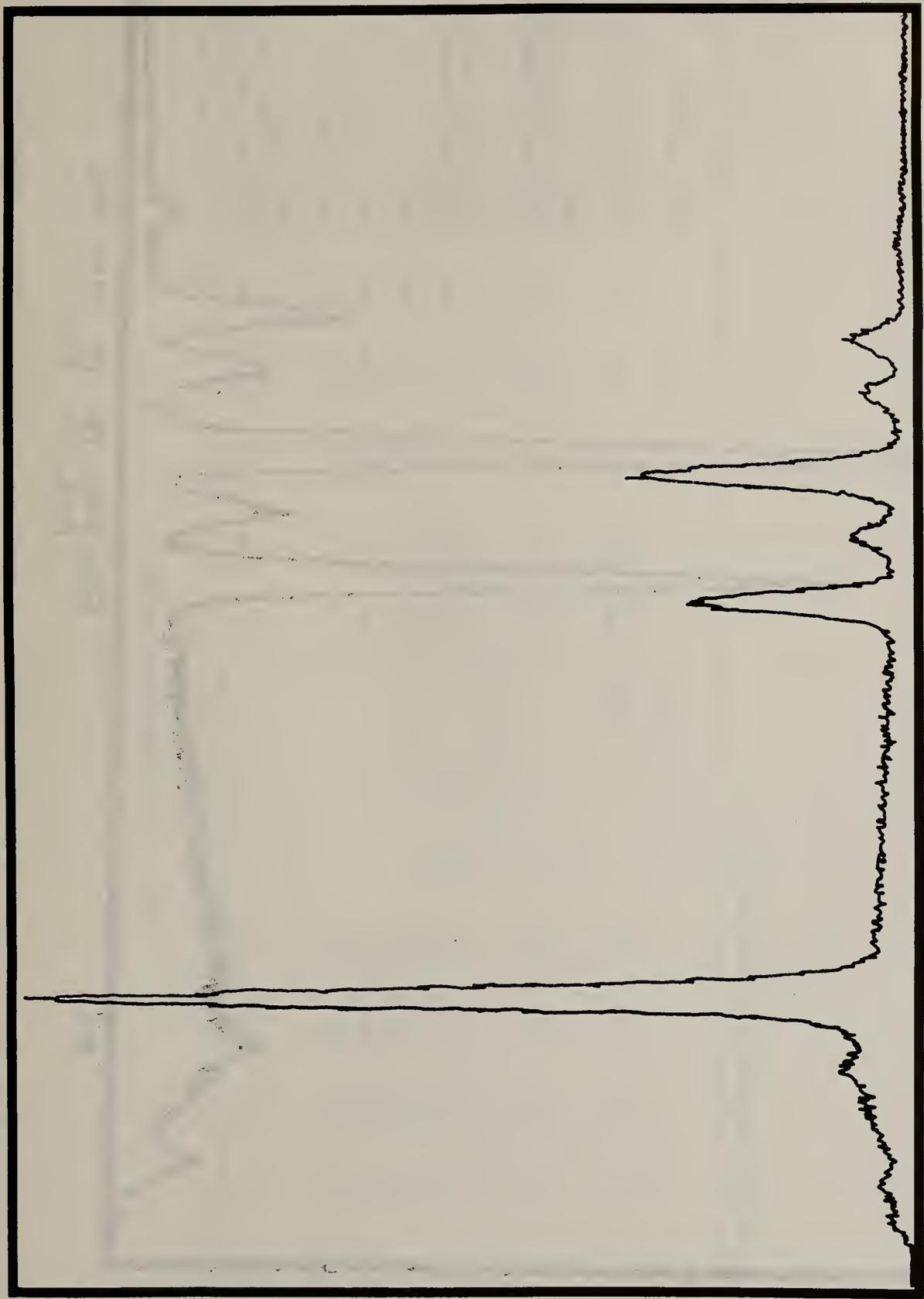
SiK  SK                    CrKα CrKβ Fe  Fe  NiKα
                                MnKα Kα  Kβ

Fig. A-3.  Microprobe analysis spectrum of the dark area within the crack.  Area #1
from Fig. A-2a.
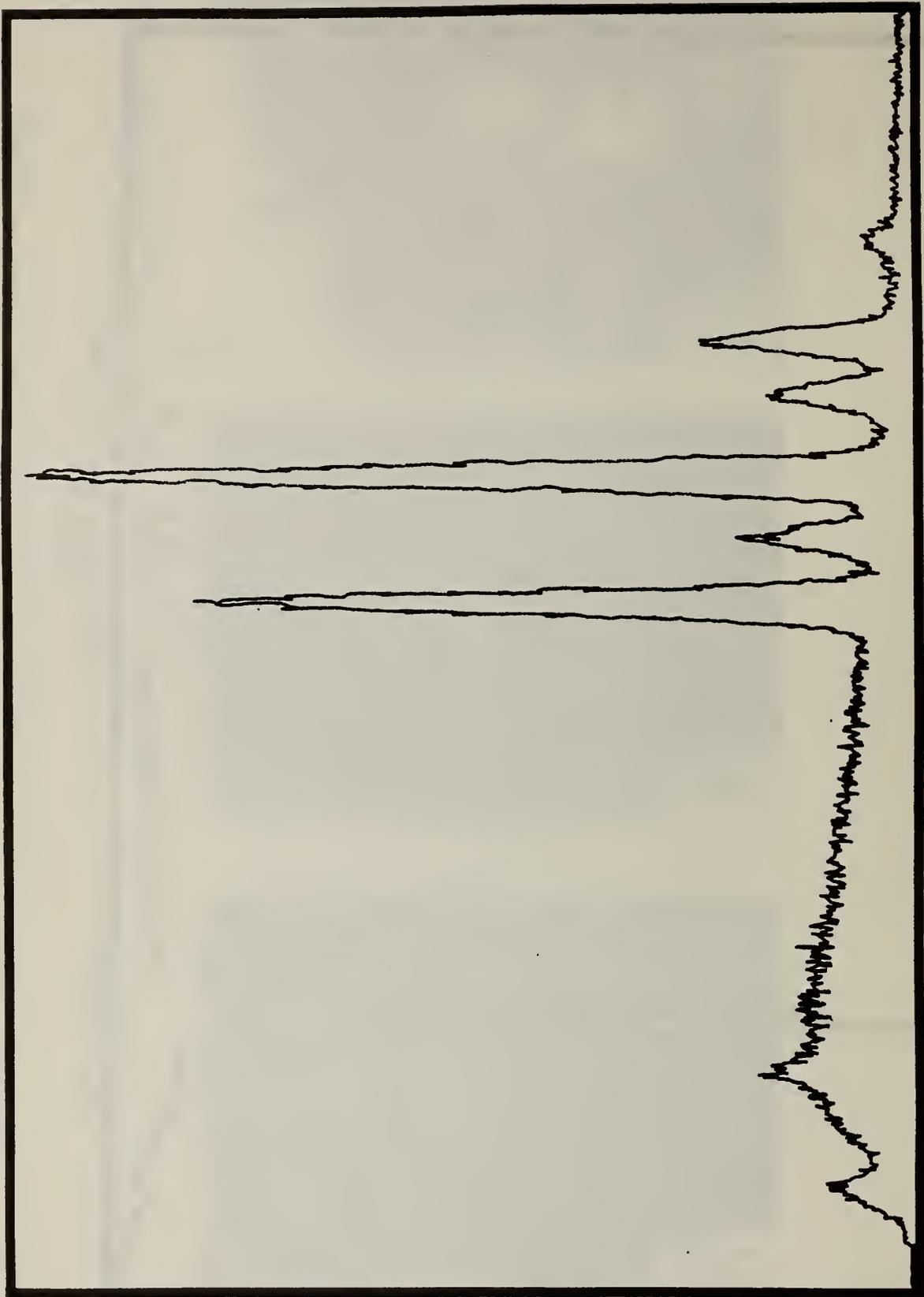
Fig. A-4. Microprobe analysis spectrum of the Type 310 specimen matrix. Area #2 from Fig. A-2a.

Table 1. Alloy Compositions, Weight %

| Alloy | C | Mn | Si | S | P | Nb | Ta | Ti | Cu | Mo | Ni | Cr | Fe | Heat Treatment |
|---|---|---|---|---|---|---|---|---|---|---|---|---|---|---|
| Type 309 | 0.07 | 1.74 | 0.70 | 0.013 | 0.018 | | | | 0.07 | 0.08 | 13.22 | 22.96 | Bal | Cold drawn, Annealed 1040-1150 °C, water quench, pickled ($HNO_3$ - HF) |
| Type 310 | 0.08 | 1.78 | 0.48 | 0.02 | 0.028 | | | | 0.17 | 0.10 | 19.59 | 24.84 | Bal | Same as Type 309 SS |
| RA 310 | 0.05 | 1.81 | 0.62 | 0.009 | 0.010 | | | | 0.06 | 0.02 | 20.02 | 24.62 | Bal | Same as Type 309 SS |
| Type 310S | 0.06 | 1.68 | 0.72 | 0.011 | 0.017 | | | | 0.14 | 0.11 | 19.60 | 24.67 | Bal | Same as Type 309 SS |
| Type 347 | 0.06 | 1.45 | 0.69 | 0.01 | 0.024 | .64 | .02 | | 0.28 | 0.43 | 9.49 | 18.21 | Bal | Cold drawn, Annealed 980-1090 °C, water quench, pickled ($HNO_3$ - HF) |
| Type 446 | 0.11 | 0.52 | 0.47 | <0.005 | 0.035 | | | | 0.03 | 0.13 | 0.59 | 25.77 | Bal | Cold drawn, Annealed 790-870 °C, water quench, pickled ($HNO_3$ - HF) |
| Incoloy 800 | 0.04 | 0.93 | 0.29 | 0.01 | 0.005 | | | 0.38 | 0.54 | 0.08 | 32.51 | 20.02 | Bal | Cold drawn, Solution annealed 980-1040 °C, pickled |
| Inconel 671 | 0.06 | | | | | | | 0.30 | | | 50.27 | 46.74 | | Cold drawn, Solution annealed 1150 °C, Pickled |

(*) From quantitative analyses performed by Chicago Spectro.

Table 2. Gas Compositions[1]

| | Oxidizing/Sulfidizing Gas[2] | | | Oxidizing/Sulfidizing/Carburizing Gas[3] | | |
|---|---|---|---|---|---|---|
| | INPUT | EQUILIBRIUM | | INPUT | EQUILIBRIUM | |
| | 1atm, 25 °C | 1atm, 450 °C | 1atm, 600 °C | 1atm, 25 °C | 1atm, 450 °C | 1atm, 600 °C |
| CO | 11.6 | 1.2 | 9.2 | 26.0 | 1.1 | 12.5 |
| $CO_2$ | 15.4 | 24.9 | 20.6 | 14.8 | 22.0 | 20.0 |
| $H_2$ | 13.0 | 16.0 | 36.3 | 26.0 | 12.8 | 32.7 |
| $CH_4$ | 10.0 | 12.5 | 2.9 | 10.0 | 11.2 | 5.5 |
| $H_2S$ | 1.0 | 1.0 | 0.9 | 1.0 | 1.0 | 0.9 |
| $H_2O$ | 49.0 | 44.4 | 30.3 | 22.2 | 34.3 | 19.4 |
| C | -- | -- | -- | -- | 17.6 | 9.0 |
| $\log P_{O_2}$ | | -28.995 | -23.919 | | -29.026 | -24.216 |
| $\log P_{S_2}$ | | -10.260 | -8.878 | | -10.086 | -8.751 |
| $\log a_c$ | | -0.043 | -0.288 | | +0.017 | +0.038 |

[1] The above gas mixtures are two of twelve mixtures being used at Battelle Columbus Laboratories and Argonne National Laboratory.

[2] This mixture corresponds to Battelle's "Gas Mixture 1A".

[3] This mixture corresponds to Battelle's "Gas Mixture 3A".

Note: The major difference between the two mixtures is the deposition of carbon from the oxidizing/sulfidizing/carburizing gas at both temperatures, the oxidizing and sulfidizing potentials being similar at each temperature.

Table 3. Properties of 310 stainless steel tested
in wet $H_2S$[1] and $H_2O/H_2S$[2] at 540 °C(1000 °F).

| Strain Rate, s$^{-1}$ | | Gas | UTS, KSI, MPa | | Elongation, % | Reduction in Area, % |
|---|---|---|---|---|---|---|
| 1.3 | $10^{-4}$ | 2 | 82 | 566 | 33.8 | 63.2 |
| 7.8 | $10^{-5}$ | 1 | 73 | 504 | 32.9 | 55.9 |
| 5.5 | $10^{-5}$ | 2 | 76 | 524 | 33.4 | 62.8 |
| 7.2 | $10^{-6}$ | 2 | 68.5 | 473 | 22.5 | 33.1 |
| 3.9 | $10^{-6}$ | 1 | 70 | 483 | 22.9 | 25.4 |
| 3.6 | $10^{-6}$ | 2 | 69 | 476 | 23.7 | 30.2 |
| 1.1 | $10^{-6}$ | 1 | 68 | 469 | 17.2 | 18.4 |
| 8.4 | $10^{-7}$ | 2 | 68 | 469 | 18.7 | 17.5 |
| 1.9 | $10^{-7}$ | 1 | -- | -- | 9.0 | 14.4 |

[1]Wet $H_2S$ = $H_2S$ saturated with water vapor at room temperature.

[2]$H_2O/H_2S$ = $H_2S$ plus steam.


Table 4. Properties of 310 S stainless steel tested
in wet $H_2S$ at 540 °C(1000 °F).

| Strain Rate, s$^{-1}$ | | UTS, KSI, MPa | | Elongation, % | Reduction in Area, % |
|---|---|---|---|---|---|
| 1.3 | $10^{-4}$ | 71.5 | 493 | 33.6 | 63.0 |
| 3.7 | $10^{-5}$ | 71.6 | 494 | 34.5 | 62.6 |
| 7.3 | $10^{-6}$ | 69.0 | 476 | 35.9 | 62.3 |
| 8.4 | $10^{-7}$ | 63.1 | 435 | 34.8 | 50.1 |
| 1.2 | $10^{-7}$ | -- | -- | 27.0 | 36.5 |


Table 5. Properties of 347 stainless steel tested
in wet $H_2S$ at 540 °C(1000 °F).

| Strain Rate, s$^{-1}$ | | UTS, KSI, MPa | | Elongation, % | Reduction in Area, % |
|---|---|---|---|---|---|
| 1.3 | $10^{-4}$ | 78.8 | 544 | 17.4 | 62.0 |
| 3.7 | $10^{-5}$ | 78.1 | 539 | 15.5 | 63.1 |
| 7.3 | $10^{-6}$ | 71.6 | 494 | 15.1 | 64.3 |
| 8.4 | $10^{-7}$ | 75.6 | 522 | 14.5 | 55.4 |
| 8.4 | $10^{-7}$ | 75.4 | 520 | 17.1 | 61.4 |
| 1.2 | $10^{-7}$ | -- | -- | 8.6 | 48.8 |

Table 6. Comparison of Type 310 SS and Type 309 SS in Various Gaseous Environments at 600 °C at a Strain Rate of $10^{-6}$/s.

| Specimen | Test Environment | Tensile Strength MPa | (psi) | Elongation % | Reduction in Area, % |
|---|---|---|---|---|---|
| 310 SS | Argon[1] | 411 | (59,500) | 18.7 | 24.2 |
| 310 SS | Helium | 368 | (53,400) | 19.9 | 28.8 |
| 310 SS | O/S/C[2] | 362 | (52,500) | 19.9 | 23.4 |
| 309 SS | Argon | 323 | (46,800) | 31.2 | 57.1 |
| 309 SS | Helium | 334 | (48,400) | 37.7 | 69.2 |
| 309 SS[3] | Helium | -- | -- | 34.3 | 62.1 |
| 309 SS | O/S/C[2] | -- | -- | 36.5 | 62.7 |

[1] Tested at 540 °C.

[2] O/S/C: oxidizing/sulfidizing/carburizing simulated coal gasification environment.

[3] Tested at a strain rate of 5 X $10^{-7}$/s.

Table 7. Summary of the Fracture Modes for the Main
Environment/Temperature Combinations for
Specimens Tested at $10^{-6}$/s.

| | 540 °C | | 450 °C | | | 600 °C | | |
|---|---|---|---|---|---|---|---|---|
| | He | $H_2S/H_2O$ | He | O/S | O/S/C | He | O/S | O/S/C |
| Type 310 | ISC[1] | ISC | D[2] | D | D | ISC | ISC | ISC |
| Type 310 S | ISC | D | D | D | D | ISC | ISC | ISC |
| Type 347 | D | D | D | D | D | SC[3] | D | SC |
| Type 309 | -- | -- | -- | -- | -- | SC | -- | SC |
| Type 446 | -- | -- | D | SC | SC | SC | SC | SC |
| Inconel 800 | -- | -- | D | D | D | SC | SC | SC |
| Incoloy 671 | -- | -- | D | SC | SC | SC | SC | SC |

[1]Intergranular secondary cracking.

[2]Ductile failure.

[3]Path of secondary cracking was not determined.
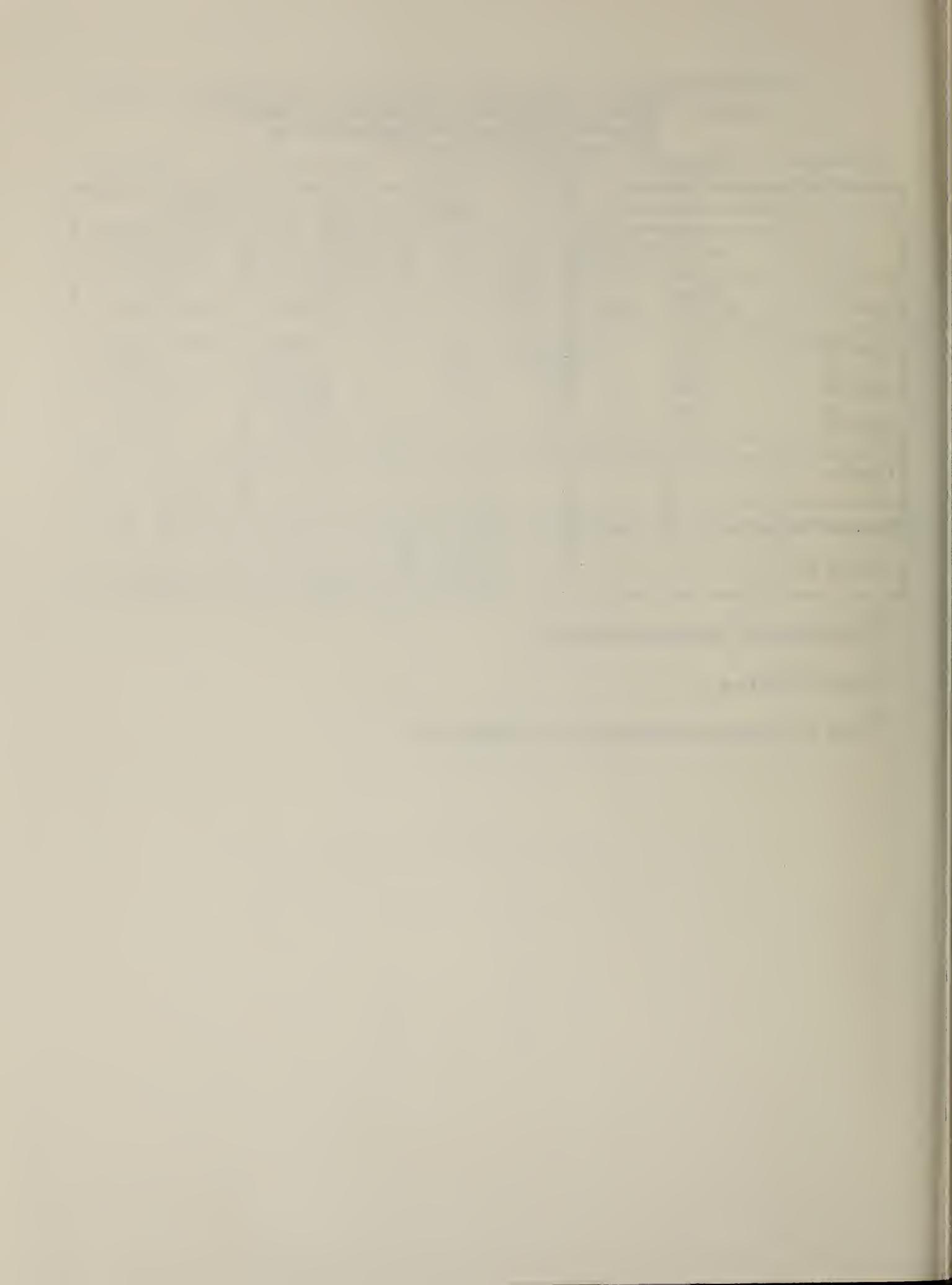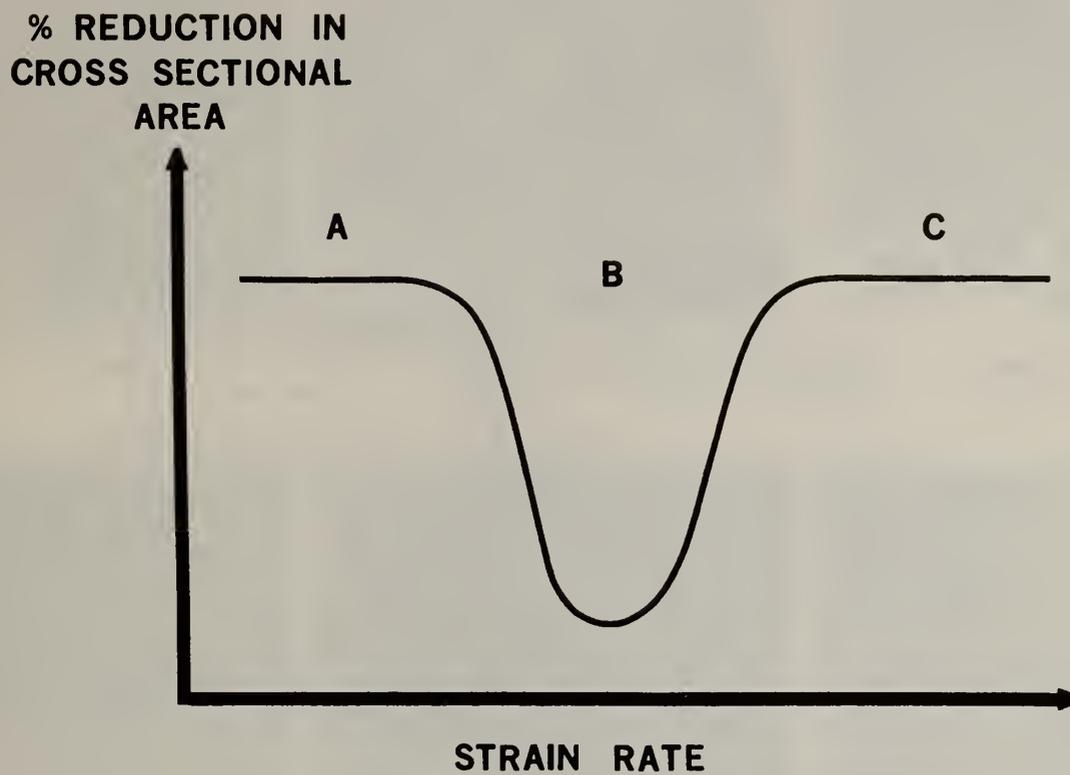
Fig. 1. Schematic representation of typical results obtained from the application of the SSRT to the study of SCC in aqueous media. The interpretation of Regions A, B and C is discussed in the text.
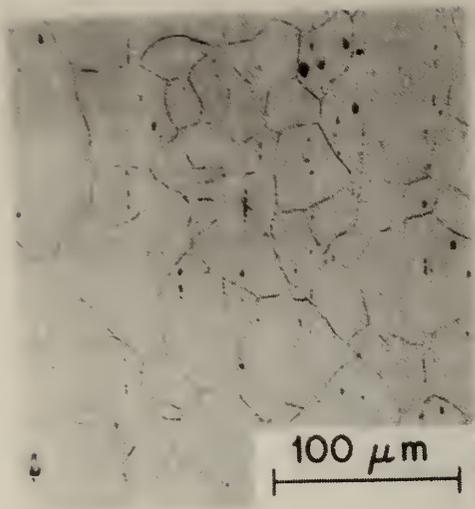
Type 309, 250 X
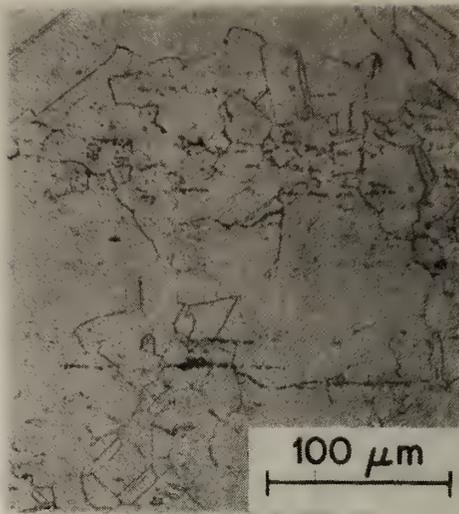
Type 310, 250 X
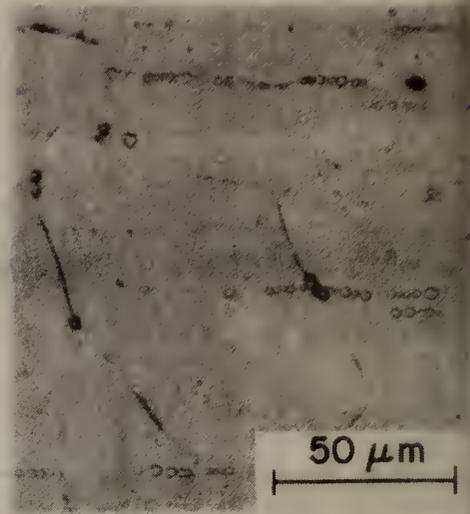
Type 310 S, 500 X
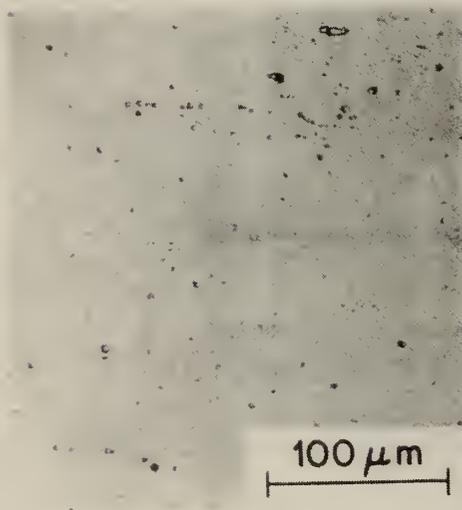
Type 347, 250 X
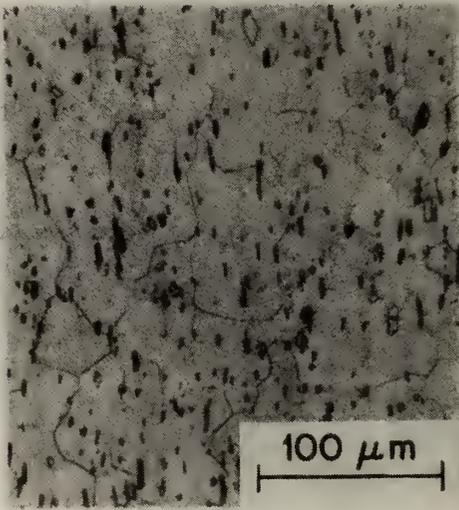
Type 446, 250 X
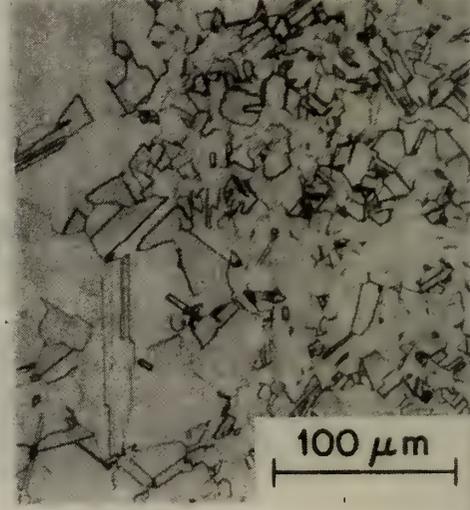
Incoloy 800, 250 X
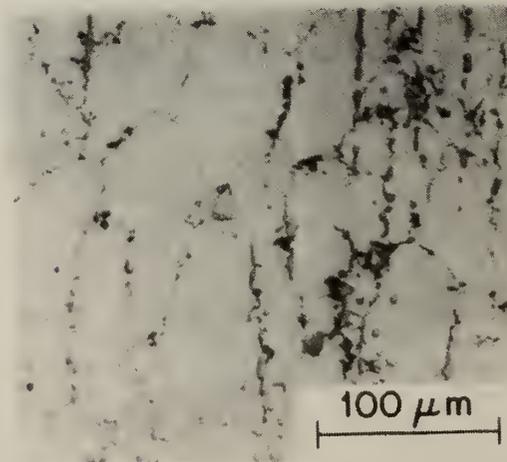
Inconel 671, 250 X

Fig. 2. Microstructures of test alloys in the as-received condition.
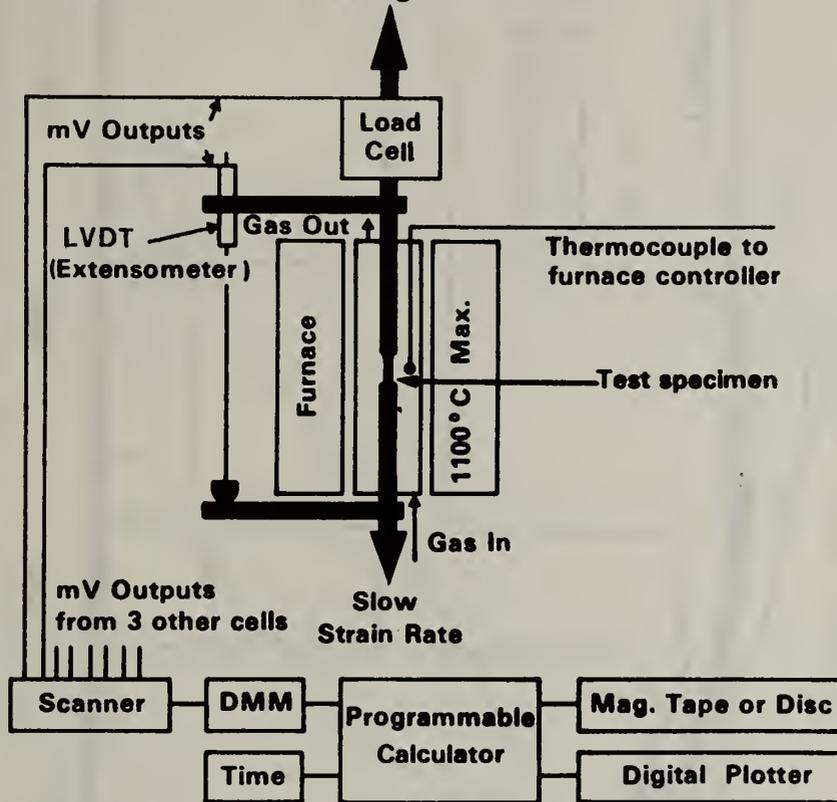
Fig. 3.  A schematic representation of the slow strain rate testing facilities.
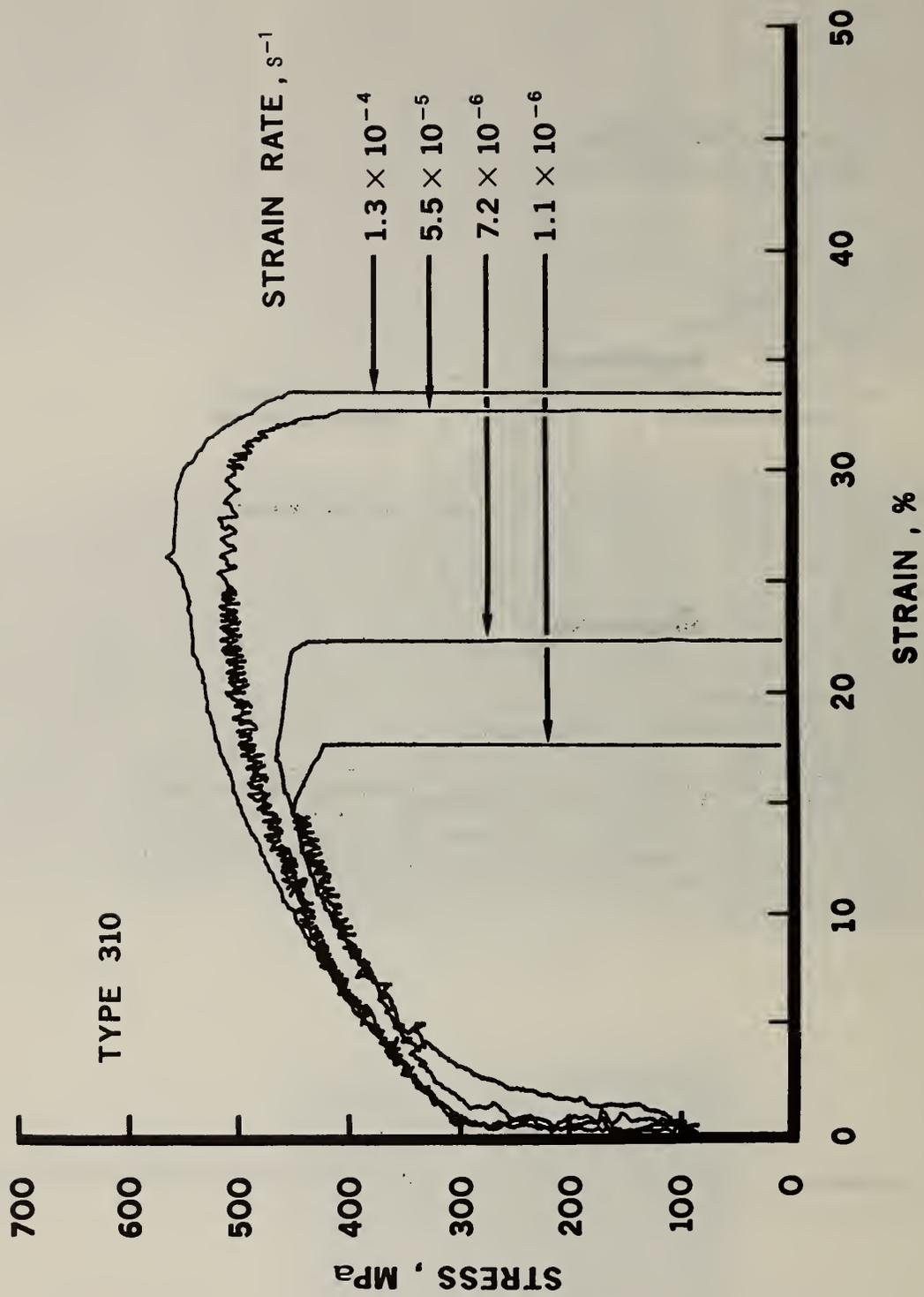
Fig. 4. Effect of strain rate on stress-strain curves of Type 310 specimens tested in $H_2O/H_2S$ at 540 °C.
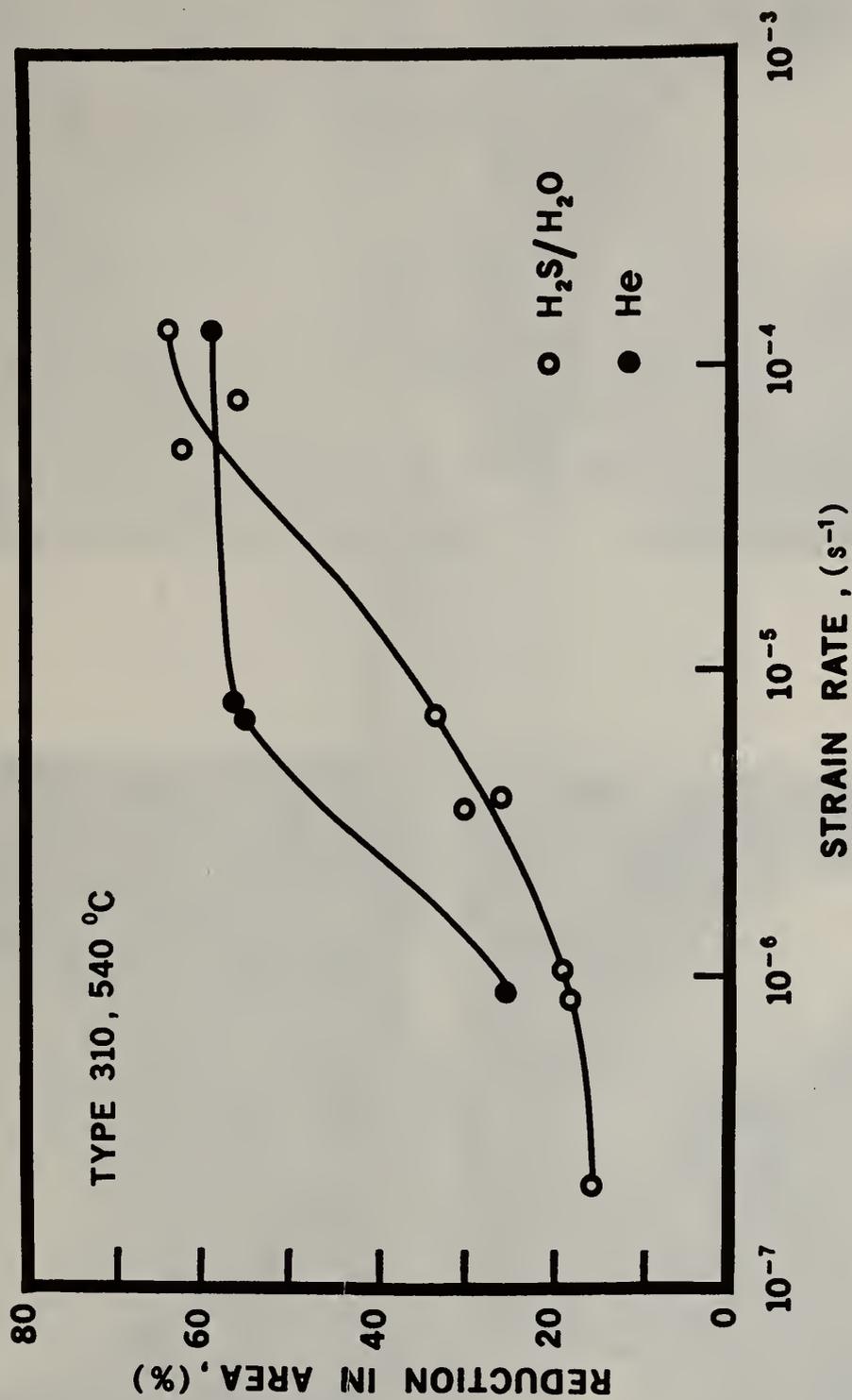
Fig. 5.  Ductility as reduction in area versus strain rate for Type 310
specimens tested in gaseous $H_2O/H_2S$ and He at 540 °C (1000 °F).

(a)  $\dot{\varepsilon} = 1.3 \times 10^{-4}$/s
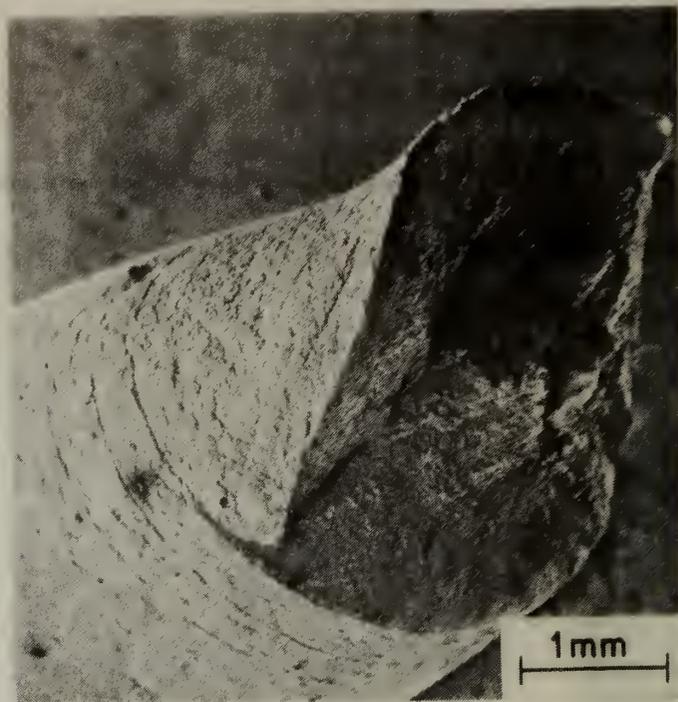
(b)  $\dot{\varepsilon} = 5.5 \times 10^{-5}$/s

(c)  $\dot{\varepsilon} = 7.2 \times 10^{-6}$/s
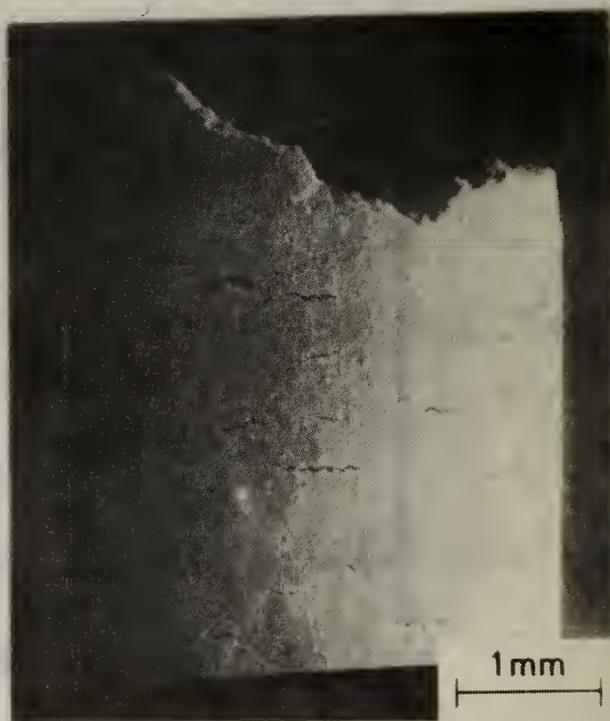
(d)  $\dot{\varepsilon} = 1.1 \times 10^{-6}$/s

Fig. 6.  Scanning electron micrographs indicating the effect of strain rate ($\dot{\varepsilon}$) on the fracture of Type 310 specimens when tested in $H_2O/H_2S$ at 540 °C (1000 °F).

Dry Purified He

Ar

Vacuum, 2 × 10⁻² Torr

Fig. 7. Cracking of Type 310 specimens in various "inert" environments when tested at 540 °C (1000 °F) at a strain rate of 10⁻⁶/s. Original magnification 7 X.
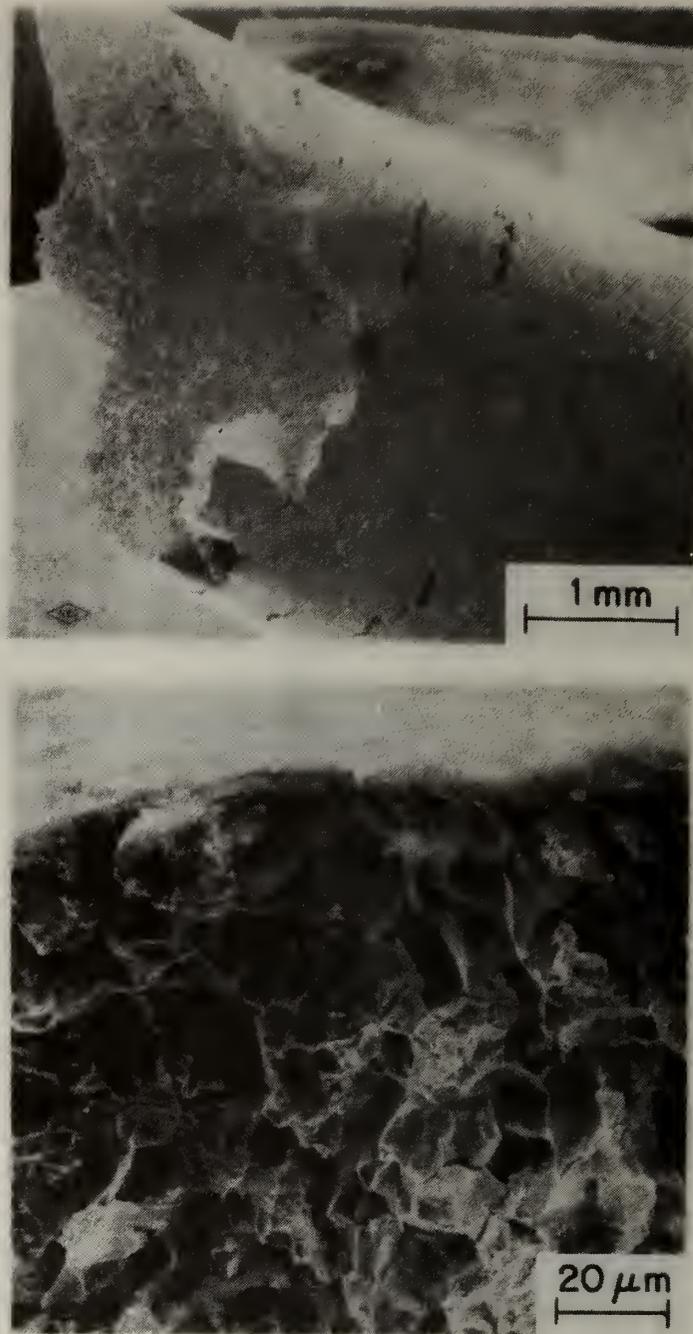
Fig. 8.  Scanning electron micrographs of a Type 310 specimen tested in $H_2$ at 540 °C at a strain rate of $10^{-6}$/s, showing the primary fracture and numerous secondary intergranular cracks (above), and the zone of intergranular failure on the primary fracture surface (below).
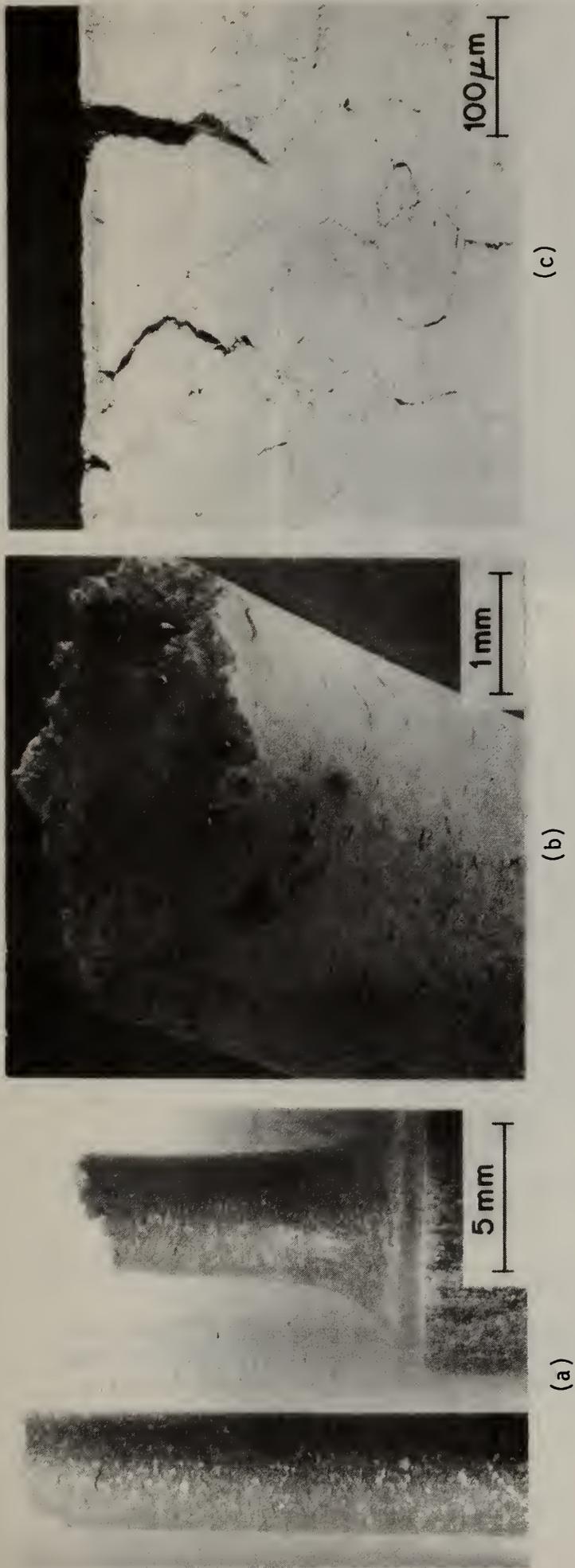
Fig. 9. Type 310 specimen tested in air at 815 °C (1500 °F) at a strain rate of $10^{-6}$/s. (a) Photomicrograph of the fractured specimen. (b) Scanning electron micrograph at the region of fracture. (c) Photomicrograph of the sectioned specimen near the fracture.
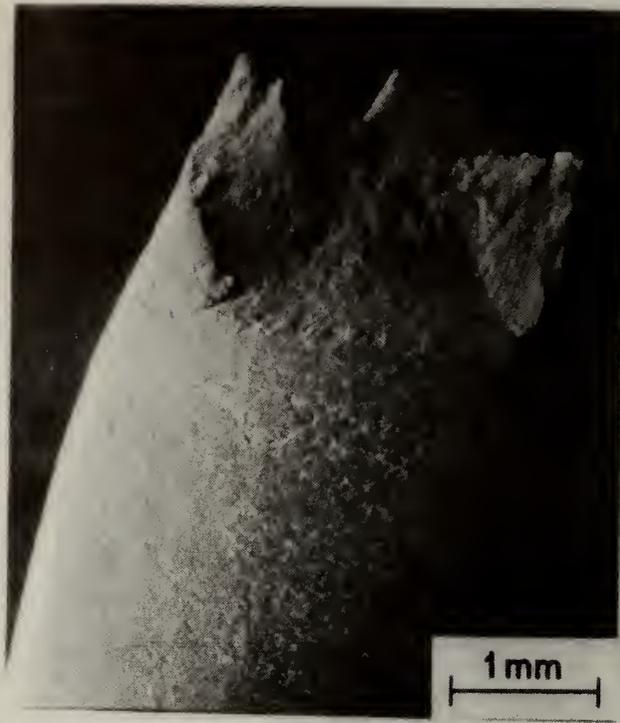
(a)



(b)

Fig. 10.  Scanning electron micrograph and photomicrograph of Type 310
specimen showing the ductile fracture and partially sensitized
grain boundaries after testing in He at 370 °C (700 °F) at a
strain rate of $10^{-6}$/s.

(a)
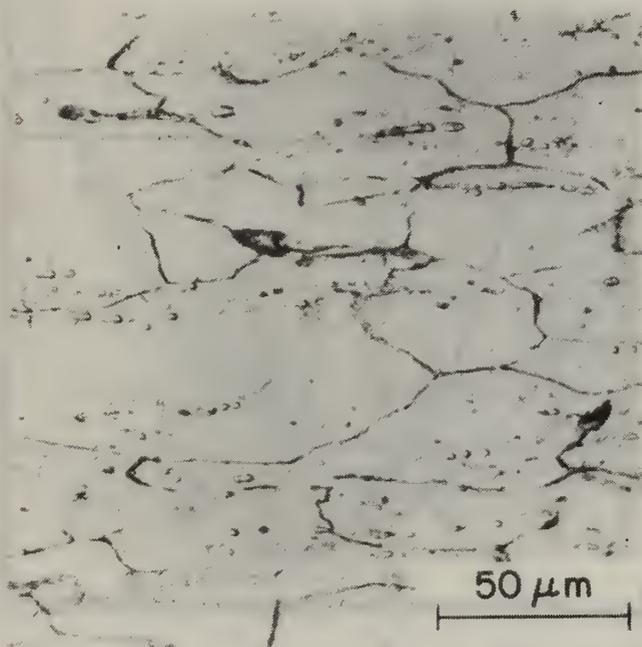


(b)

Fig. 11.  Scanning electronmicrograph and photomicrograph of Type 310
specimen showing the ductile fracture and partially sensitized
grain boundaries after testing in $H_2$ at 450 °C (840 °F) at a
strain rate of $10^{-6}$/s.
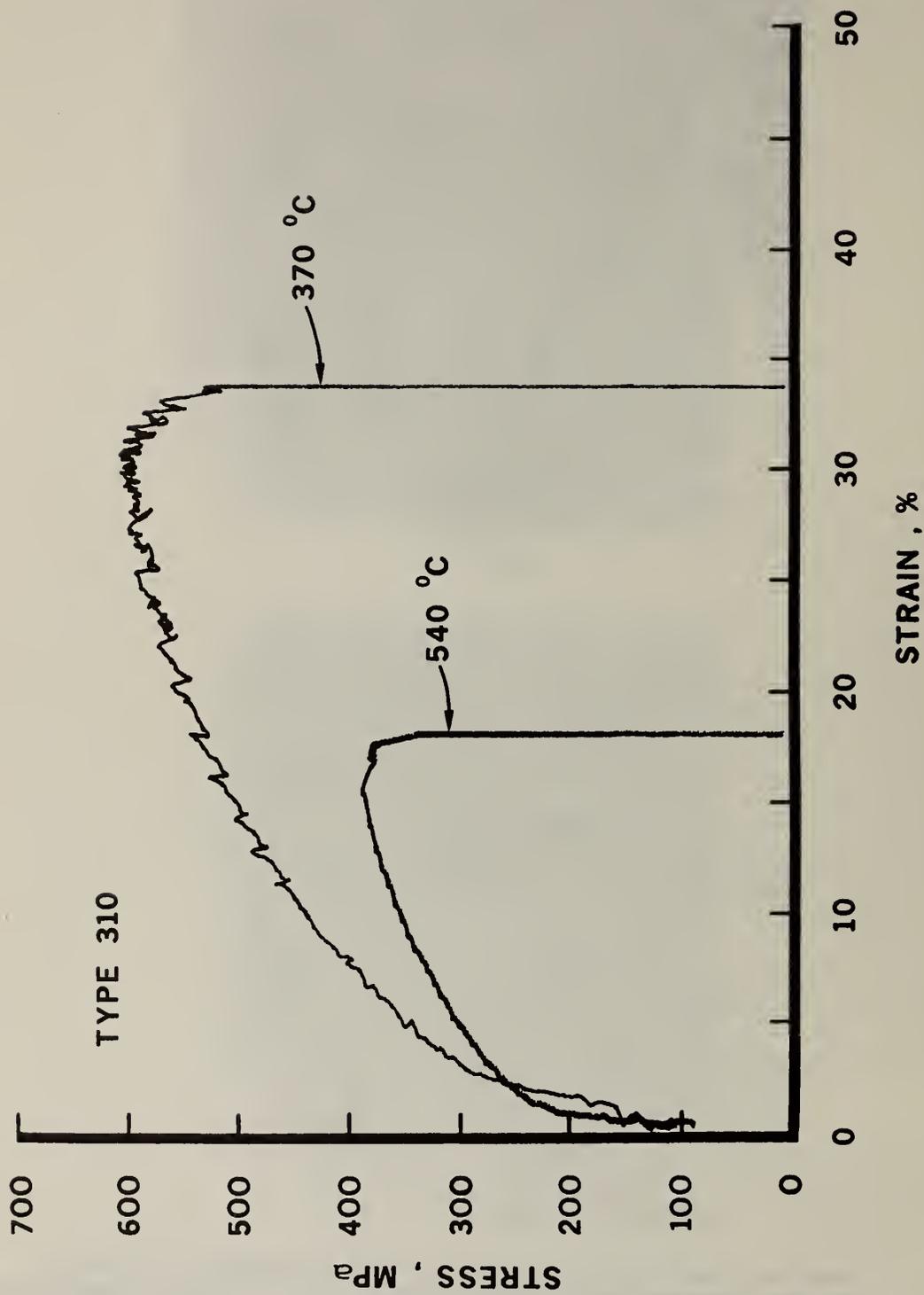
Fig. 12. Stress-strain curves for Type 310 specimens showing the effect of temperature when tested in dry He (passed through inert gas purifier) at a strain rate of $8.43 \times 10^{-7}$/s.
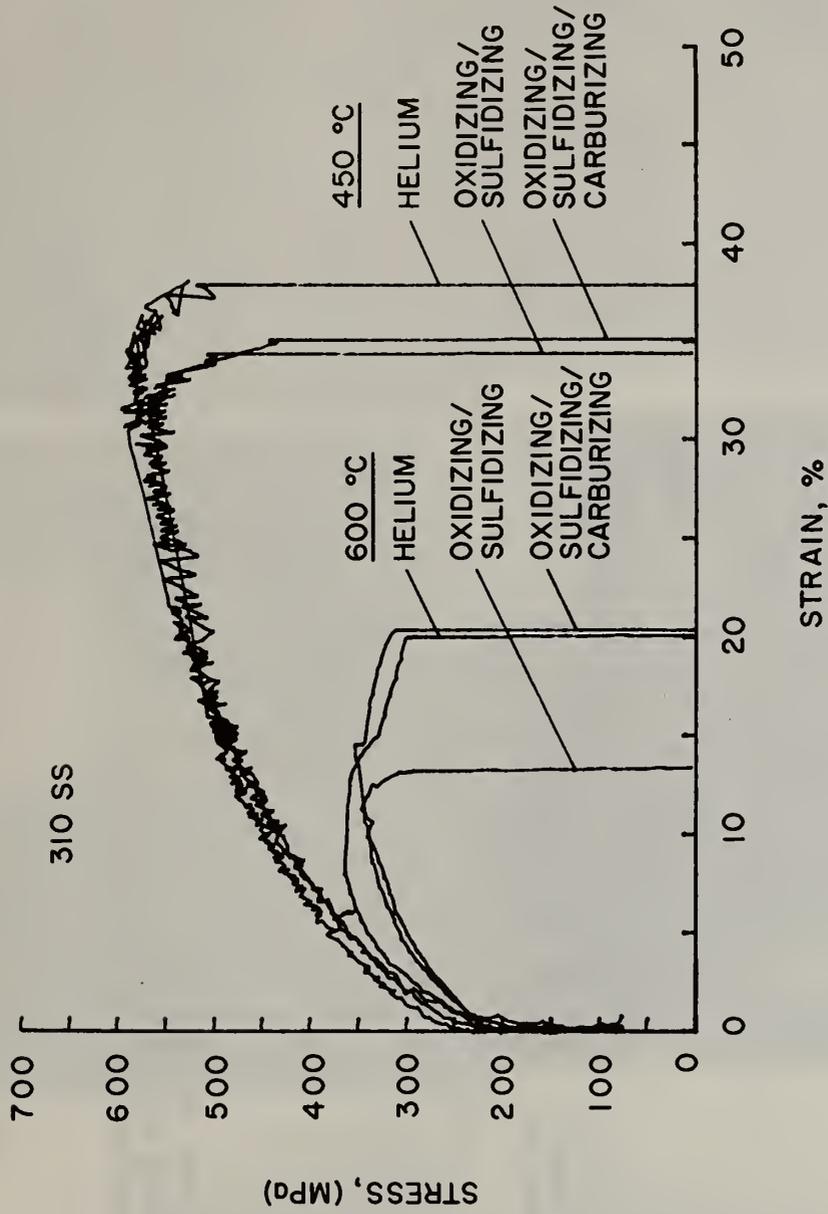
Fig. 13. Stress-strain curves for Type 310 specimens tested at 450 °C (840 °F) and 600 °C (1100 °F) in He and in oxidizing/sulfidizing and oxidizing/sulfidizing/carburizing coal gasification environments at a strain rate of 1 X 10⁻⁶/s.
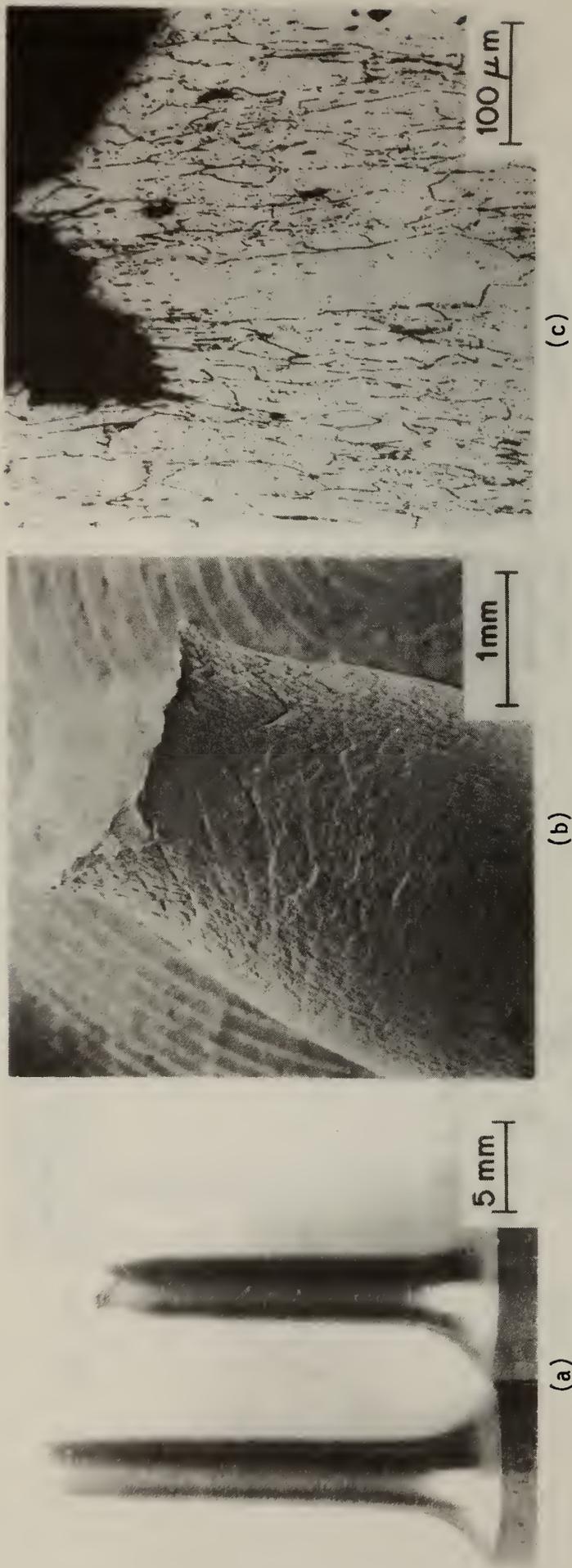
UTS — 602 MPa(87,300 psi)
Elongation — 37.9%
RA — 64.6%

Fig. 14. Type 310 specimen tested in He at 450 °C at a strain rate of $1 \times 10^{-6}$/s. (a) Photomicrograph of the fractured specimen. (b) Scanning electron micrograph at the region of fracture. (c) Photomicrograph of the sectioned specimen near the fracture.

(a)

(b)

(c)

5 mm

2 mm

200 μm
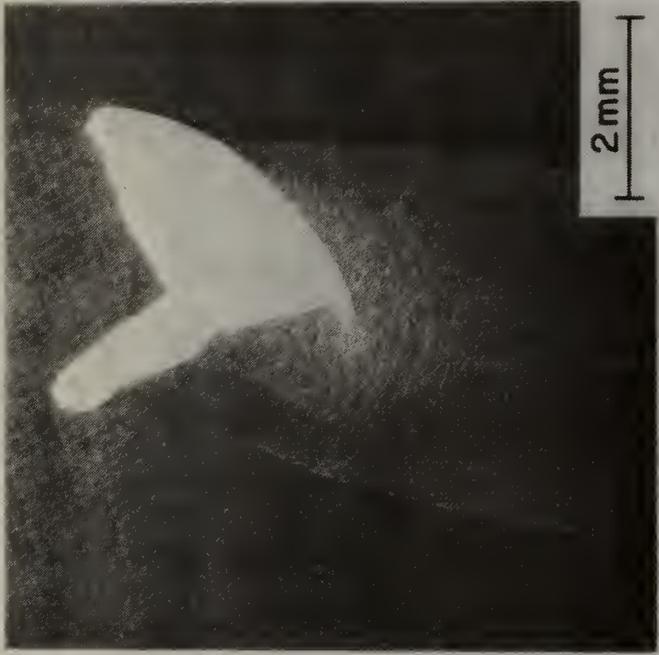
UTS —— 581 MPa (84,200 psi)
Elongation —— 35.4%
RA —— 55.1%

Fig. 15. Type 310 specimen tested in the oxidizing-sulfidizing
environment at 450 °C at a strain rate of 1 x 10⁻⁶/s.
(a) Photomicrograph of the fractured specimen.
(b) Scanning electron micrograph at the region of fracture.
(c) Photomicrograph of the sectioned specimen near the fracture.
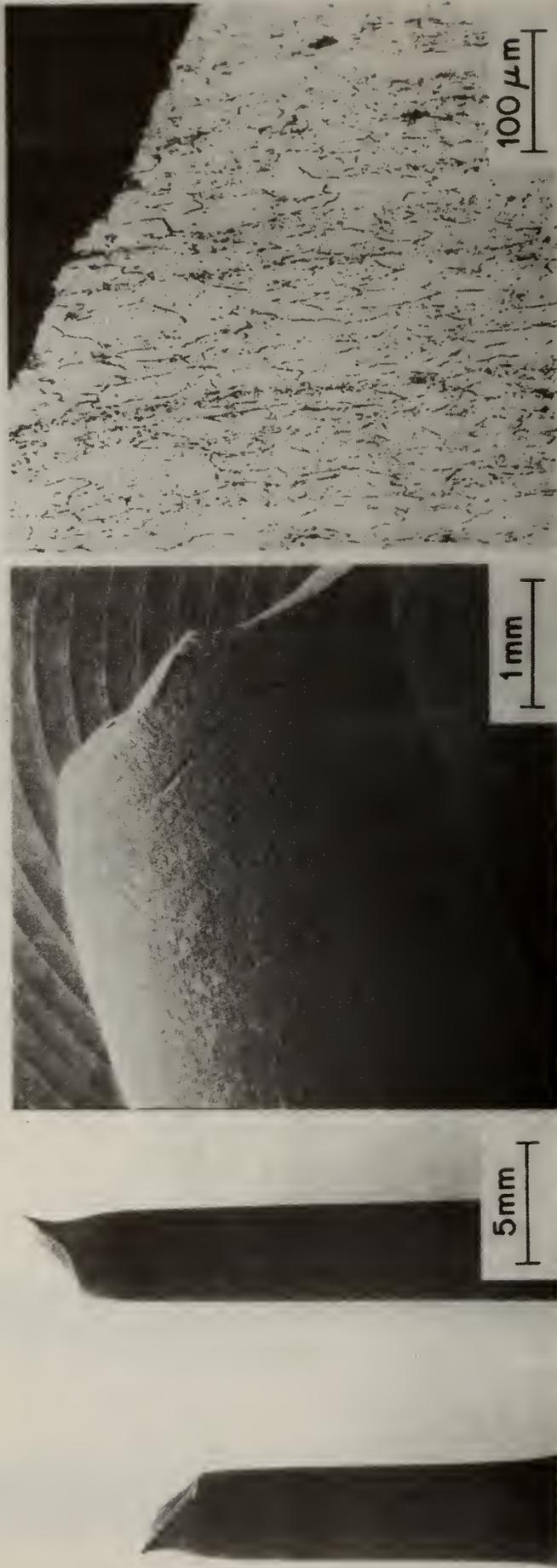
(a)

(b)

(c)

UTS ——— 598 MPa (86,700 psi)
Elongation ——— 35.6%
RA ——— 60.2%

Fig. 16.  Type 310 specimen tested in the oxidizing-sulfidizing-
carburizing environment at 450 °C at a strain rate of
$1 \times 10^{-6}$/s.
(a) Photomicrograph of the fractured specimen.
(b) Scanning electron micrograph at the region of fracture.
(c) Photomicrograph of the sectioned specimen near the fracture.

(a)

(b)

(c)

| 5 mm |
| 1mm |
| 100 μm |

UTS ——— 368 MPa (53,400 psi)
Elongation ——— 19.9%
RA ——— 28.8%

Fig. 17.  Type 310 specimen tested in dry He at 600 °C at a
strain rate of 1 x 10⁻⁶/s.
(a) Photomicrograph of fractured specimen.
(b) Scanning electron micrograph at the region of fracture.
(c) Photomicrograph of the sectioned specimen near the fracture.
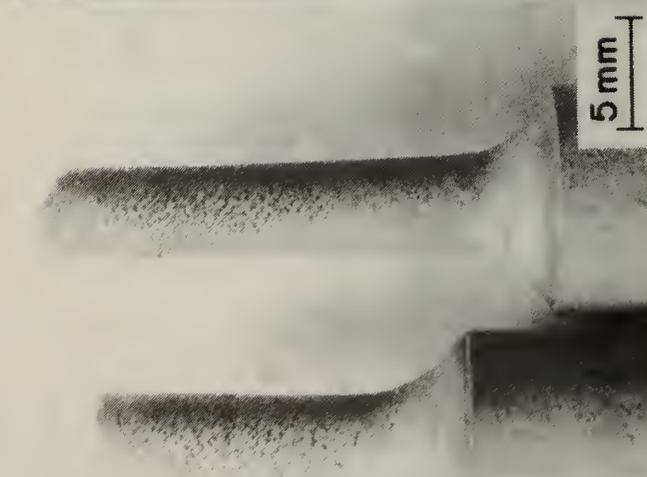
UTS — 347 MPa (50,300 psi)
Elongation — 14.0%
RA — 21.6%

Fig. 18. Type 310 specimen tested in the oxidizing-sulfidizing environment at 600 °C at a strain rate of 1 X 10⁻⁶/s. (a) Photomicrograph of fractured specimen. (b) Scanning electron micrograph at the region of fracture. (c) Photograph of the sectioned specimen near the fracture.

(a)

(b)

(c)

UTS        — 362 MPa (52,500 psi)
Elongation — 19.9%
RA         — 23.4%

Fig. 19.  Type 310 specimen tested in the oxidizing-sulfidizing-
          carburizing environment at 600 °C at a strain rate of
          1 x 10⁻⁶/s.
          (a) Photomicrograph of the fractured specimen.
          (b) Scanning electron micrograph at the region of fracture.
          (c) Photomicrograph of the sectioned specimen near the fracture.
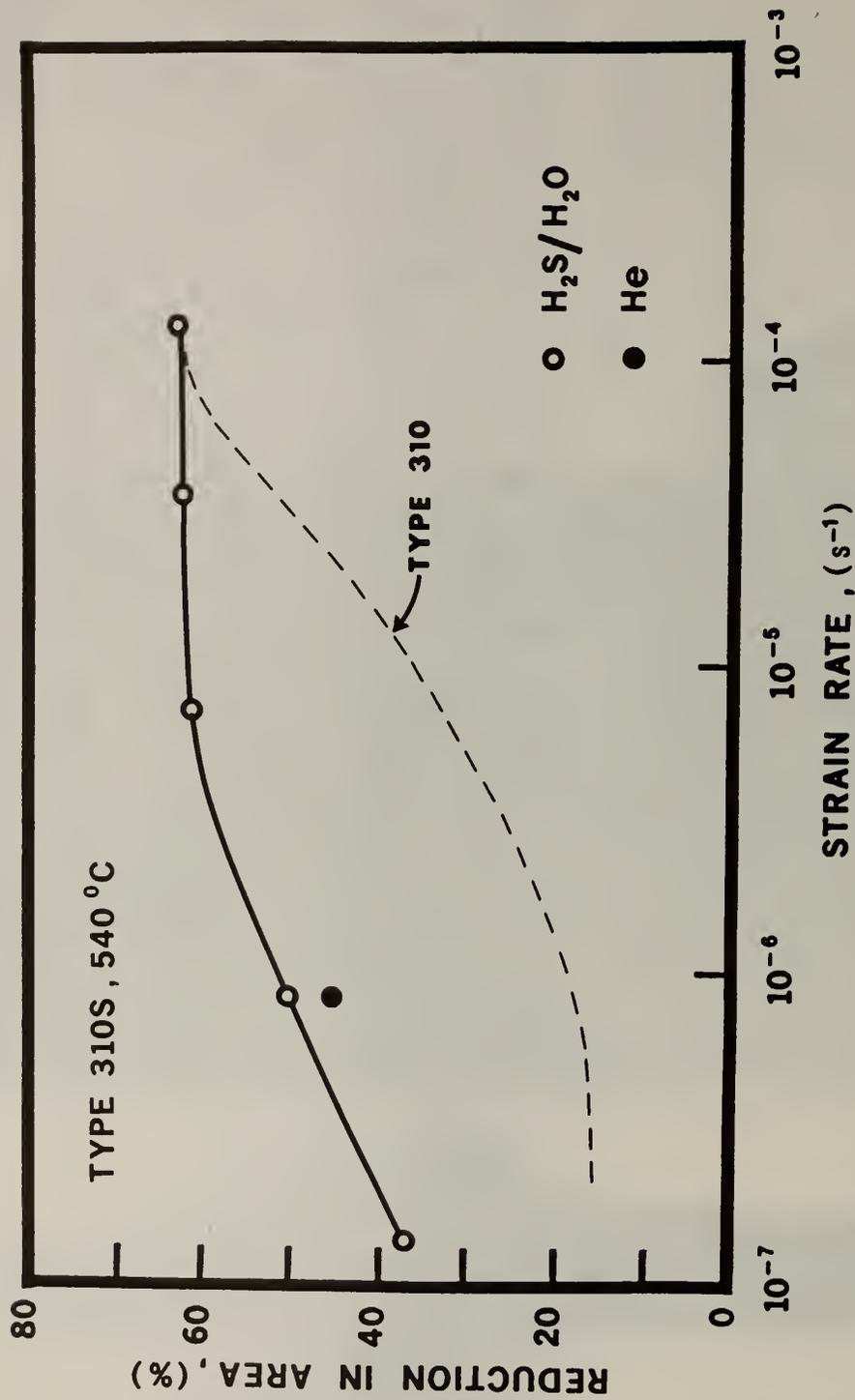
Fig. 20. Ductility as reduction in area versus strain rate for Type 310S specimens tested in gaseous $H_2O/H_2S$ and He at 540 °C (1000 °F). Type 310 curve is shown for comparison.
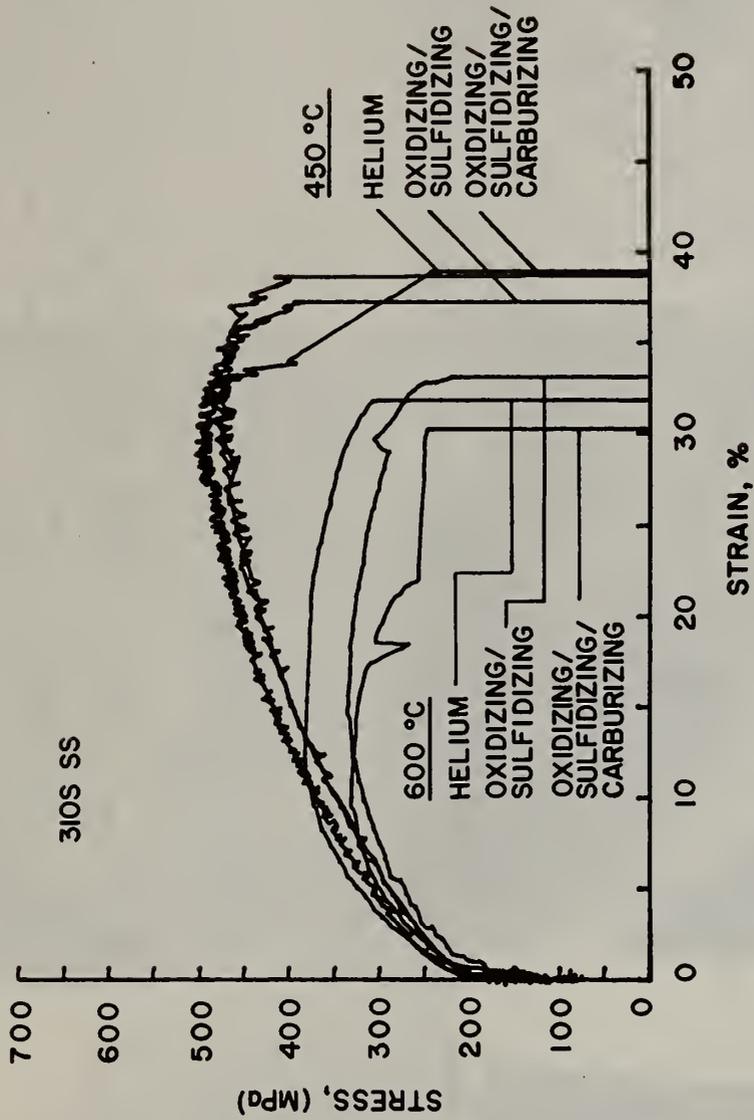
Fig. 21.  Stress-strain curves for 310S steel tested at 450 °C (840 °F) and 600 °C (1100 °F) in He and in oxidizing/sulfidizing and oxidizing/sulfidizing/carburizing coal gasification environments at a strain rate of 1 X 10⁻6/s.
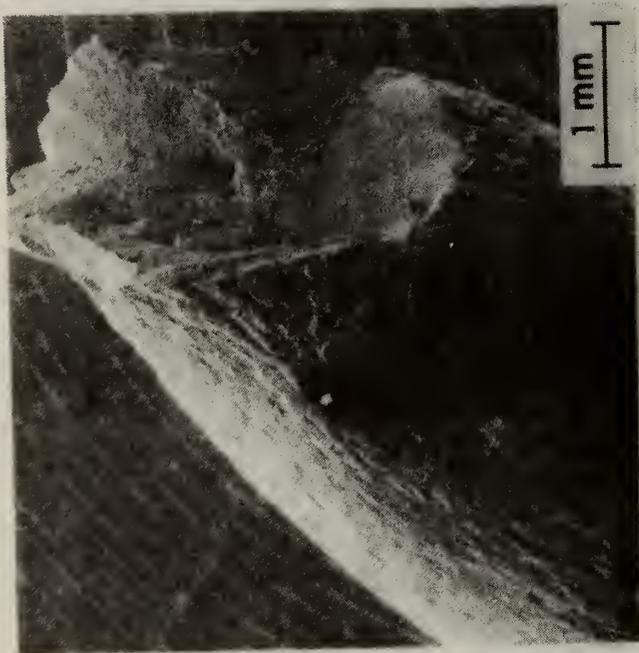
UTS ——— 518 MPa (75,100 psi)
Elongation ——— 38.9%
RA ——— 63.7%

Fig. 22.   Type 310S stainless steel tested in He at 450 °C at a strain
rate of 1 X 10⁻⁶/s.  (a) Photomicrograph of the fractured
specimen.  (b) Scanning electron micrograph at the region of
fracture.  (c) Photomicrograph of the sectioned specimen near the
fracture.
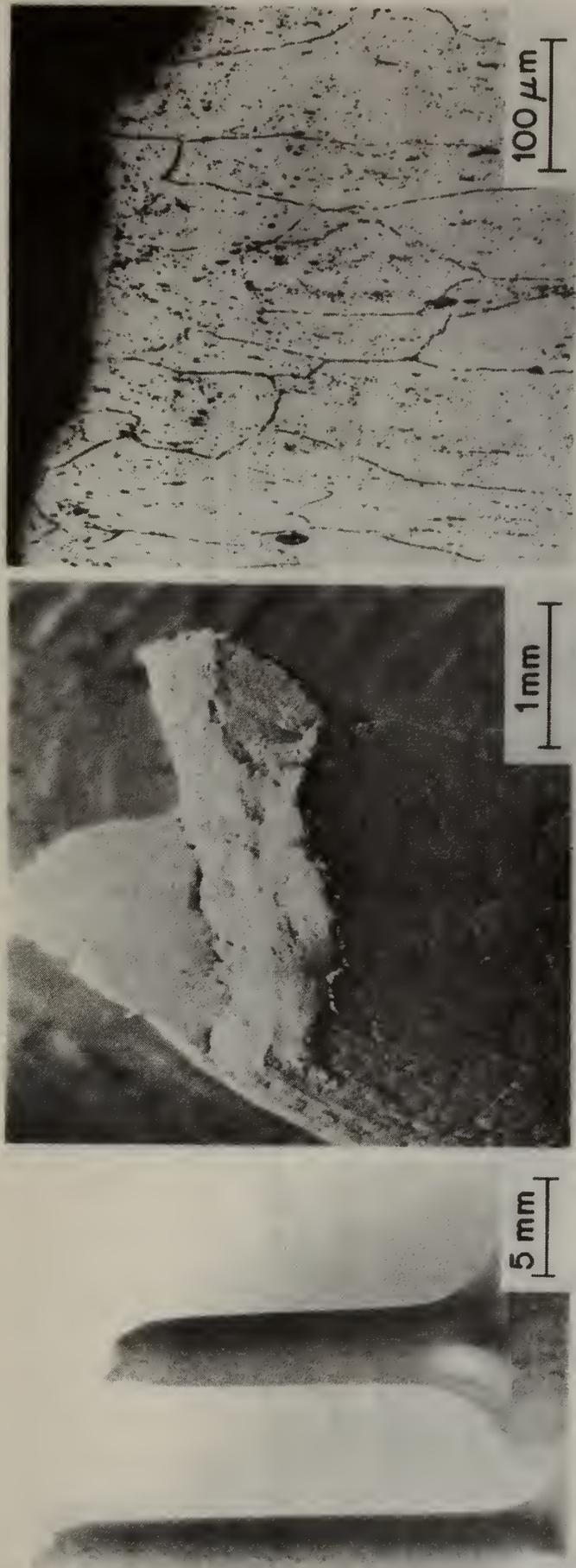
(a)  (b)  (c)

UTS — 519 MPa (75,200 psi)
Elongation — 38.6%
RA — 65.1%

Fig. 23.  Type 310S stainless steel tested in the oxidizing-
sulfidizing environment at 450 °C at a strain rate
of 1 x 10⁻⁶/s.
(a) Photomicrograph of the fractured specimen.
(b) Scanning electron micrograph at the region of fracture.
(c) Photomicrograph of the sectioned specimen near the fracture.

(c)

(b)

(a)
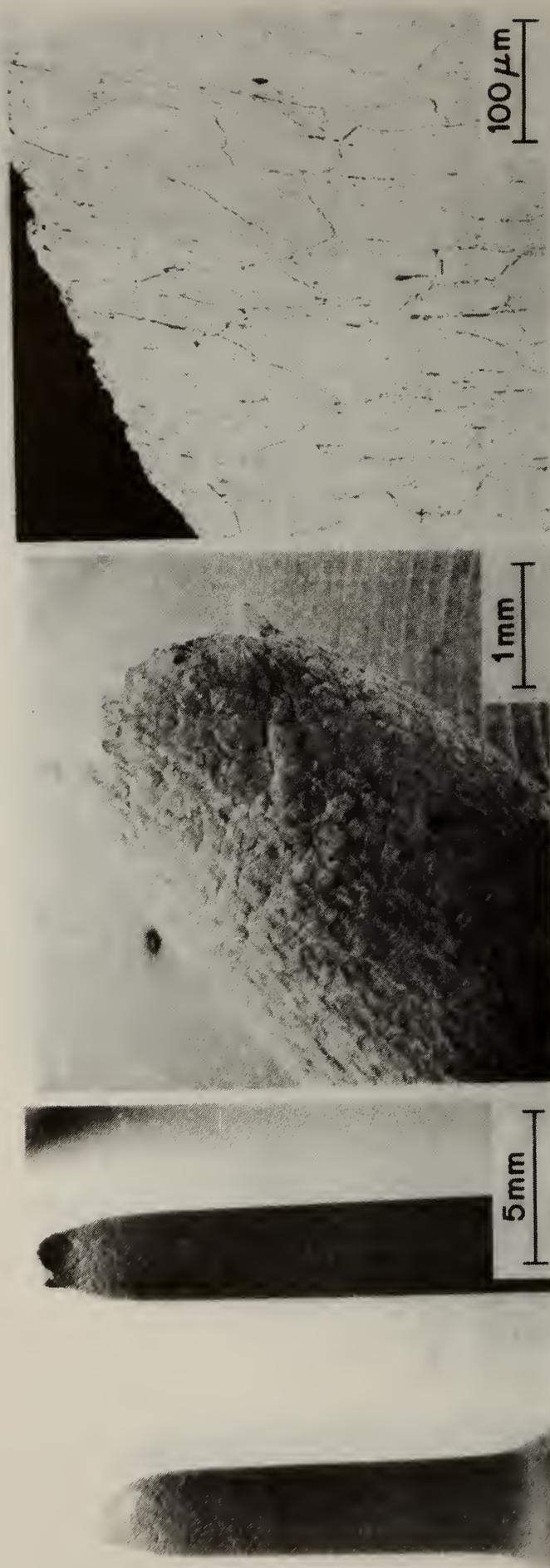
UTS      — 513 MPa (74,400 psi)
Elongation — 38.8%
RA       — 69.9%

Fig. 24.   Type 310S stainless steel tested in the oxidizing-sulfidizing-carburizing environment at 450 °C at a strain rate of $1 \times 10^{-6}$/s.
(a) Photomicrograph of the fractured specimen.
(b) Scanning electron micrograph at the region of fracture.
(c) Photomicrograph of the sectioned specimen near the fracture.
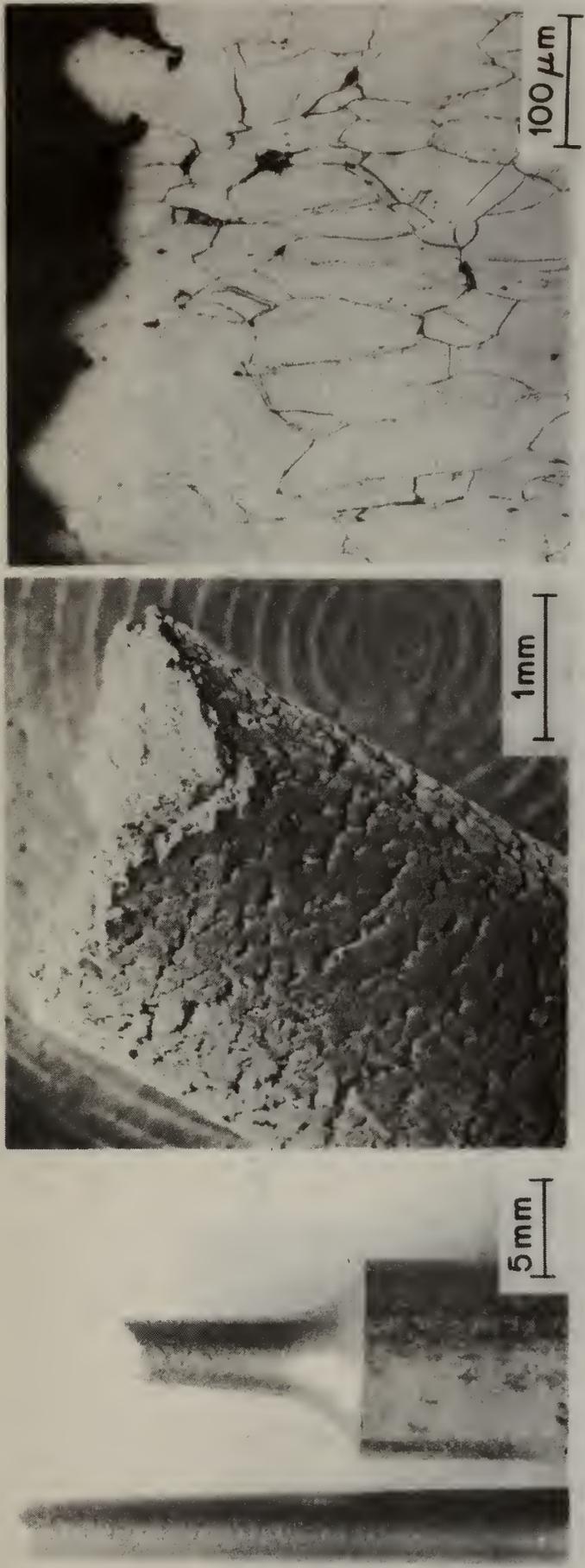
(a)

(b)

(c)

UTS ——— 437 MPa (63,400 psi)
Elongation —— 31.9%
RA —— 42.8%

Fig. 25.   Type 310S stainless steel tested in dry He at 600 °C
at a strain rate of 1 x 10⁻⁶/s.
(a) Photomicrograph of the fractured specimen.
(b) Scanning electron micrograph at the region of fracture.
(c) Photomicrograph of the sectioned specimen near the fracture.

(a)

(b)

(c)
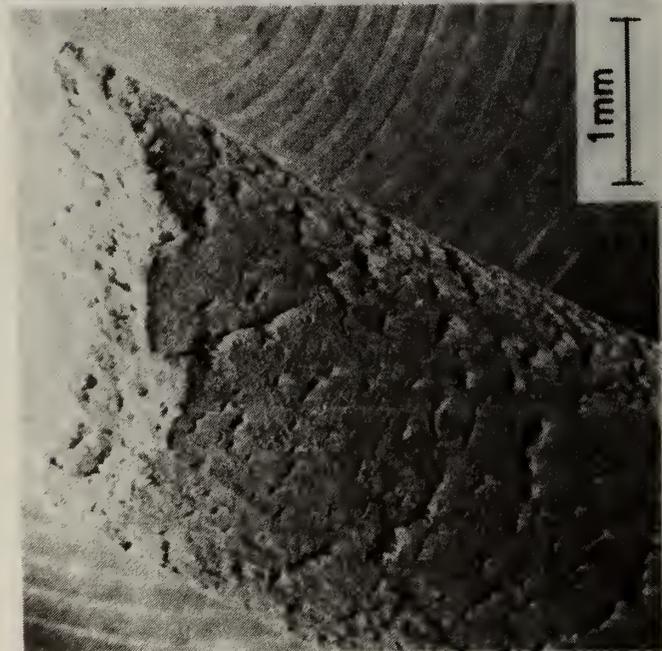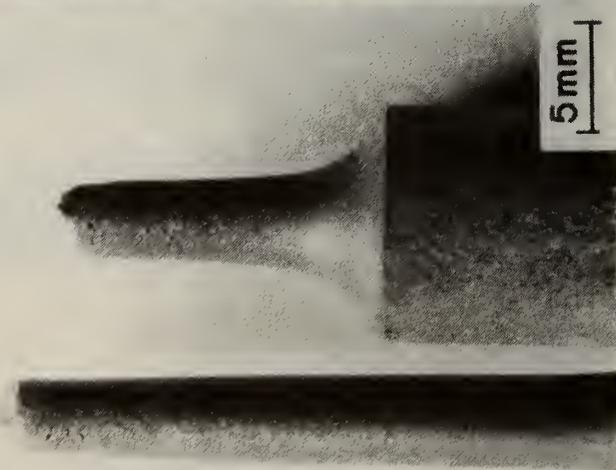
UTS — 376 MPa (54,500 psi)
Elongation — 32.8%
RA — 43.9%

Fig. 26.  Type 310S stainless steel tested in the oxidizing-sulfidizing environment at 600 °C at a strain rate of $1 \times 10^{-6}$/s.
(a) Photomicrograph of the fractured specimen.
(b) Scanning electron micrograph at the region of fracture.
(c) Photomicrograph of the sectioned specimen near the fracture.
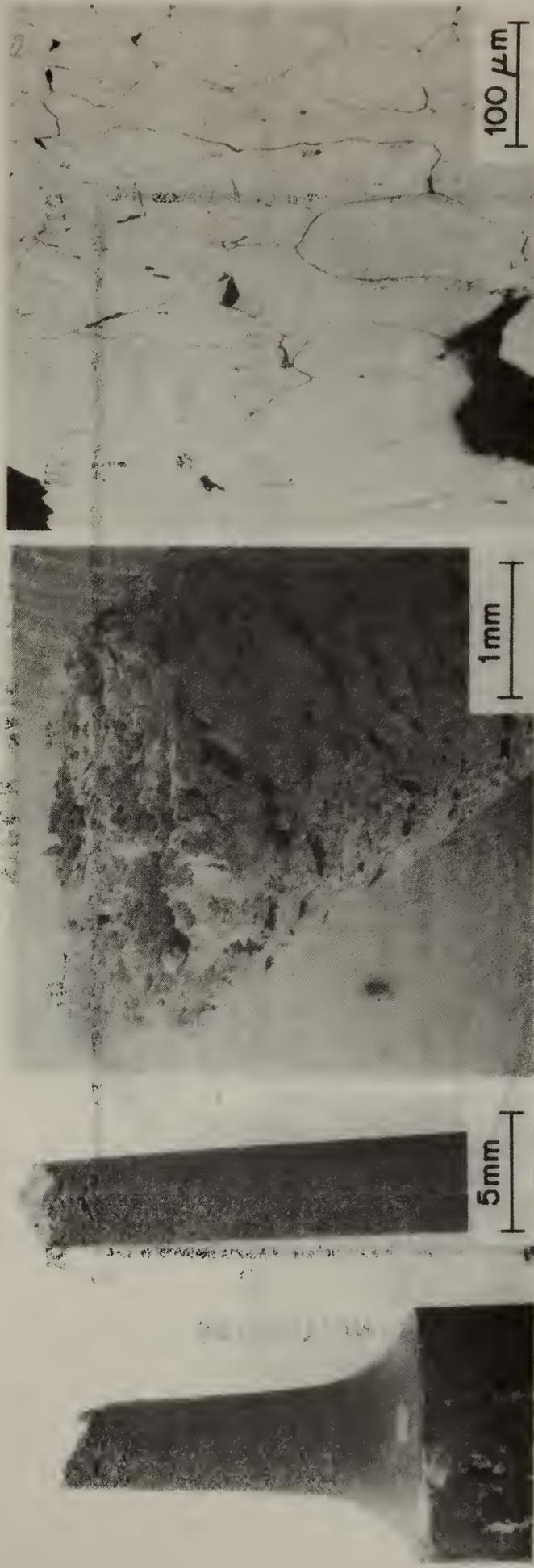
UTS — 336 MPa (48,700 psi)
Elongation — 30.3%
RA — 33.8%

Fig. 27.  Type 310S stainless steel tested in the oxidizing-sulfidizing-carburizing environment at 600 °C at a strain rate of $1 \times 10^{-6}$/s.
(a) Photomicrograph of the fractured specimen.
(b) Scanning electron micrograph at the region of fracture.
(c) Photomicrograph of the sectioned specimen.
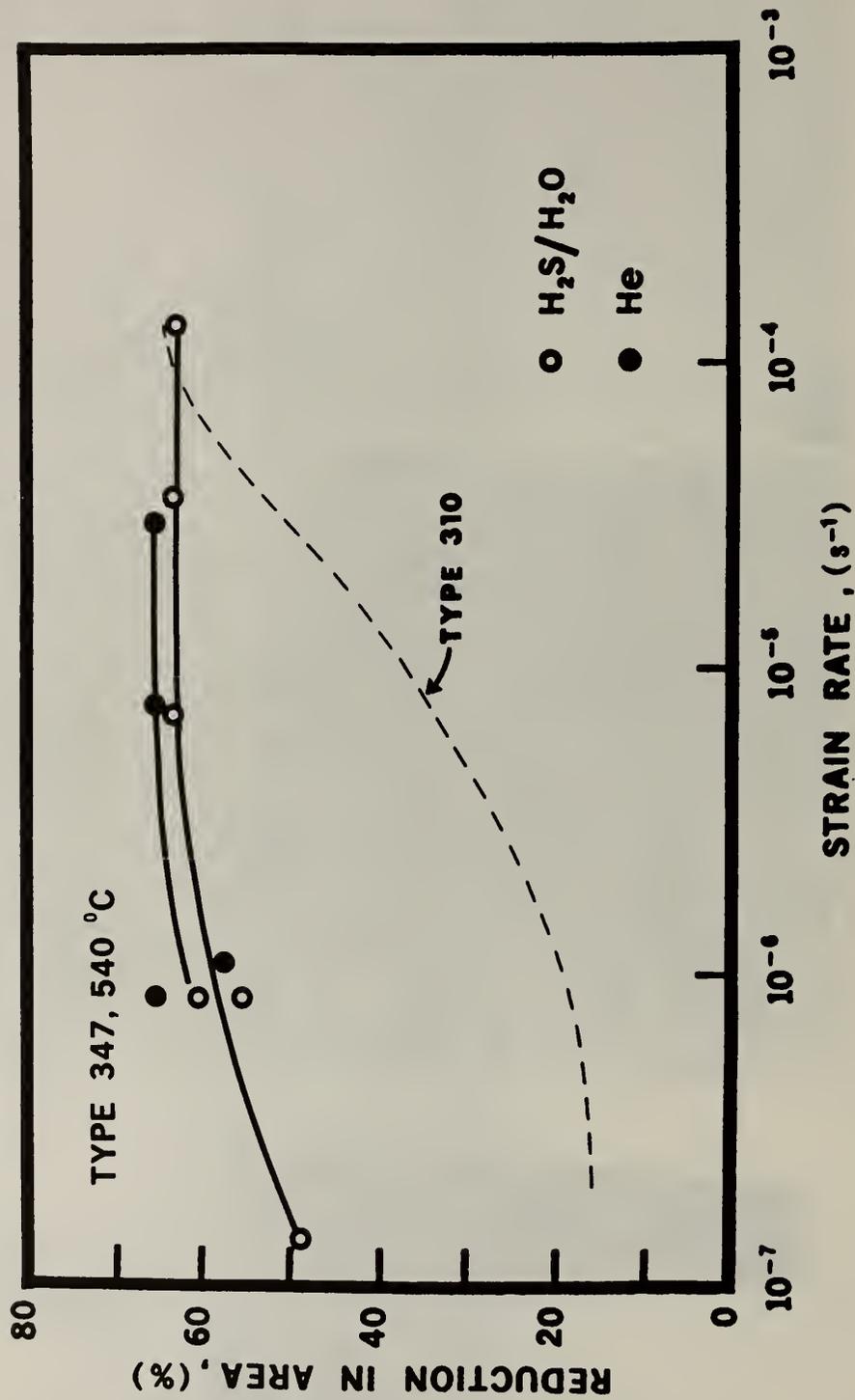
Fig. 28.  Ductility as reduction in area versus strain rate for Type 347 specimens tested in gaseous $H_2O/H_2S$ and He at 540 °C (1000 °F).  Type 310 curve is shown for comparison.
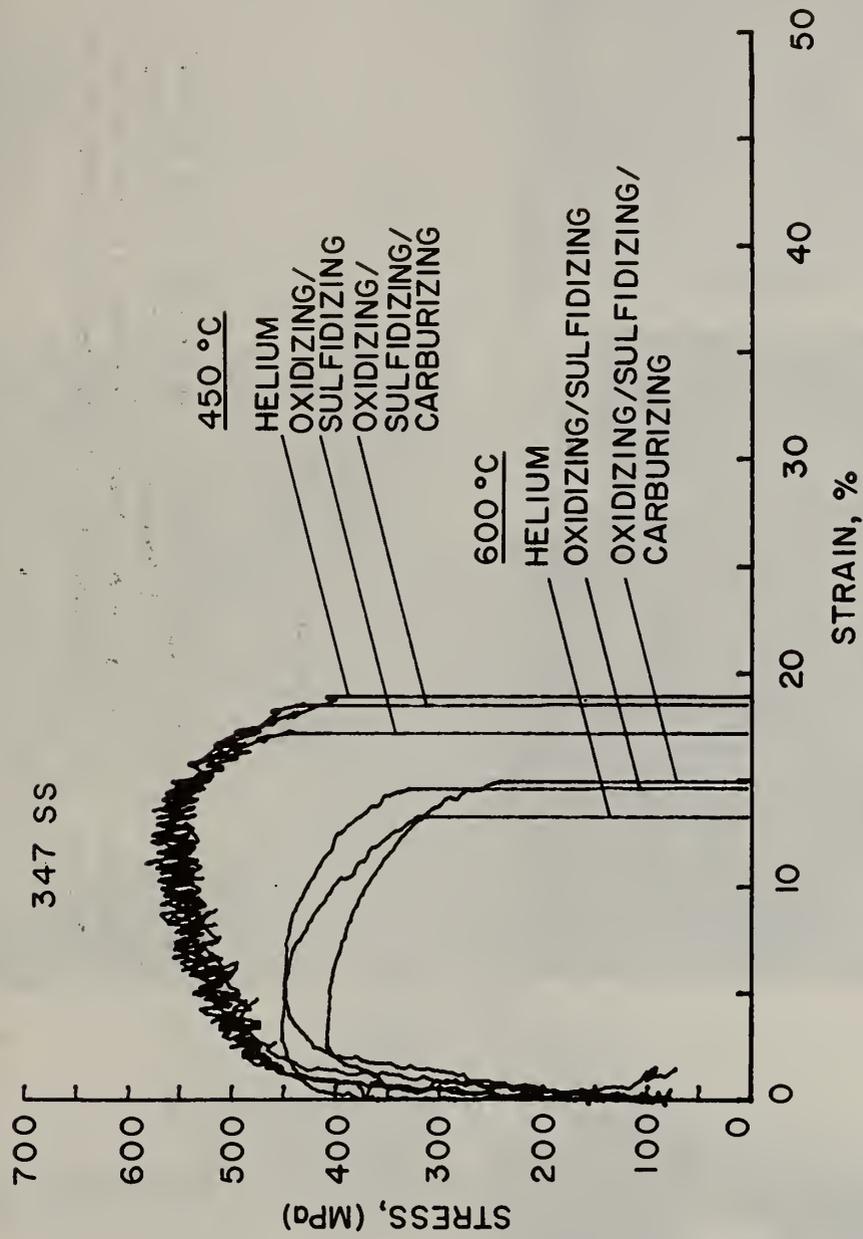
Fig. 29. Stress-strain curves for Type 347 specimens tested at 450 °C (840 °F) and 600 °C (1100 °F) in He and in oxidizing/sulfidizing and oxidizing/sulfidizing/ carburizing coal gasification environments at a strain rate of 1 X 10⁻⁶/s.
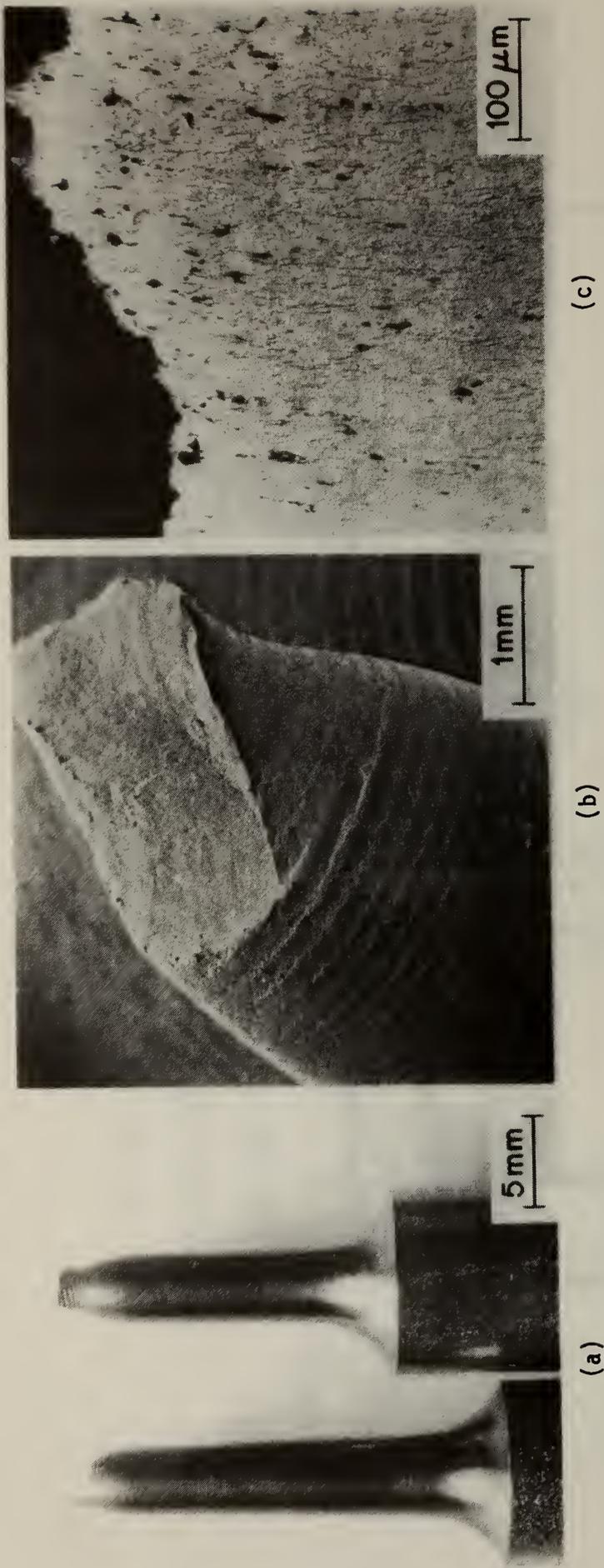
UTS — 568 MPa (82,300 psi)
Elongation — 18.8%
RA — 65.2%

Fig. 30. Type 347 stainless steel tested in He at 450 °C at a strain rate of 1 X 10⁻⁶/s. (a) Photomicrograph of the fractured specimen. (b) Scanning electron micrograph at the region of fracture. (c) Photomicrograph of the sectioned specimen near the fracture.

(a)

(b)

(c)

5 mm

2 mm

200 μm
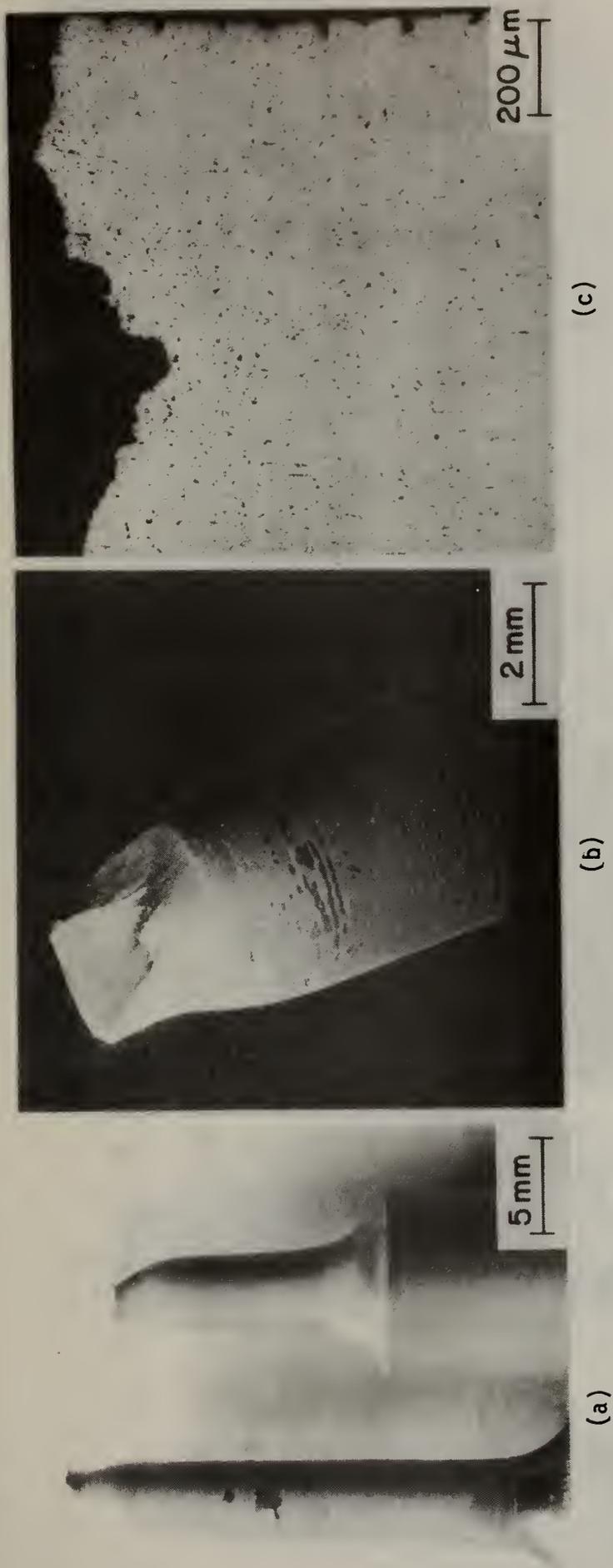
UTS        — 591 MPa (85,700 psi)
Elongation — 17.0%
RA         — 60.2%

Fig. 31.  Type 347 stainless steel tested in the oxidizing-sulfidizing environment at 450 °C at a strain rate of 1 X 10-6/s. (a) Photomicrograph of the fractured specimen. (b) Scanning electron micrograph at the region of fracture. (c) Photomicrograph of the sectioned specimen near the fracture.
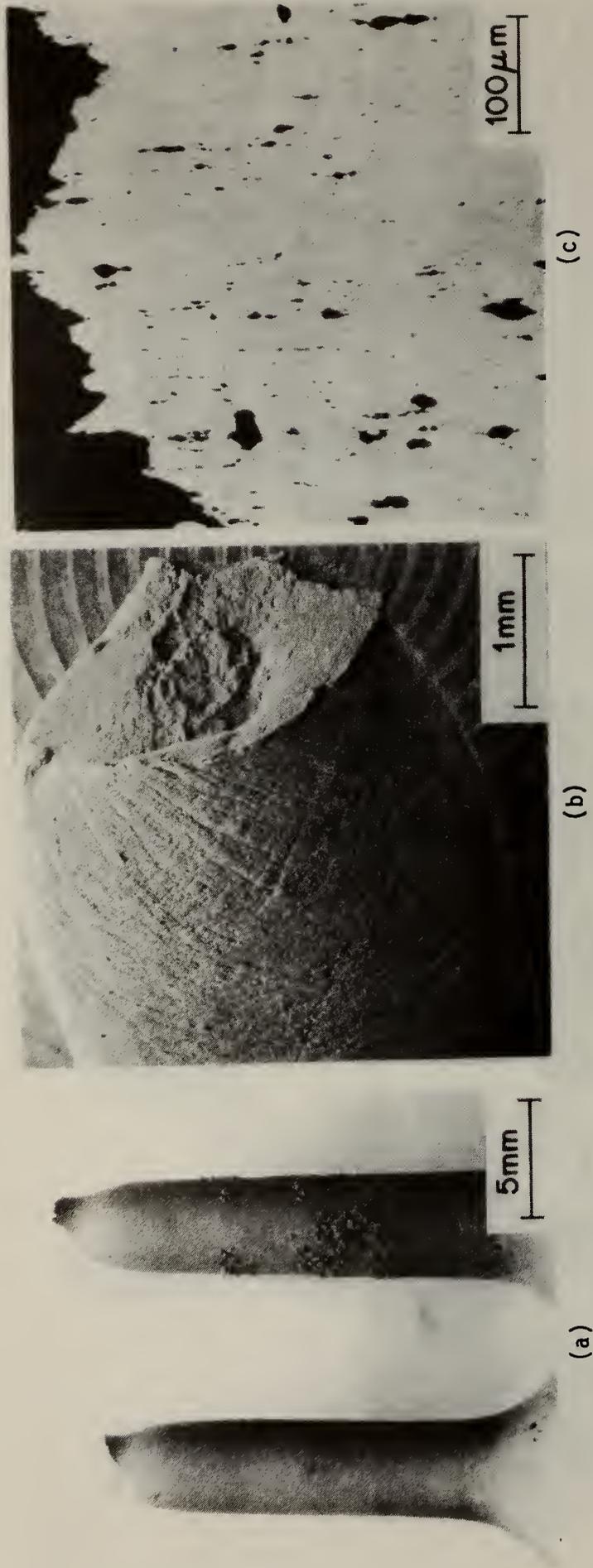
UTS ——— 590 MPa (85,500 psi)
Elongation ——— 18.4%
RA ——— 59.7%

Fig. 32.  Type 347 stainless steel tested in the oxidizing-sulfidizing-carburizing enviroment at a strain rate of 1 x 10⁻⁶/s.
(a) Photomicrograph of the fractured specimen.
(b) Scanning electron micrograph at the region of fracture.
(c) Photomicrograph of the sectioned specimen near the fracture.

(a)

(b)

(c)

5mm

1 mm

100 μm

UTS ——— 451 MPa (65,300 psi)
Elongation —— 13.4%
RA ——— 52.2%

Fig. 33. Type 347 stainless steel tested in He at 600 °C at a strain
rate of 1 X 10⁻⁶/s. (a) Photomicrograph of the fractured
specimen. (b) Scanning electron micrograph at the region
of fracture. (c) Photomicrograph of the sectioned specimen
near the fracture.

(a)

(b)

(c)
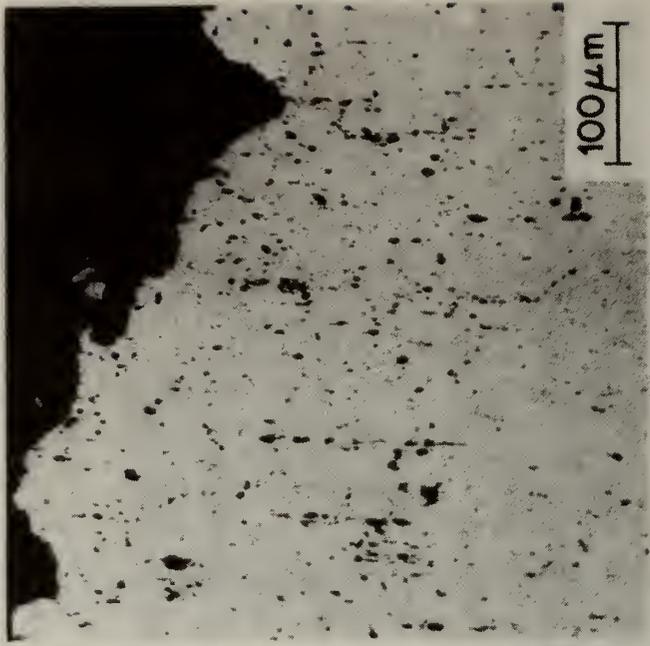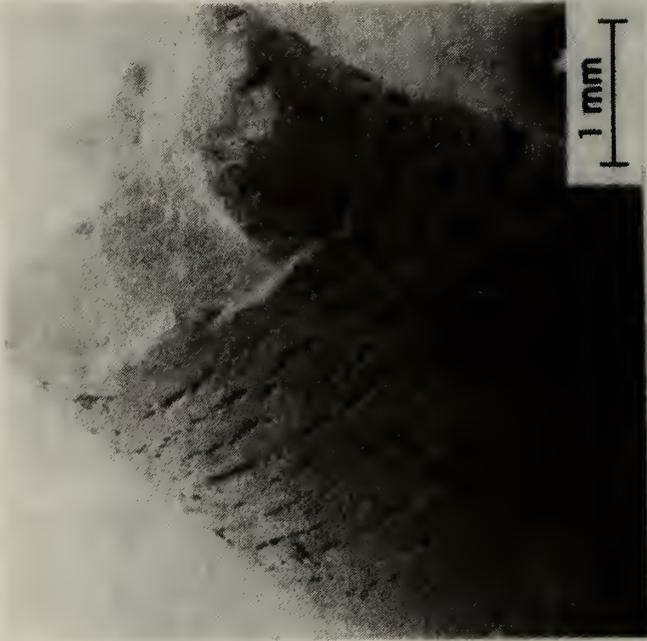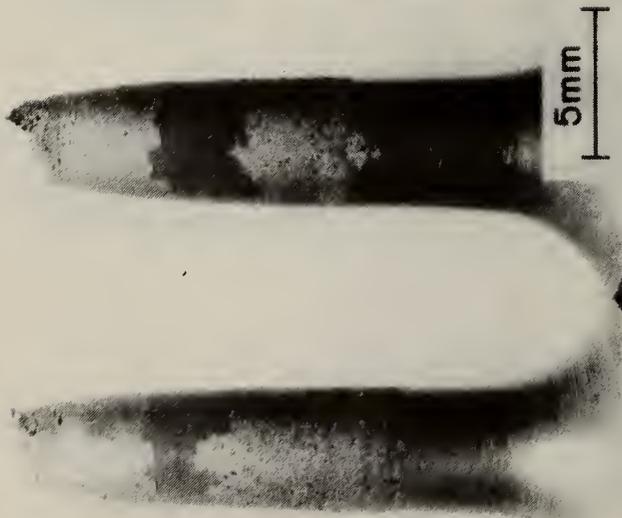
UTS      — 426 MPa (61,700 psi)
Elongation — 14.8%
RA       — 58.3%

Fig. 34.  Type 347 stainless steel tested at 600 °C in the oxidizing-sulfidizing-carburizing environment at a strain rate of 1 X 10⁻⁶/s.  (a) Photomicrograph of the fractured specimen.  (b) Scanning electron micrograph at the region of fracture.  (c) Photomicrograph of the sectioned specimen near the fracture.

(a)

5 mm

(b)

2 mm

(c)

200 μm
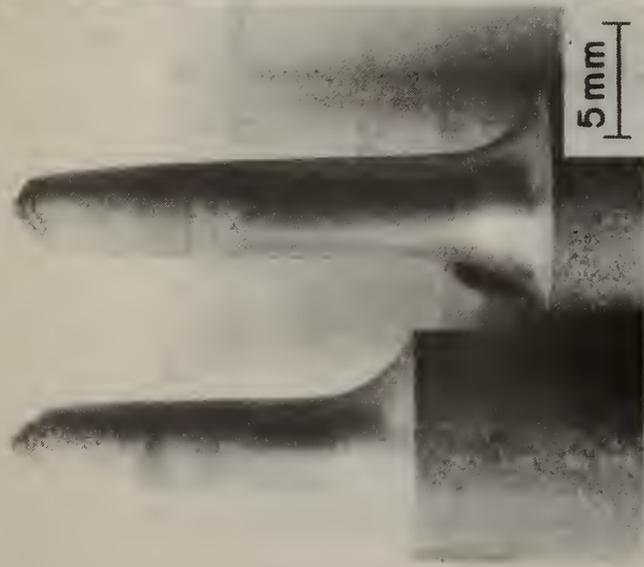
UTS —— 460 MPa (66,600 psi)
Elongation —— 14.5%
RA —— 46.0%

Fig. 35. Type 347 stainless steel tested in the oxidizing-sulfidizing environment at 600 °C at a strain rate of 1 X 10$^{-6}$/s. (a) Photomicrograph of the fractured specimen. (b) Scanning electron micrograph at the region of fracture. (c) Photomicrograph of the sectioned specimen near the fracture.
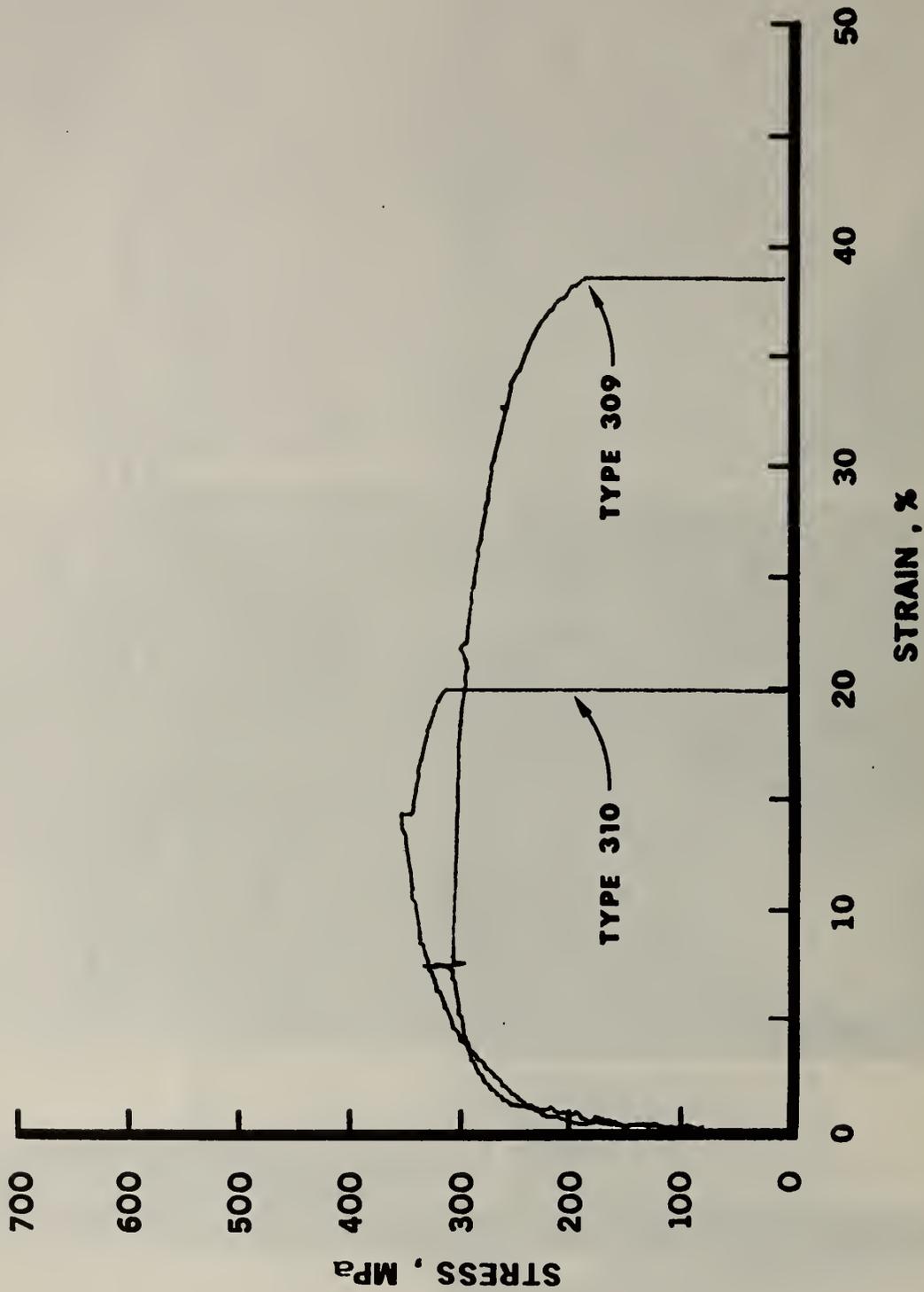
Fig. 36.  Comparison stress-strain curves of Types 309 and 310 specimens
tested at a strain rate of $10^{-6}$/s in He at 600 °C.

(a)                            (b)                          (c)
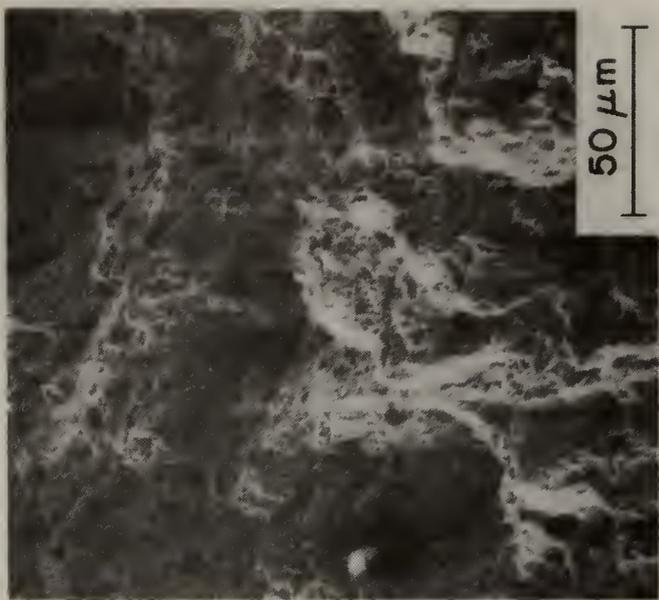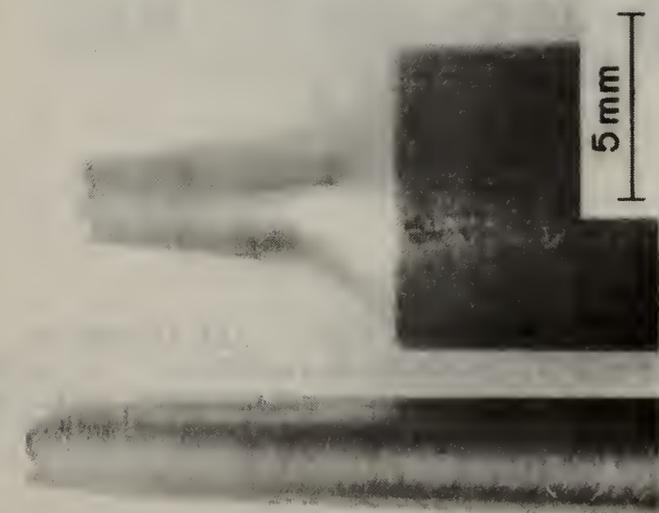
UTS &mdash; 334 MPa (48,400 psi)
Elongation &mdash; 37.7%
RA &mdash; 69.2%

Fig. 37.  Type 309 specimen tested in He at 600 °C and strain rate of
1 X 10⁻⁶/s.  (a) Photomicrograph of fractured specimen (5 X).
(b) SEM at the region of fracture (20 X).  (c) SEM of fractured
surface near edge (500 X).
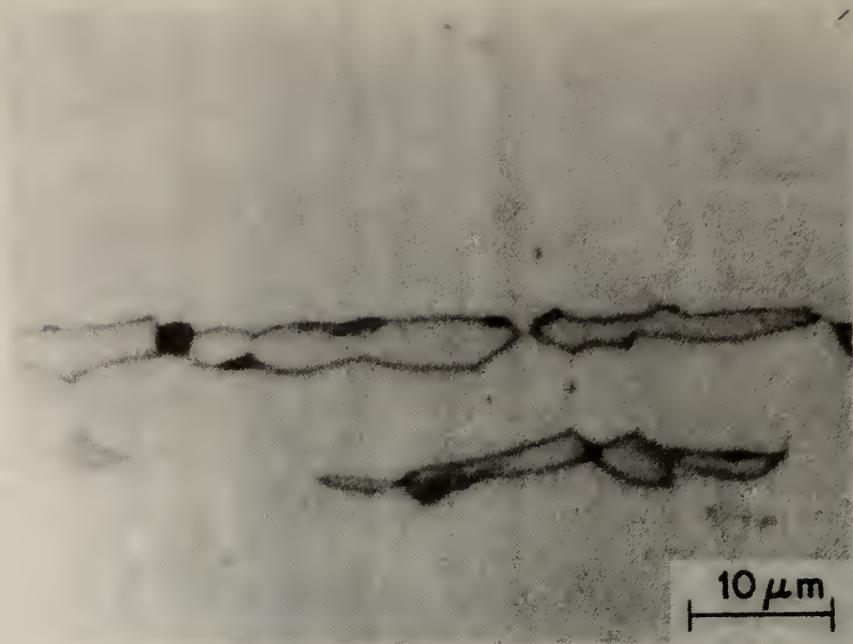
(a)
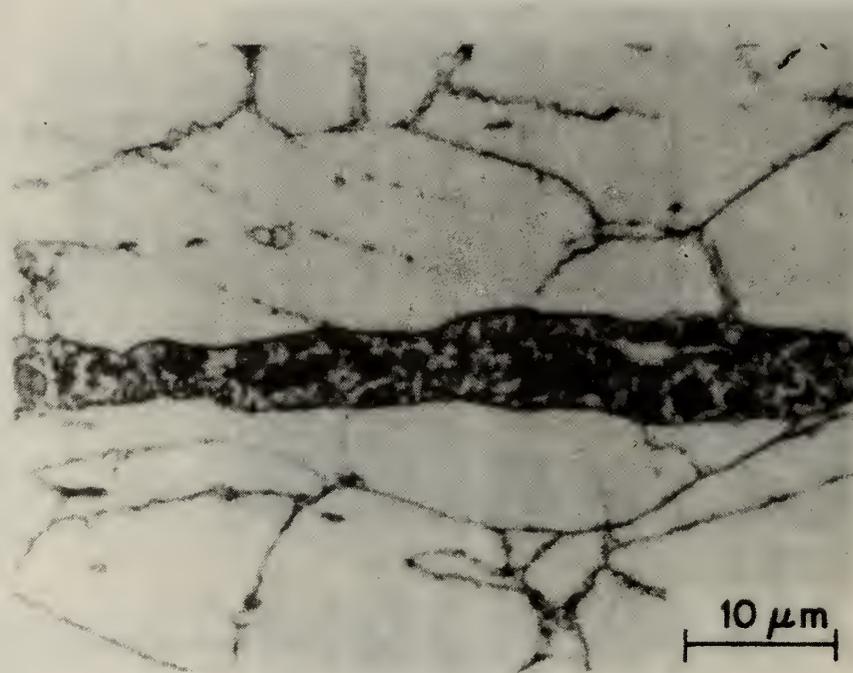


(b)

Fig. 38.  Microstructure of Type 309 stainless steel.  (a) Islands of
          ferrite in austenite matrix, as-received condition.  (b) Islands
          of ferrite transformed to mixed ferrite and carbides, which were
          indentified by chemical etchants, after being tested at 600 °C
          in He at a strain rate of $10^{-6}$/s.
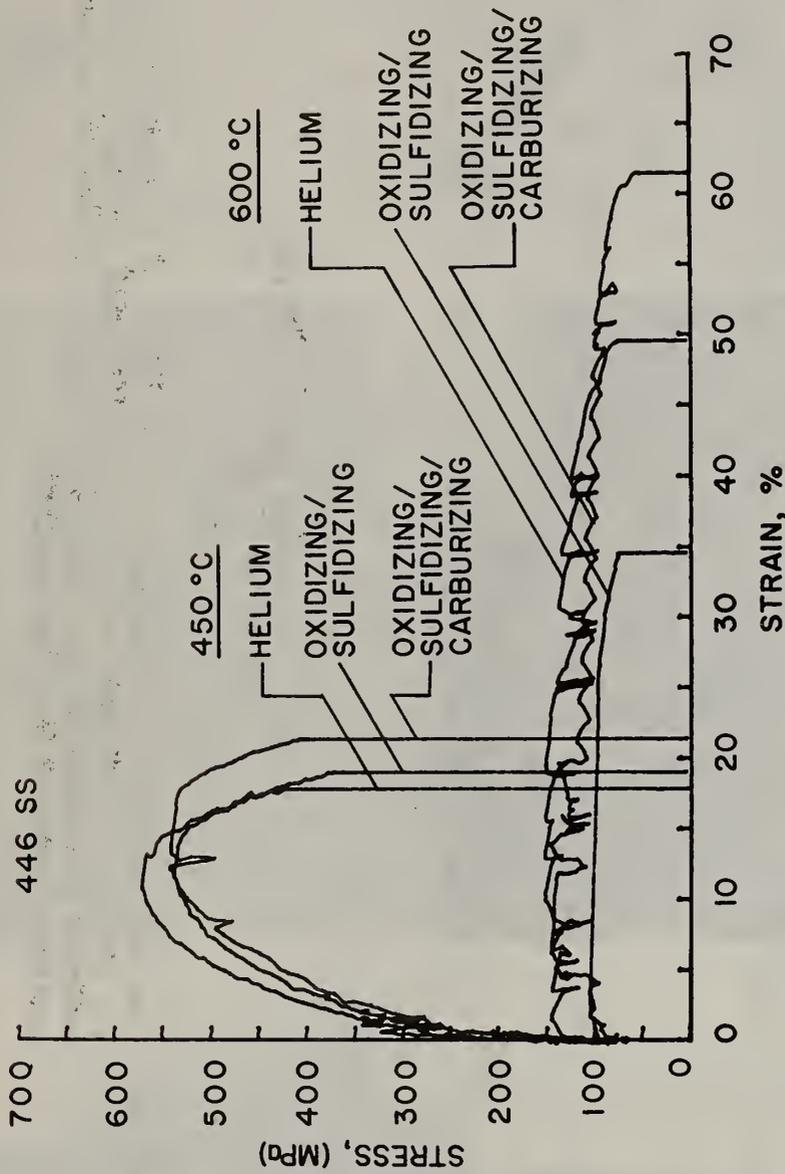
Fig. 39. Stress-strain curves for Type 446 specimens tested at 450 °C (840 °F) and 600 °C (1100 °F) in He and in oxidizing/sulfidizing and oxidizing/ sulfidizing/carburizing coal gasification environments at a strain rate of 1 X 10-6/s.
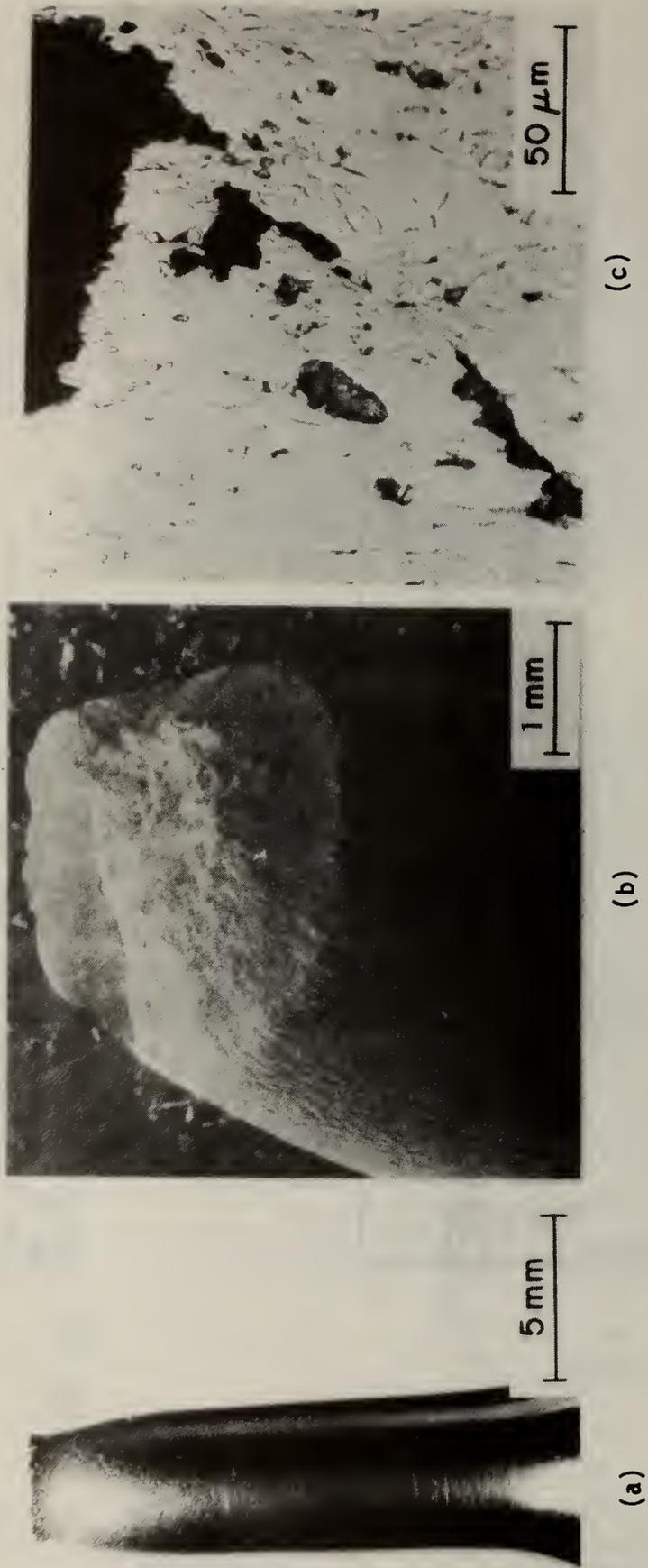
UTS — 586 MPa (85,000 psi)
Elongation — 17.3%
RA — 57.0%

Fig. 40.  Type 446 stainless steel tested in He at 450 °C at a strain rate of
1 X 10-6/s.  (a) Photomicrograph of the fractured specimen.  (b) Scanning
electron micrograph at the region of fracture.  (c) Photomicrograph of the
sectioned specimen near the fracture.

(a)

(b)

(c)

| 5 mm | 1 mm | 100 μm |

UTS        — 552 MPa (80,000 psi)
Elongation — 19.3%
RA         — 61.4%

Fig. 41.  Type 446 stainless steel tested in the oxidizing/sulfidizing environment
at 450 °C at a strain rate of 1 X 10⁻⁶/s.  (a) Photomicrograph of the
fractured specimen.  (b) Scanning electron micrograph at the region of
fracture.  (c) Photomicrograph of the sectioned specimen near the fracture.

(c)

(b)
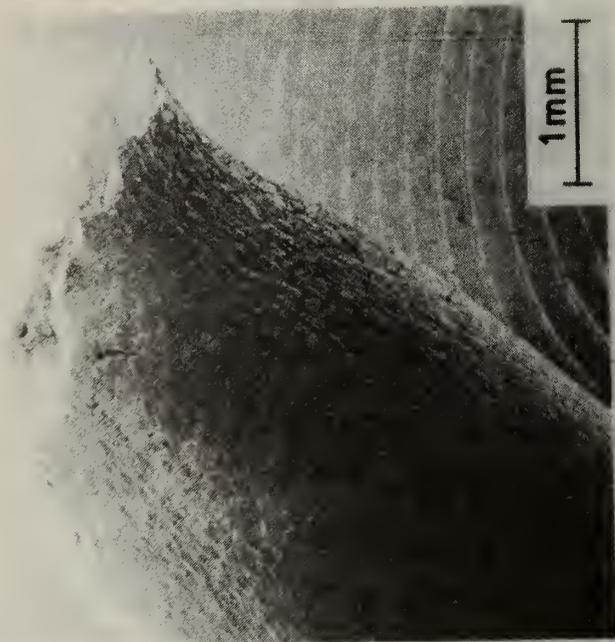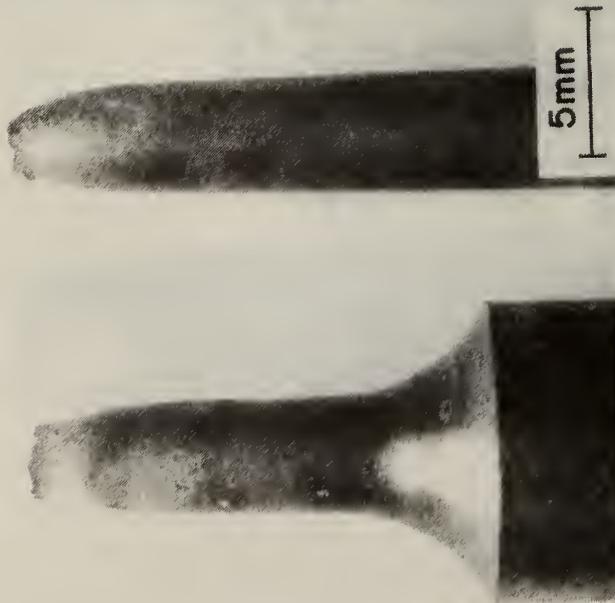
UTS ——— 574 MPa (83,200 psi)
Elongation —— 21.0%
RA —— 58.0%

(a)

Fig. 42.  Type 446 stainless steel tested in the oxidizing/sulfidizing/
carburizing environment at 450 °C at a strain rate of 1 X 10⁻⁶/s.
(a) Photomicrograph of the fractured specimen.  (b) Scanning
electron micrograph at the region of fracture.  (c) Photomicrograph
of the sectioned specimen near the fracture.

(a)                               (b)                            (c)
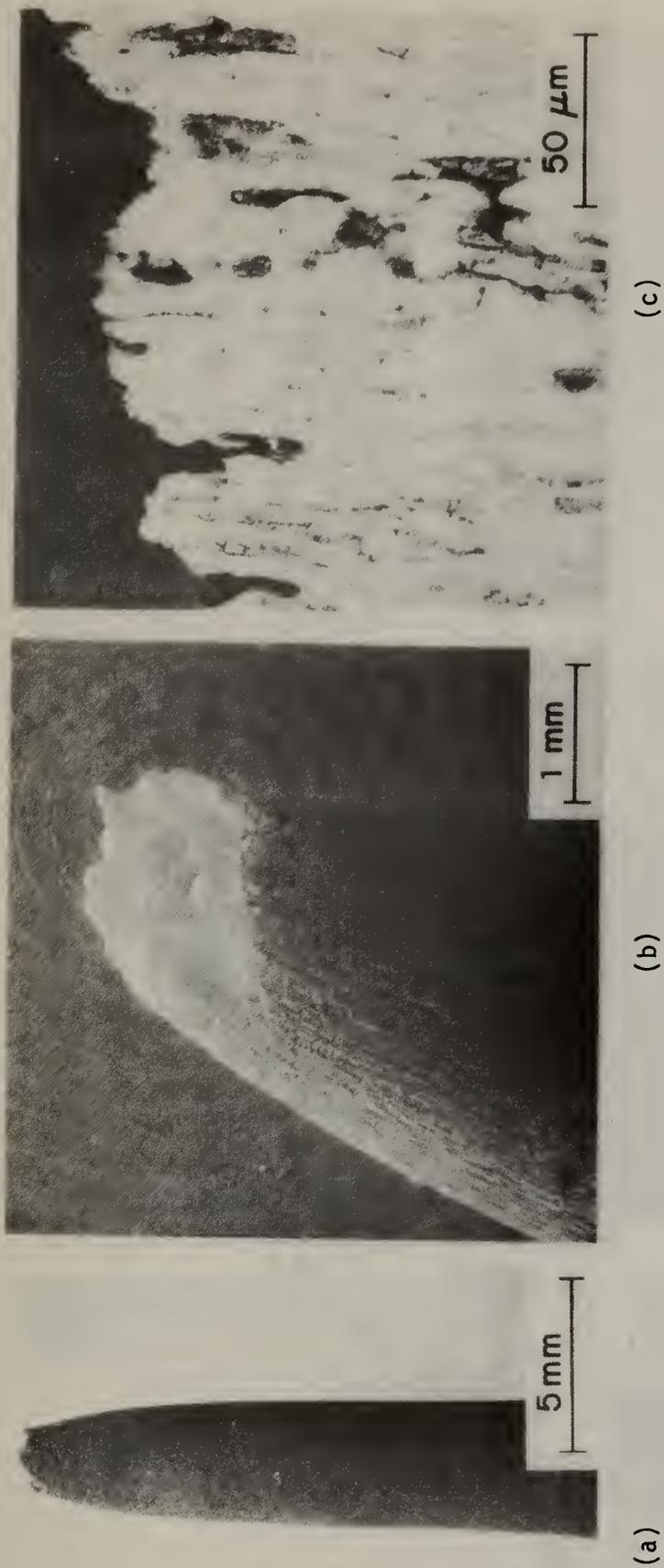
UTS       — 152 MPa (22,000 psi)
Elongation — 62.0%
RA        — 86.2%

Fig. 43.   Type 446 stainless steel tested in He at 600 °C at a strain rate of
1 X 10-6/s.  (a) Photomicrograph of the fractured specimen.  (b) Scanning
electron micrograph at the region of fracture.  (c) Photomicrograph of
the sectioned specimen near the fracture.
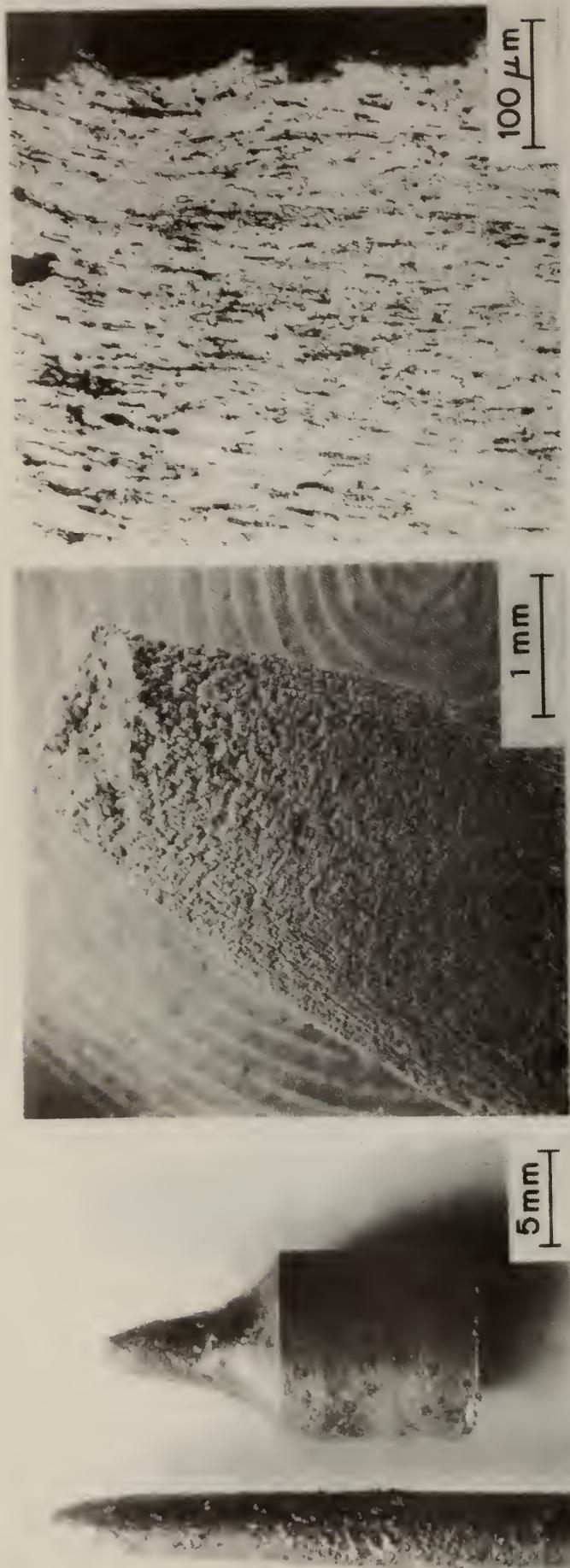
(a)

(b)

(c)

UTS ——— 109 MPa (15,800 psi)
Elongation ——— 34.7%
RA ——— 88.3 %

Fig. 44.  Type 446 stainless steel tested in the oxidizing/sulfidizing environment
at 600 °C at a strain rate of 1 X 10⁻⁶/s.  (a) Photomicrograph of the
fractured specimen.  (b) Scanning electron micrograph at the region of
fracture.  (c) Photomicrograph of the sectioned specimen near the fracture.

(c)

(b)
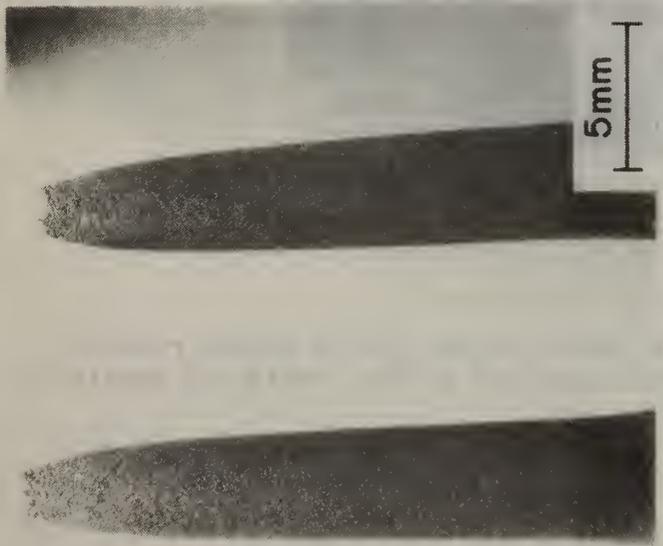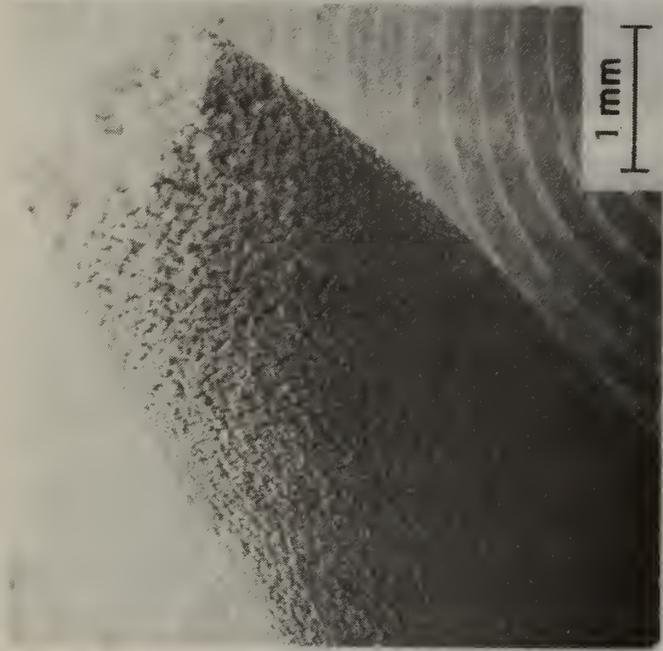
| UTS | — | 160 MPa (23,200 psi) |
| Elongation | — | 49.5% |
| RA | — | 83.3% |

(a)

Fig. 45.   Type 446 stainless steel tested in the oxidizing/sulfidizing/
carburizing environment at 600 °C at a strain rate of $1 \times 10^{-6}$/s.
(a) Photomicrograph of the fractured specimen.   (b) Scanning
electron micrograph at the region of fracture.   (c) Photomicrograph
of the sectioned specimen near the fracture.
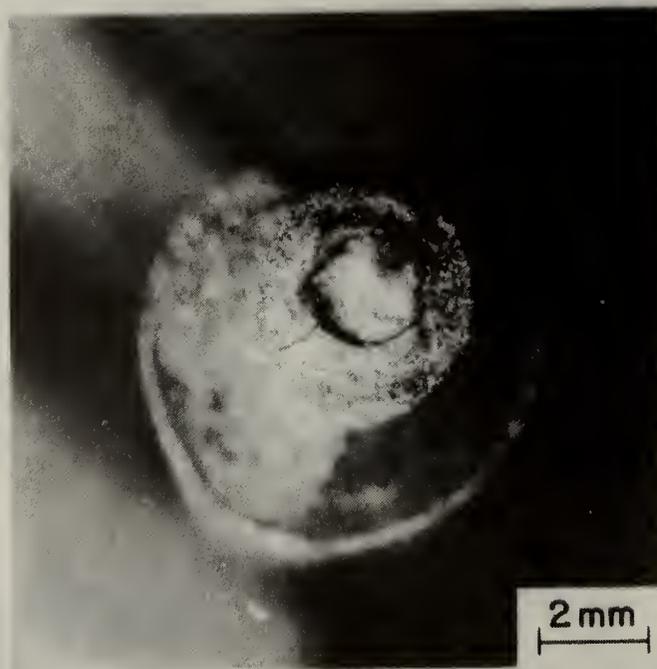
Fig. 46.  In 800 specimen tested at 540 °C in wet $H_2S$ at strain rate of 1.7 X 10$^{-7}$/s showing large amount of surface scale and remaining metal.
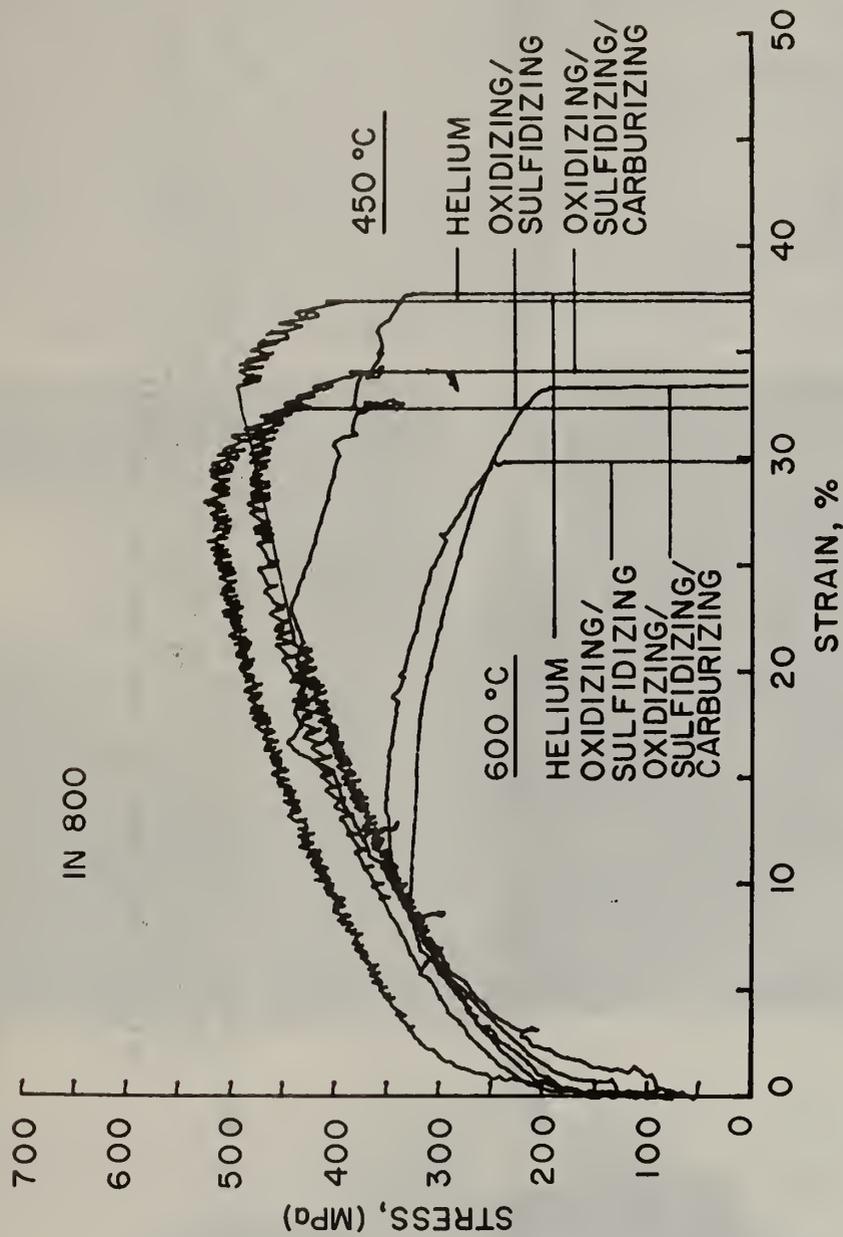
Fig. 47.  Stress-strain curves for Incoloy 800 tested at 450 °C (840 °F) and 600 °C (1100 °F) in He and in oxidizing/sulfidizing and oxidizing/sulfidizing/carburizing coal gasification environments at a strain rate of 1 X 10⁻6/s.

(c)

(b)

(a)
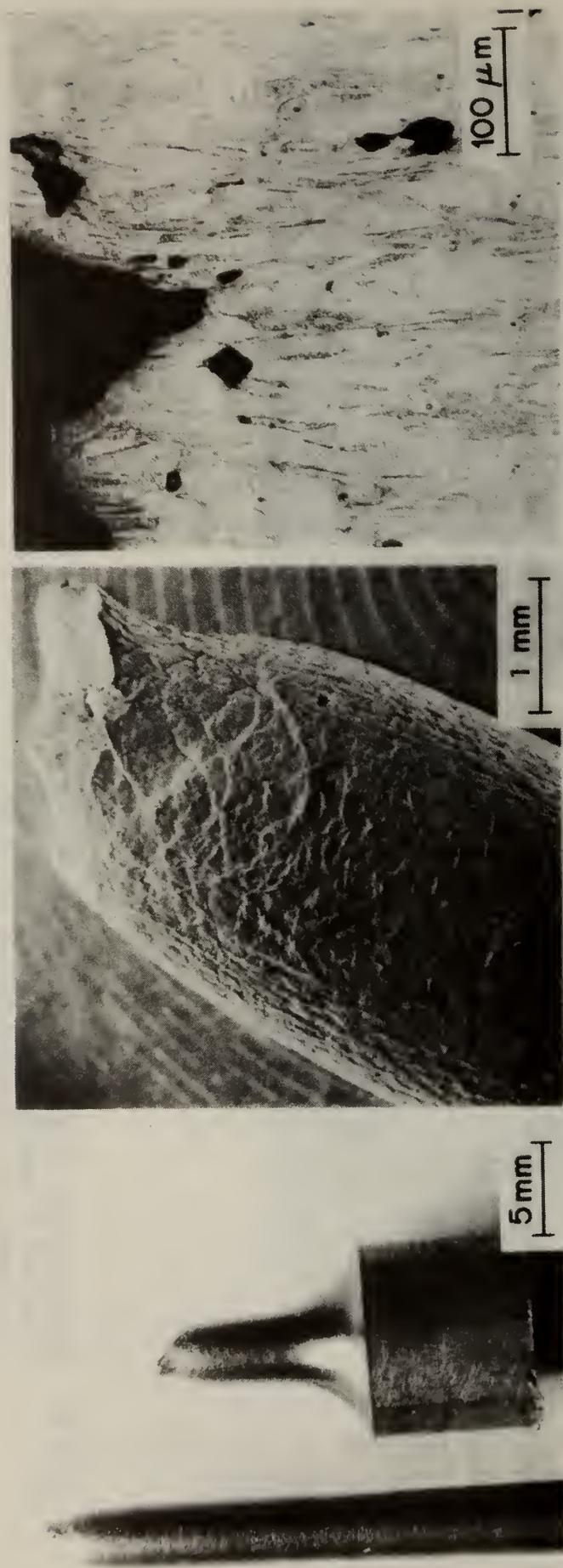
UTS ——— 526 MPa (76,200 psi)
Elongation ——— 37.3%
RA ——— 72.1%

Fig. 48.  Incoloy 800 tested in He at 450 °C at a strain rate of 1 X 10$^{-6}$/s.
(a) Photomicrograph of the fractured specimen.  (b) Scanning
electron micrograph at the region of fracture.  (c) Photomicrograph
of the sectioned specimen near the fracture.

(a)

(b)

(c)

UTS       — 544 MPa (78,900 psi)
Elongation — 32.6%
RA        — 65.8%

Fig. 49.   Incoloy 800 tested in the oxidizing/sulfidizing environment at
           450 °C at a strain rate of 1 X 10⁻⁶/s.  (a) Photomicrograph of
           the fractured specimen.  (b) Scanning electron micrograph at
           the region of fracture.  (c) Photomicrograph of the sectioned
           specimen near the fracture.

(a)

5 mm

(b)

1 mm

(c)

100 μm
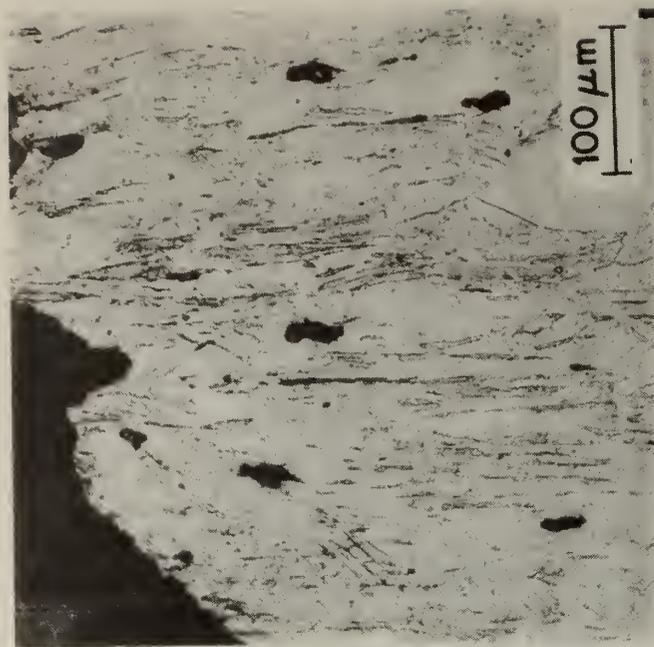
UTS ——— 551 MPa (79,800 psi)
Elongation ——— 34.3%
RA ——— 70.5%

Fig. 50. Incoloy 800 tested in the oxidizing/sulfidizing/carburizing environment at 450 °C at a strain rate of 1 X 10⁻⁶/s. (a) Photomicrograph of the fractured specimen. (b) Scanning electron micrograph at the region of fracture. (c) Photomicrograph of the sectioned specimen near the fracture.

(a)

(b)

(c)

UTS      — 467 MPa (67,700 psi)
Elongation — 37.1%
RA       — 60.1%

Fig. 51.   Incoloy 800 tested in He at 600 °C at a strain rate of
           1 X 10-6/s.   (a) Photomicrograph of the fractured specimen.
           (b) Scanning electron micrograph at the region of fracture.
           (c) Photomicrograph of the sectioned specimen near the fracture.

(a)

5 mm

(b)

2 mm

(c)

200 μm
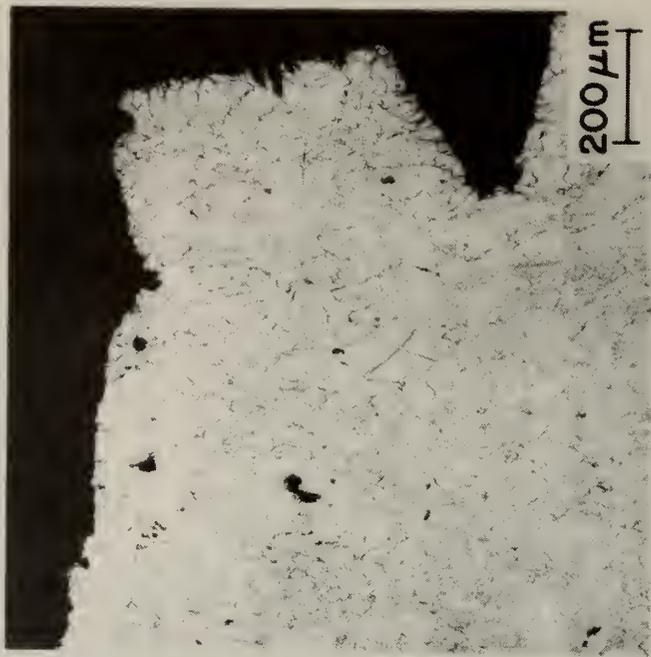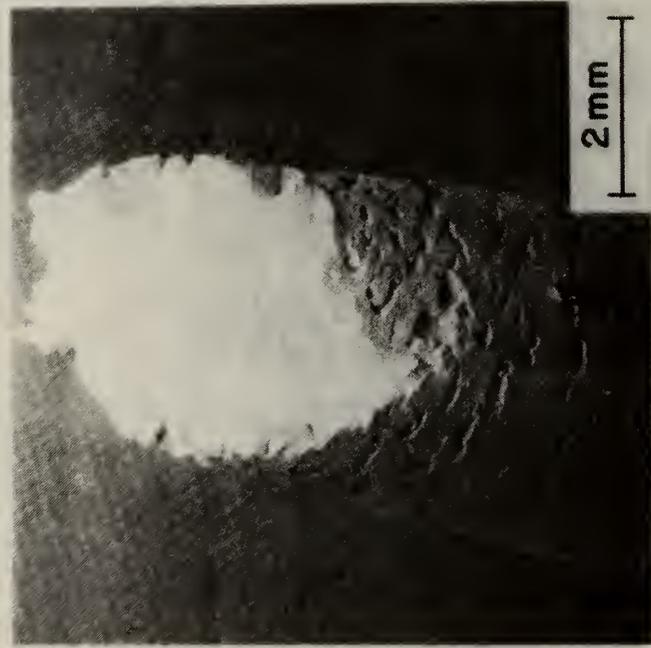
UTS — 368 MPa (53,400 psf)
Elongation — 29.4%
RA — 49.4%

Fig. 52.  Incoloy 800 tested in the oxidizing/sulfidizing environment at
600 °C at a strain rate of 1 X 10⁻⁶/s.  (a) Photomicrograph of
the fractured specimen.  (b) Scanning electron micrograph at the
region of fracture.  (c) Photomicrograph of the sectioned specimen
near the fracture.
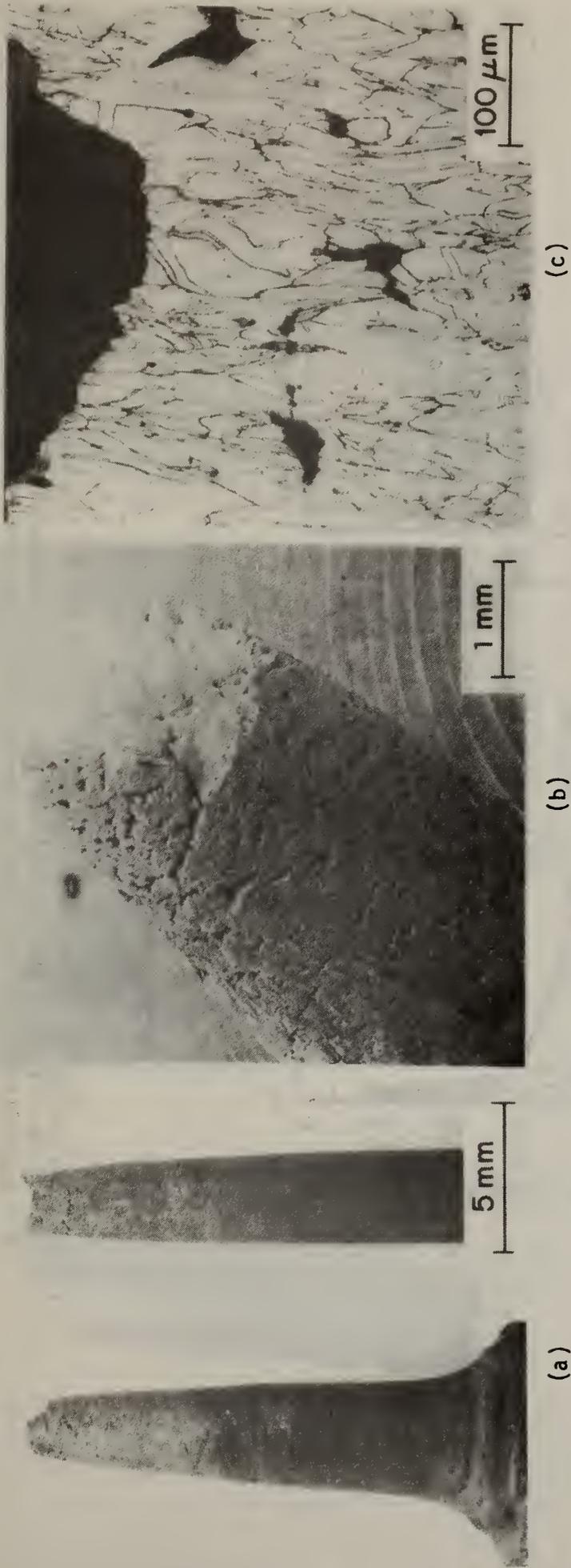
UTS     — 353 MPa (51,100 psi)
Elongation — 32.7%
RA       — 61.7%

Fig. 53.   Incoloy 800 tested in the oxidizing/sulfidizing/carburizing
environment at 600 °C at a strain rate of 1 X 10-6/s.
(a) Photomicrograph of the fractured specimen.   (b) Scanning
electron micrograph at the region of fracture.   (c) Photo-
micrograph of the sectioned specimen near the fracture.
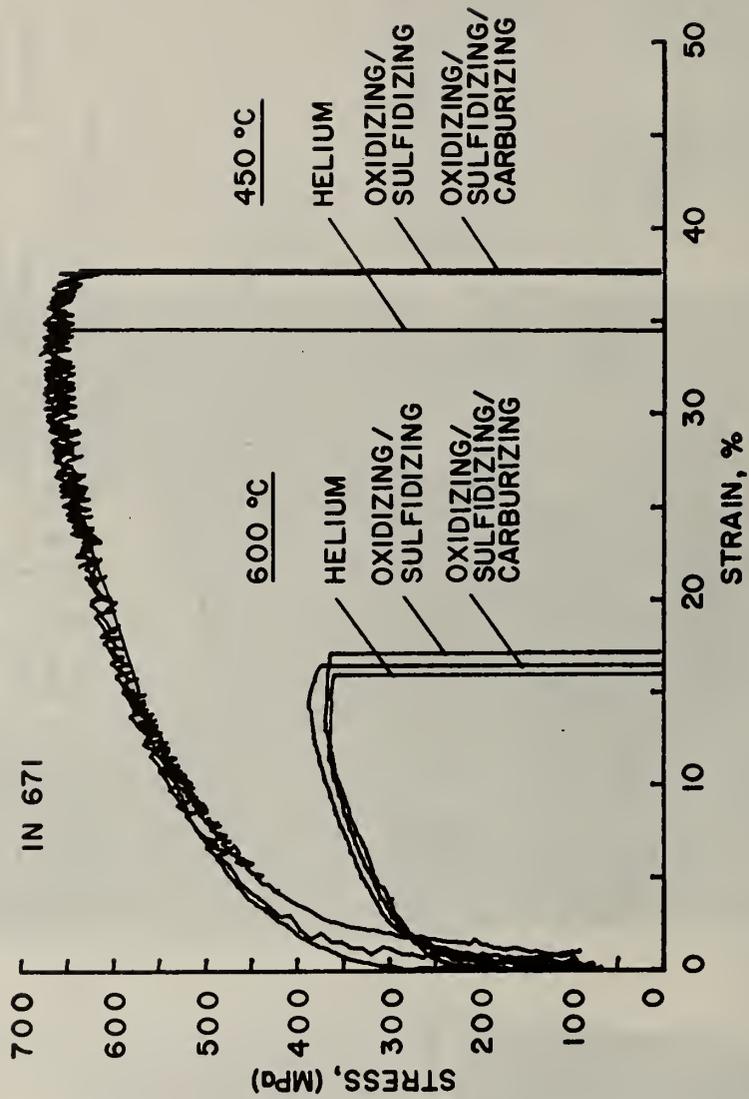
Fig. 54. Stress-strain curves for Inconel 671 tested at 450 °C (840 °F) and 600 °C (1100 °F) in He and in oxidizing/sulfidizing and oxidizing/sulfidizing/carburizing coal gasification environments at a strain rate of 1 × 10$^{-6}$/s.

(a)

(b)

(c)

5 mm

1 mm

50 μm
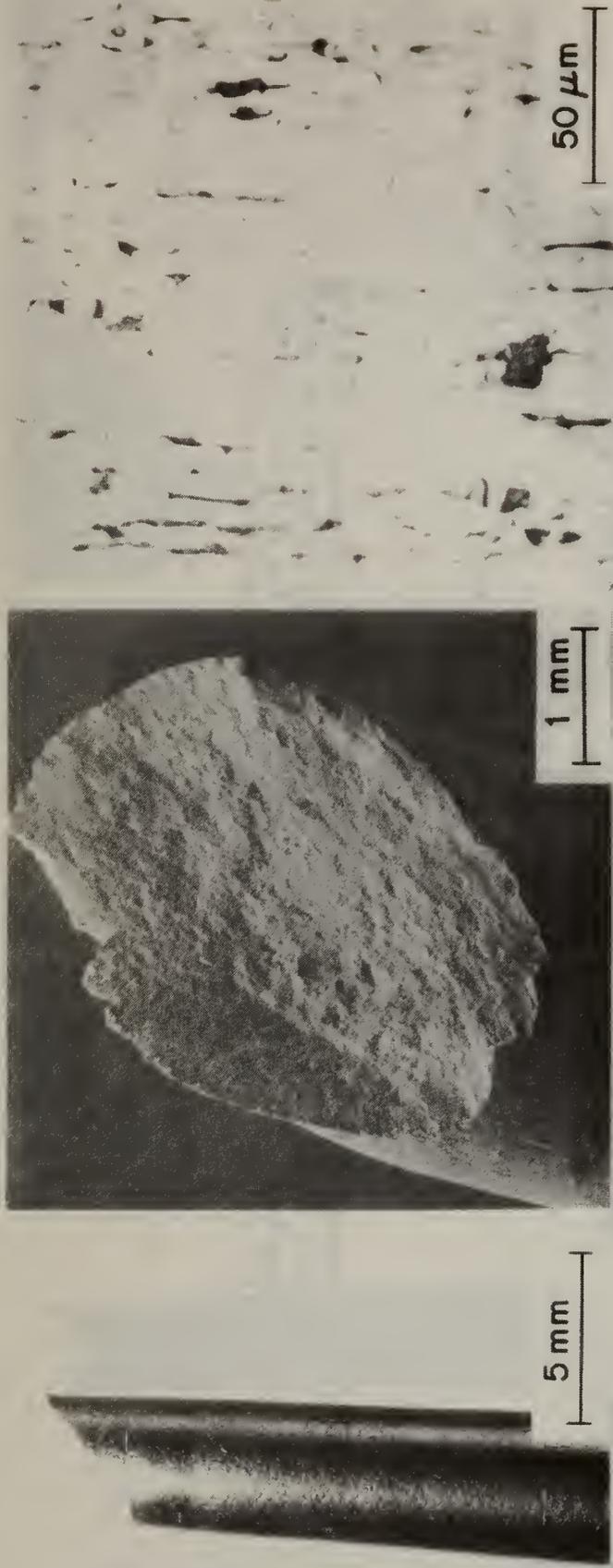
UTS ——— 680 MPa (98,600 psi)
Elongation ——— 32.8%
RA ——— 37.7%

Fig. 55. Inconel 671 tested in He at 450 °C at a strain rate of 1 X 10$^{-6}$/s.
(a) Photomicrograph of the fractured specimen. (b) Scanning
electron micrograph at the region of fracture. (c) Photomicrograph
of the sectioned specimen near the fracture.
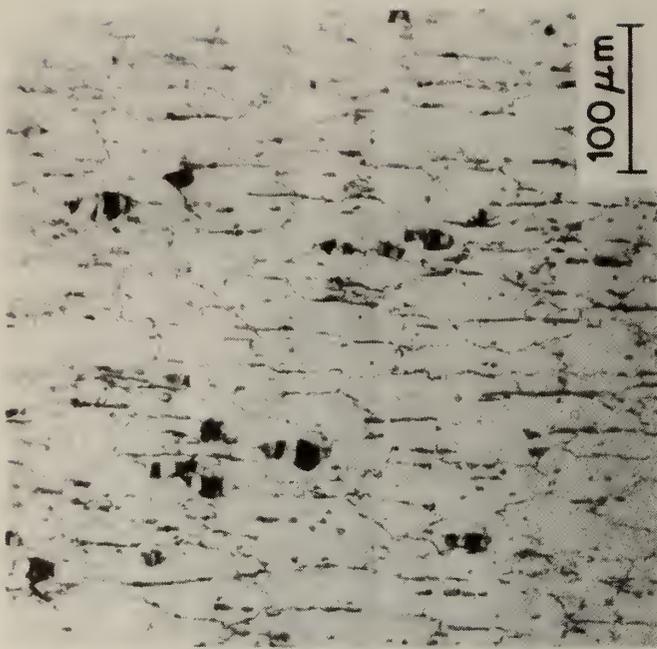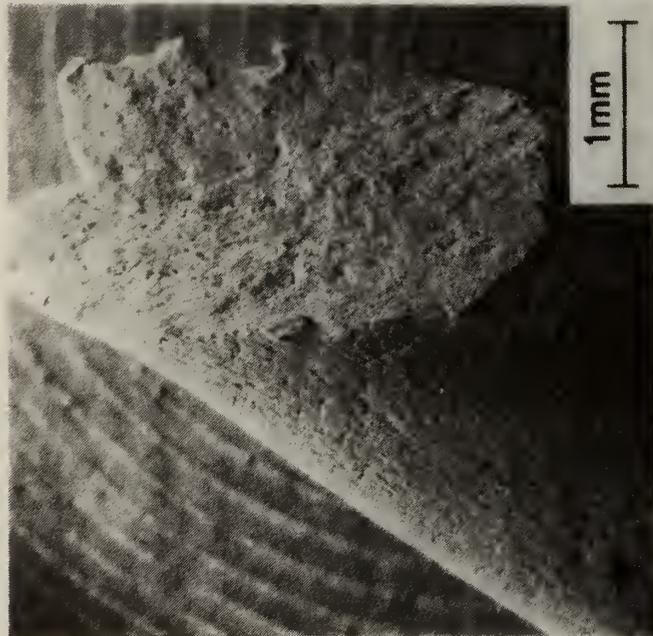
UTS —— 670 MPa (97,100 psi)
Elongation —— 38.6%
RA —— 45.3%
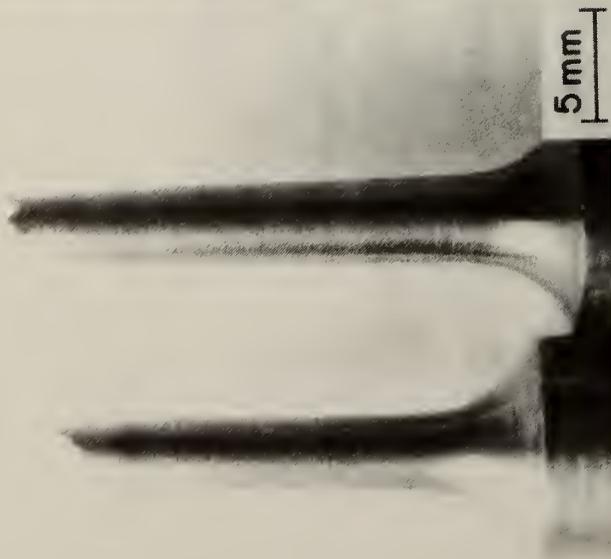
Fig. 56.  Inconel 671 tested in the oxidizing/sulfidizing environment at 450 °C
at a strain rate of 1 X 10⁻⁶/s.  (a) Photomicrograph of the fractured
specimen.  (b) Scanning electron micrograph at the region of fracture.
(c) Photomicrograph of the sectioned specimen near the fracture.

(a)

5 mm

(b)

1 mm

(c)

100 μm
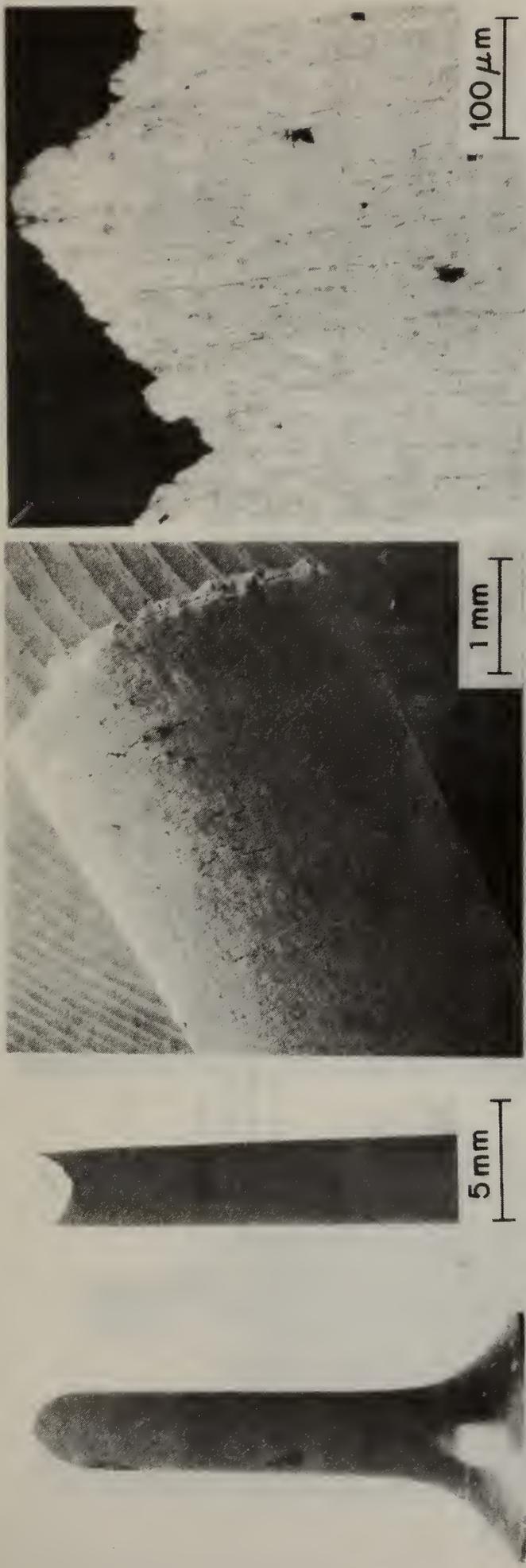
UTS      — 676 MPa (97,900 psi)
Elongation — 38.0%
RA       — 39.3%

Fig. 57.   Inconel 671 tested in the oxidizing/sulfidizing/carburizing environment at 450 °C at a strain rate of 1 X 10⁻⁶/s. (a) Photomicrograph of the fractured specimen. (b) Scanning electron micrograph at the region of fracture. (c) Photomicrograph of the sectioned specimen near the fracture.

(c)

(b)

(a)
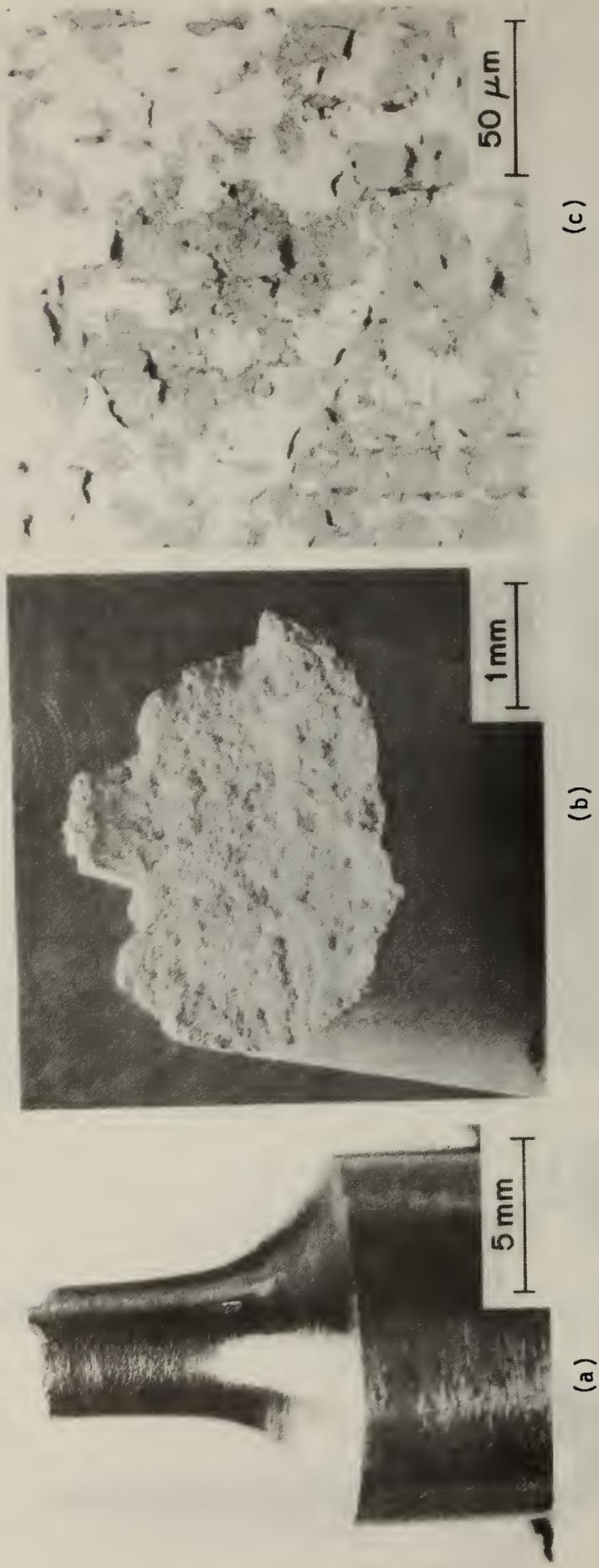
| | |
|---|---|
| UTS | — 416 MPa (60,300 psi) |
| Elongation | — 16.1% |
| RA | — 16.3% |

Fig. 58.  Inconel 671 tested in He at 600 °C at a strain rate of $1 \times 10^{-6}$/s.
(a) Photomicrograph of the fractured specimen.  (b) Scanning electron
micrograph at the region of fracture.  (c) Photomicrograph of the
sectioned specimen near the fracture.

(a)

(b)

(c)

5 mm

1 mm

100 μm
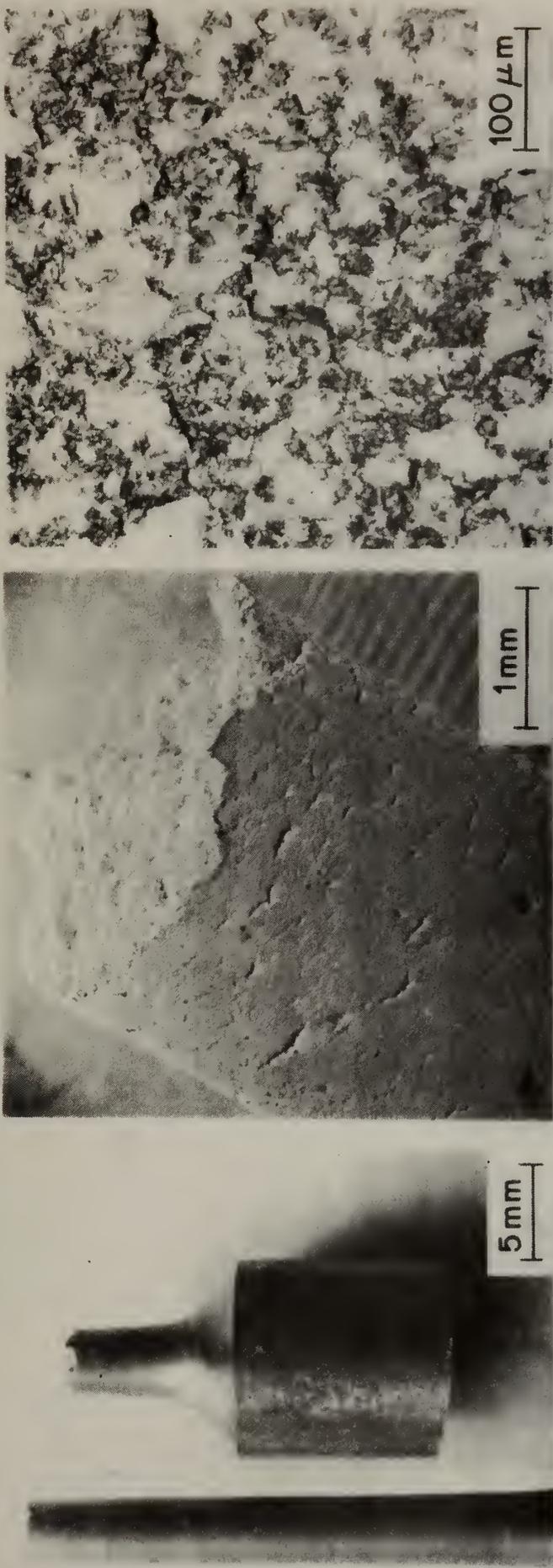
UTS ——— 397 MPa (57,600 psi)
Elongation ——— 17.5%
RA ——— 20.7%

Fig. 59. Inconel 671 tested in the oxidizing/sulfidizing environment at 600 °C
at a strain rate of 1 X 10⁻6/s. (a) Photomicrograph of the fractured
specimen. (b) Scanning electron micrograph at the region of fracture.
(c) Photomicrograph of the sectioned specimen near the fracture.
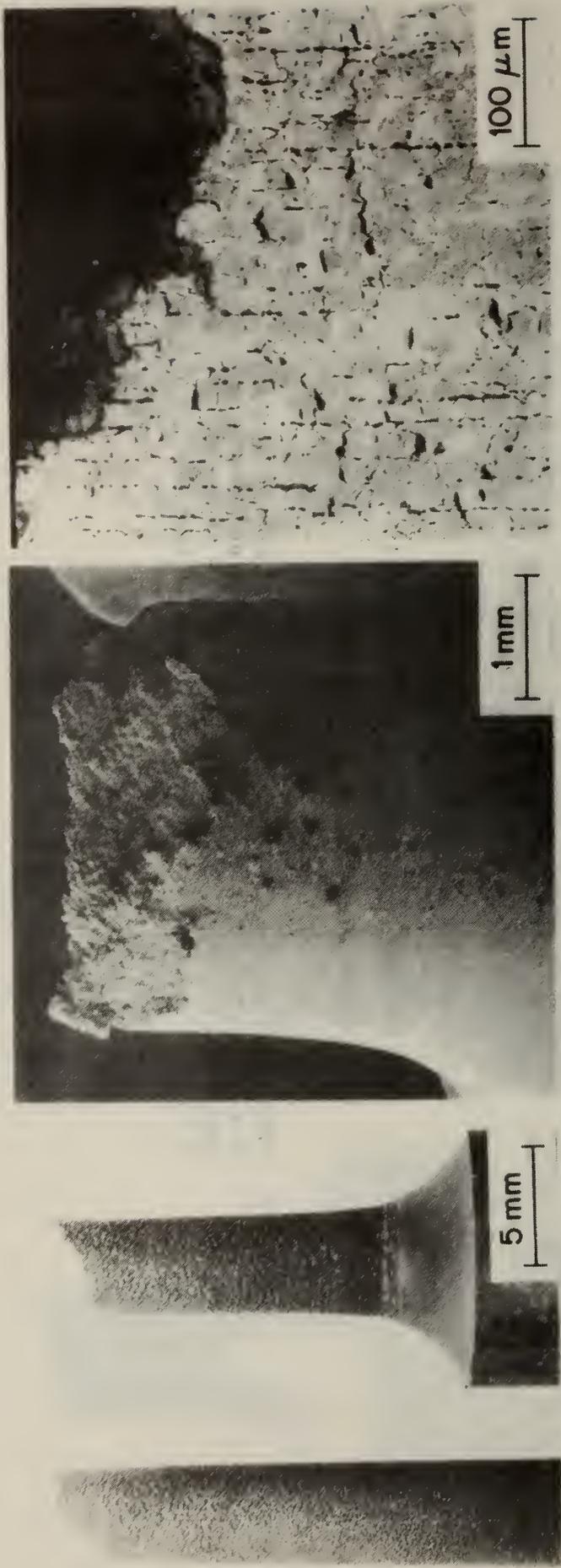
(a)

(b)

(c)

UTS — 448 MPa (64,900 psi)
Elongation — 16.3%
RA — 16.8%

Fig. 60. Inconel 671 tested in the oxidizing/sulfidizing/carburizing environment at 600 °C at a strain rate of 1 X 10⁻⁶/s. (a) Photomicrograph of the fractured specimen. (b) Scanning electron micrograph at the region of fracture. (c) Photomicrograph of the sectioned specimen near the fracture.
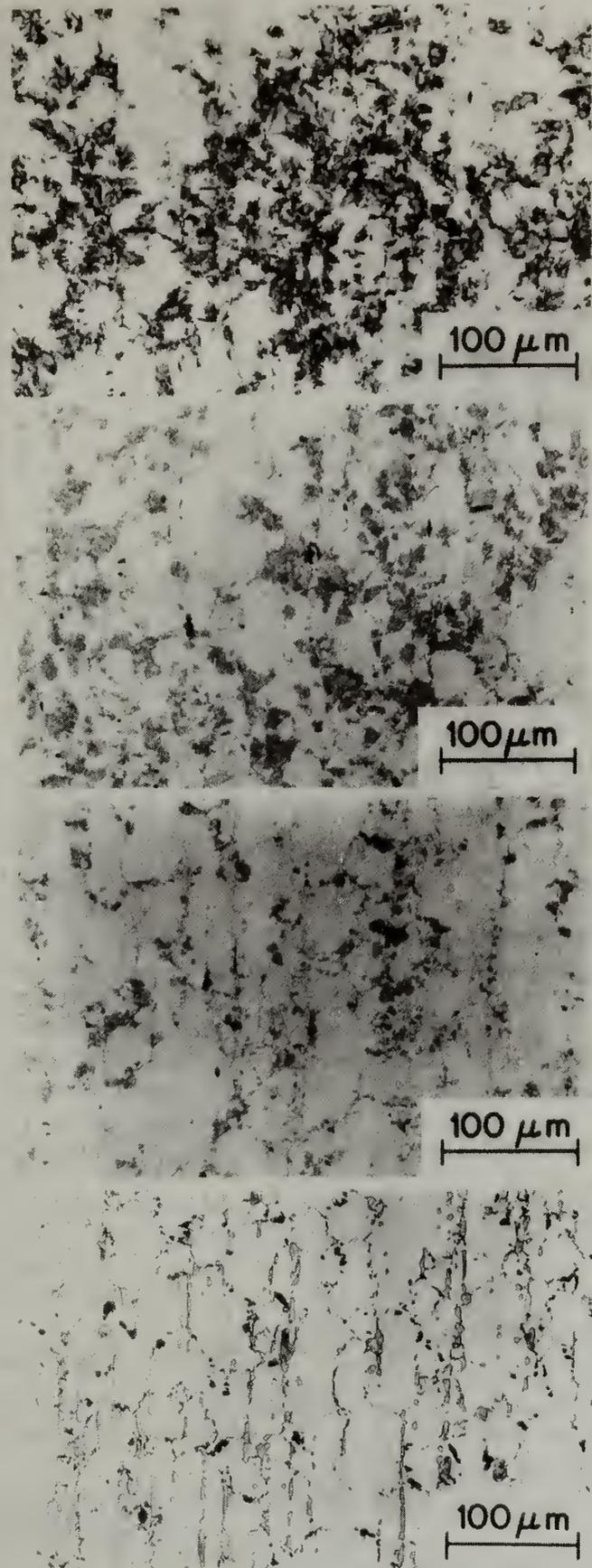
Fig. 61. Inconel 671 tested at 600 °C in oxidizing/sulfidizing/carburizing environment at 1 X 10<sup>-6</sup>/s. (Top to Bottom) Alpha-chromium phase present in alloy due to combined effects of temperature and strain. Progressing from maximum strain (fracture surface) to a smaller strain (near shoulder area of reduced section). 200 ᵞ.

| U.S. DEPT. OF COMM.<br>BIBLIOGRAPHIC DATA<br>SHEET | 1. PUBLICATION OR REPORT NO.<br><br>NBSIR 81-2191 (DoE) | 2. Gov't. Accession No. | 3. Recipient's Accession No. |
|---|---|---|---|

| 4. TITLE AND SUBTITLE<br><br>The Use of the Slow Strain Rate Technique for the Evaluation of Structural Materials for Application in High-temperature Gaseous Environments | 5. Publication Date |
|---|---|
| | 6. Performing Organization Code<br>561 |

| 7. AUTHOR(S)<br><br>G. M. Ugiansky and C. E. Johnson | 8. Performing Organ. Report No. |
|---|---|

| 9. PERFORMING ORGANIZATION NAME AND ADDRESS<br><br>NATIONAL BUREAU OF STANDARDS<br>DEPARTMENT OF COMMERCE<br>WASHINGTON, DC 20234 | 10. Project/Task/Work Unit No. |
|---|---|
| | 11. Contract/Grant No. |

| 12. SPONSORING ORGANIZATION NAME AND COMPLETE ADDRESS (Street, City, State, ZIP)<br>Department of Energy<br>Division of Systems Engineering/Energy Technology<br>Mail Stop GTN C-155<br>Washington, DC 20545 | 13. Type of Report & Period Covered<br><br>Final |
|---|---|
| | 14. Sponsoring Agency Code |

15. SUPPLEMENTARY NOTES

☐ Document describes a computer program; SF-185, FIPS Software Summary, is attached.

16. ABSTRACT *(A 200-word or less factual summary of most significant information. If document includes a significant bibliography or literature survey, mention it here.)*

The slow strain rate technique has been evaluated as an accelerated test for determining the performance of structural materials in simulated coal gasification environments. Seven alloys, namely Types 309, 310, 310S, 347 and 446 stainless steels; Incoloy 800; and Inconel 671, were tested at temperatures from 370 $^\circ$C to 1040 $^\circ$C at strain rates from $10^{-4}$ to $10^{-7}$/s in $H_2S$ plus water, gaseous mixtures of CO, $CO_2$, $H_2$, $CH_4$, $H_2S$, and $H_2O$, and in nominally inert environments of He and Ar. Type 310 steel, the most extensively studied material, showed a marked reduction in mechanical properties at low strain rates (<$10^{-5}$/s) in $H_2S/H_2O$ at 540 $^\circ$C, and this was associated with the occurrence of a large degree of secondary intergranular cracking in addition to the main ductile fracture mode. The occurrence of the secondary cracking was taken as the primary indication of embrittlement in subsequent tests. Of particular significance, it occurred to some degree in all alloys tested in the simulated coal-gasification environments at 600 $^\circ$C. Consequently, the mechanism(s) of the embrittlement phenomena remain uncertain; a number of possible causes including creep and several environmentally-induced fracture processes are outlined. It is shown that the overall results of the test program are in good agreement with in-plant experience. It is concluded that the slow strain rate technique is an effective method for evaluating the performance of structural materials in the elevated-temperature gaseous environments.

17. KEY WORDS *(six to twelve entries; alphabetical order; capitalize only the first letter of the first key word unless a proper name; separated by semicolons)*

Austenitic stainless steels; coal gasification; elevated temperatures; ferritic stainless steel; gaseous environments; nickel alloy 671; nickel alloy 800; slow strain rate test; structural materials

| 18. AVAILABILITY | [X] Unlimited | 19. SECURITY CLASS<br>(THIS REPORT) | 21. NO. OF<br>PRINTED PAGES |
|---|---|---|---|
| ☐ For Official Distribution. Do Not Release to NTIS | | UNCLASSIFIED | |
| ☐ Order From Sup. of Doc., U.S. Government Printing Office, Washington, DC 20402, SD Stock No. SN003-003- | | 20. SECURITY CLASS<br>(THIS PAGE) | 22. Price |
| ☐ Order From National Technical Information Service (NTIS), Springfield, VA. 22161 | | UNCLASSIFIED | |